Conversion of n-pentenes over H-ZSM-5

Michele Cowley

BSc. Hons. (Chem.)

(UOVS)

Submitted to the University of Cape Town
in partial fulfillment of the requirements for the degree of
Master of Science (Applied Science)

Catalysis Research Unit
Department of Chemical Engineering
University of Cape Town
Rondebosch
Cape Town
South Africa

February 2002

To my parents

Acknowledgements

Sasol Technology (Pty) Ltd for making this MSc possible and for financial support.

Dr. Klaus P. Möller, my supervisor, for his guidance and input.

Prof. E. van Steen for helpful suggestions.

Mr. W. Böhringer for his assistance in sorting out the unknowns in the GC results.

A. de Klerk for continued support and discussions.

Syncat, Richardsbay, for supplying the H-ZSM-5.

The Catalyst Characterisation Group at R&D for performing analyses, especially B. Breedt.

The GC laboratory at SCI for performing GC-MS analyses, in particular A. Tolmay.

The shift personnel at FTRC, for valuable assistance in running the reactor continuously.

My colleagues at FTRC, for showing interest and Johann Rademann for help with thermodynamic calculations.

Family and friends for support.

My sister, Vanessa, for her encouragement.

My husband, André, for his support and encouragement.

Abstract

The skeletal isomerisation of 1-pentene provides the feed stock 2-methyl-2-butene and 2-methyl-1-butene for the production of tertiary amyl methyl ether (TAME), an octane booster for petrol. Benzene, toluene, xylenes and ethylbenzene (BTX+EB) are good or even better octane boosters, although the use of benzene is limited due to its carcinogenic nature. From an industrial point of view, these compounds are therefore of importance.

The conversion of 1-pentene over H-ZSM-5 zeolite catalyst was studied in a fixed-bed micro reactor. Experiments were performed at temperatures ranging from 150°C-400°C, at low weight hourly space velocities (WHSV) and at pressures of 2 bar to 5 bar with argon or hydrogen as carrier gas.

Results showed that double-bond isomerisation, and oligomerisation, with some skeletal isomerisation and cracking, were the main reactions at the lower end (up to 270°C) of the temperature range studied. At higher temperatures, aromatics (BTX+ EB as well as higher aromatics) were the main products. Carbon of graphitic nature was formed at the highest temperature (400°C).

The major changes resulting from an increase in WHSV were a decrease in BTX+EB and an increase in higher aromatics. The nature of the carbon content on the spent catalyst could be shifted from graphitic to aromatic by increasing the WHSV.

Increasing the pressure with hydrogen as carrier gas resulted in a significantly lower aromatics content (especially the higher aromatics), while light products (C_2-C_4) and paraffins were increased.

The reaction pathway indicated by the experiments is:

Double-bond isomerisation ⟶ Oligomerisation ⟶

Cracking + Skeletal isomerisation ⟶ Cyclisation ⟶ Aromatisation.

Table of contents

List of tables

Chapter 1

Chapter 2

Chapter 3

Appendix IV

List of figures

Chapter 1

Chapter 2

Chapter 3

Chapter 4

Introduction

The original objective of this dissertation was to investigate the skeletal isomerisation of n-pentenes over H-mordenite, Pt/H-mordenite and H-ZSM-5. Several factors contributed to the actual experiments being performed using only H-ZSM-5 as catalyst. Since H-ZSM-5 is a medium pore zeolite known to catalyse a wide range of reactions including aromatisation, the focus of this study was no longer restricted to skeletal isomerisation only.

Chapter 1 Literature Review

1.1 ZSM-5

1.1.1 Zeolites

The word "zeolite" is derived from the Greek "zeo" (to boil) and "lithos" (stone). Cronstedt gave the name "zeolites" to materials which began bubbling on strong heating (Roland and Kleinschmidt, 1998).

Zeolites are molecular sieves with an oxide framework of aluminium and silicon (Thomas and Thomas, 1997) (Figure 1.1). These framework silicates are built from interlocking tetrahedrons of SiO_4^{4-} and AlO_4^{5-}. The definition of zeolites is usually given as crystalline, hydrated aluminosilicates with a framework structure (Roland and Kleinschmidt, 1998). In general, the term "zeolite" is broadly used for any microporous material with cages and/or channels of molecular dimension (3 to 10 Å diameter) and which is capable of accommodating water and other molecules in its intracrystallite spaces.

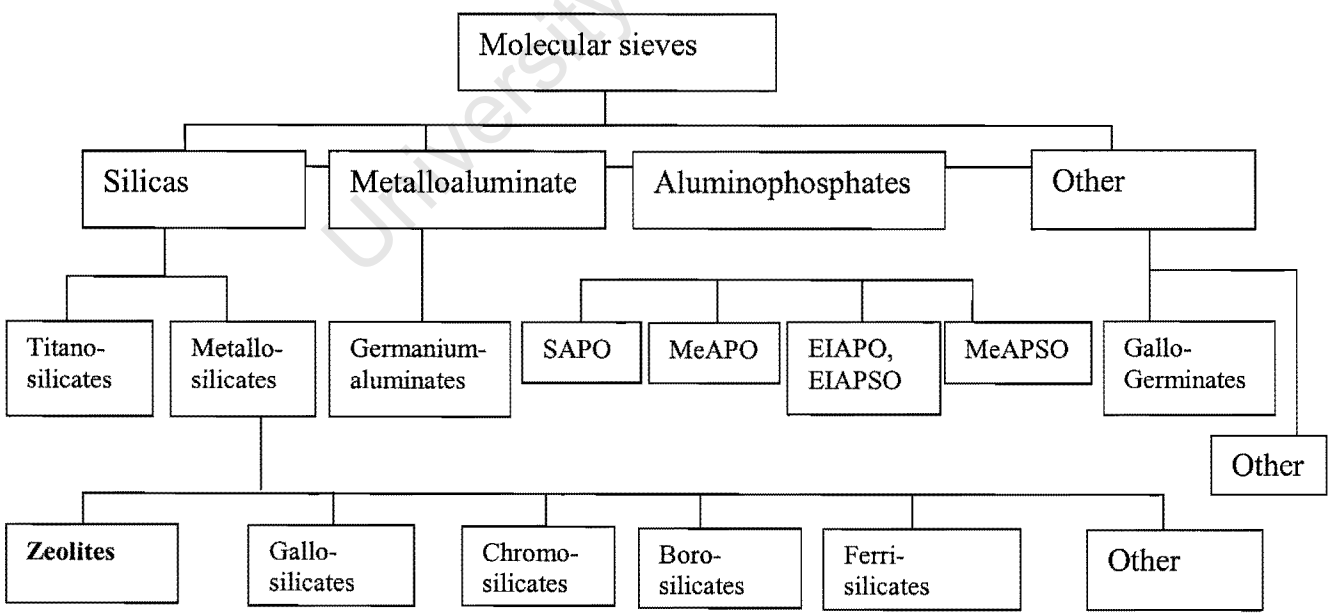

Figure 1.1 Family of molecular sieves

The specific characteristics of zeolites can be attributed to their pore size. The shape selectivity observed when using zeolites as catalysts can be classified as: reactant, product, or transition state selectivity. The shape selective effects are categorised according to whether the pore size limits a) the entrance of the reactant molecule, b) the product molecule exiting or c) the formation of the required transition state (Jacobs and Martens, 1991, Chen et al., 1989, Csicsery, 1985.):

a) Reactant selectivity occurs when the zeolite acts as a molecular sieve to exclude some reactant molecules from the intracrystalline voids based on the size and structure of the reactant molecule. Only reactant molecules that are small enough will diffuse through the catalyst pores (Figure 1.2).

b) Product selectivity arises due to discrete diffusivities of the reaction products in the pores of the zeolite crystals. Only molecules with the proper shape and size can pass through the zeolite channels as products. Products that are too bulky are either converted to less bulky molecules or eventually cause catalyst deactivation by blocking the pores (Figure 1.3).

c) Transition state selectivity (spatiospecific selectivity) is found when the spatial configuration around a transition state located in the intracrystalline volume is such that only certain configurations are possible. Certain reactions are prevented since the transition states required are too big for the pores. Spatiospecific selectivity could be one of the most important properties of ZSM-5. Transition state selectivity is independent of crystal size and activity but depends on pore diameter and zeolite type (Chen et al., 1989) (Figure 1.4).

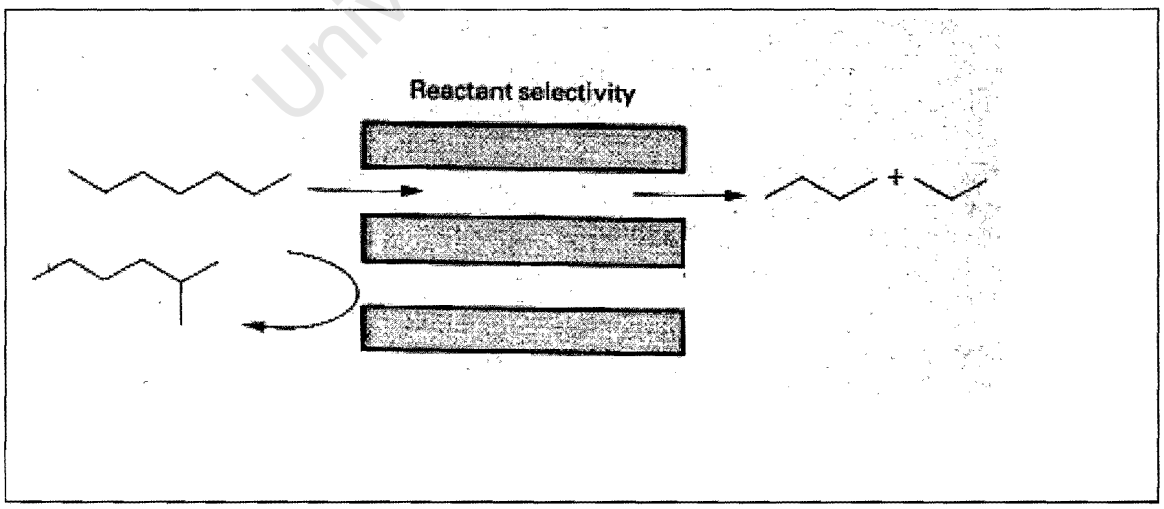

Figure 1.2 Reactant shape selectivity (from Csicsery, S.M., 1985)

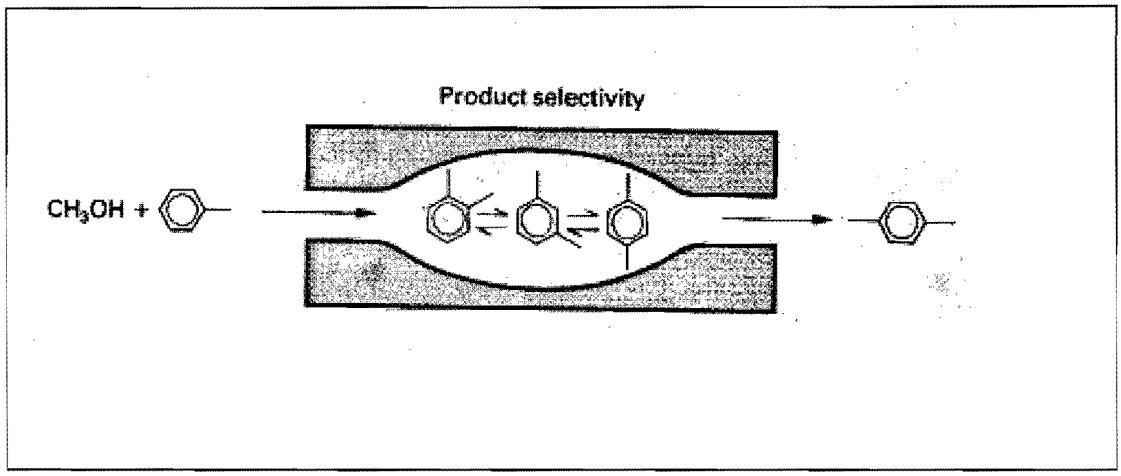

Figure 1.3 Product shape selectivity (from Csicsery, S.M., 1985)

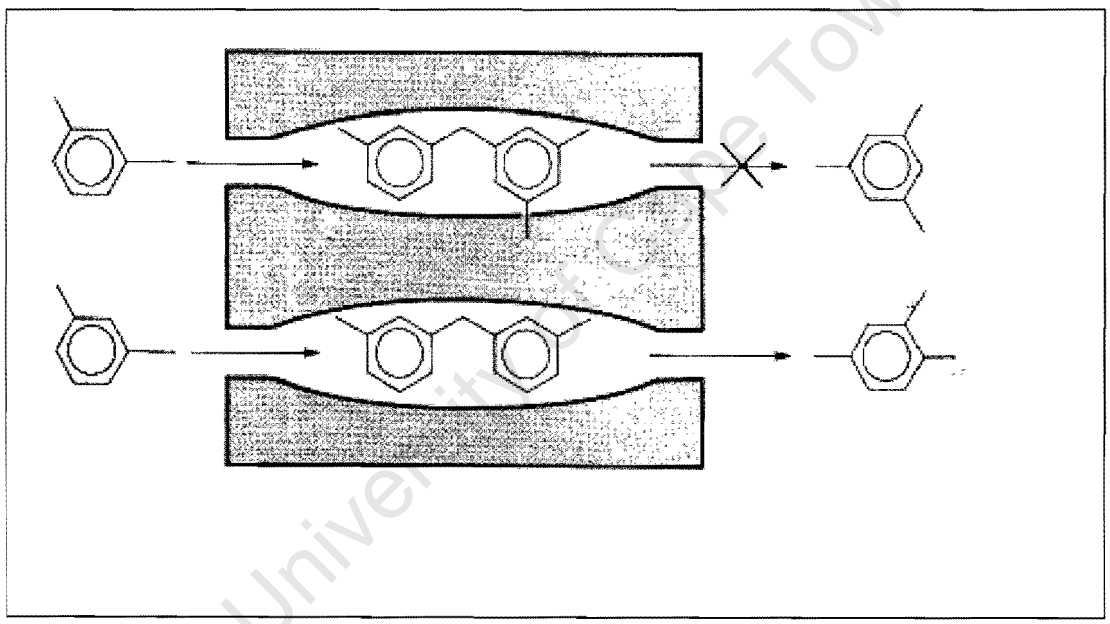

Figure 1.4 Restricted transition state selectivity (from Csicsery, S.M., 1985)

1.1.2 Structure and properties of ZSM-5

ZSM-5 is a synthetic zeolite, which does not have a naturally occurring mineral analogue (Thomas et al., 1997). The acronym ZSM stands for Zeolite Socony Mobil, indicating the laboratory in which it was first synthesised. ZSM-5 represents a family of zeolites of the MFI structure type, which have a wide range of variation of the SiO_2/Al_2O_3 ratio (about 5-∞) (Roland and Kleinschmidt, 1998). ZSM-5 is represented by the formula $Na_n[Al_nSi_{96-n}O_{192}]$~16 H_2O, with n<27.

Material of this formula crystallises with orthorhombic symmetry, space group Pnma. (Thomas et al., 1997). Cell parameters are: a=20.090 Å , b=19.738 Å, and c=13.142 Å, alpha = 90°, beta = 90°, gamma = 90° and volume = 5211.13 $Å^3$. The framework density (FD) is 17.9 T atoms/1000 $Å^3$ (i.e. number of tetrahedral atoms per 1 nm^3), with FD_{Si} = 18.4 T/1000 $Å^3$ (Meier and Olsen, 1992).

ZSM-5 has a two-dimensional structure consisting of two intersecting 10-membered rings: a straight channel of pore size 5.3 x 5.6 [010] and a sinusoidal channel of pore size 5.1 x 5.5 [100]. The third dimension arises from the intersection cavities (ca. 9 Å), although these intersections do not form a third channel. The structure viewed along [010] is shown in Figure 1.5.

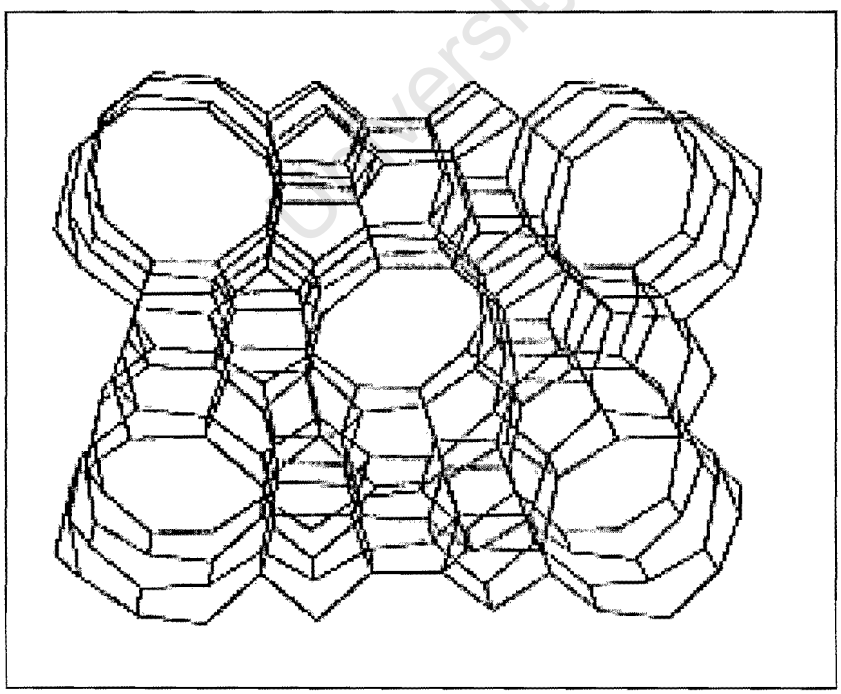

Figure 1.5 MFI framework viewed along [010] (Meier and Olson, 1992)

The acidity of ZSM-5 can be altered by substituting Al^{3+} in the place of the tetrahedral Si^{4+}, which requires additional positive charge to compensate for the resulting negative charge. When the additional positive charge is obtained by H^+, Brønsted acid sites are created. It is the acidity of the H-ZSM-5 that gives rise to its catalytic activity in acid based reactions.

A Brønsted acid is a substance capable of donating a proton, while a Lewis acid is a substance capable of accepting an electron pair to form a covalent bond (Morrison and Boyd, 1987). When zeolites are transformed into the hydrogen form, they are solid acids capable of showing both Brønsted and Lewis acidity. Brønsted acid sites are protons attached to framework oxygen atoms (bridging hydroxyl groups between two cations). One acidic hydrogen can be accommodated for every tetrahedrally bonded aluminium in the zeolite (Figure 1.6). Brønsted acid sites are transformed to Lewis acid sites upon removal of water by heating, e.g. dehydration during calcination of a zeolite (Figure 1.7).

Dealumination is not normally used to increase the SiO_2/Al_2O_3 ratio of zeolites, as with other zeolites, e.g. mordenite, since it can be obtained directly as a high-silica molecular sieve by hydrothermal synthesis (Roland and Kleinschmidt, 1998).

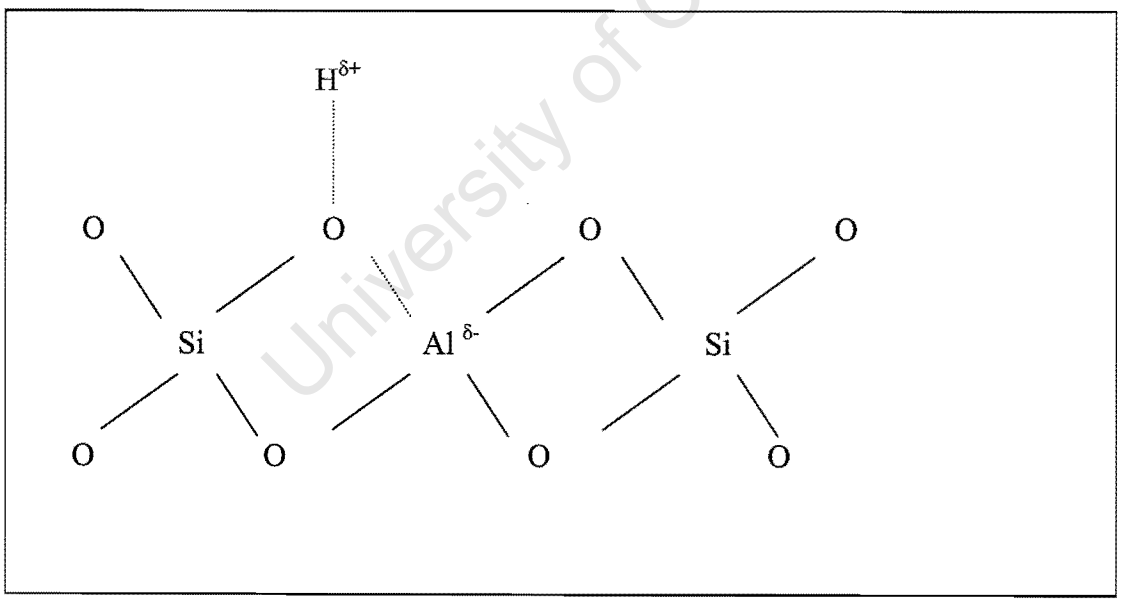

Figure 1.6 Brønsted acid site (Thomas and Thomas, 1997)

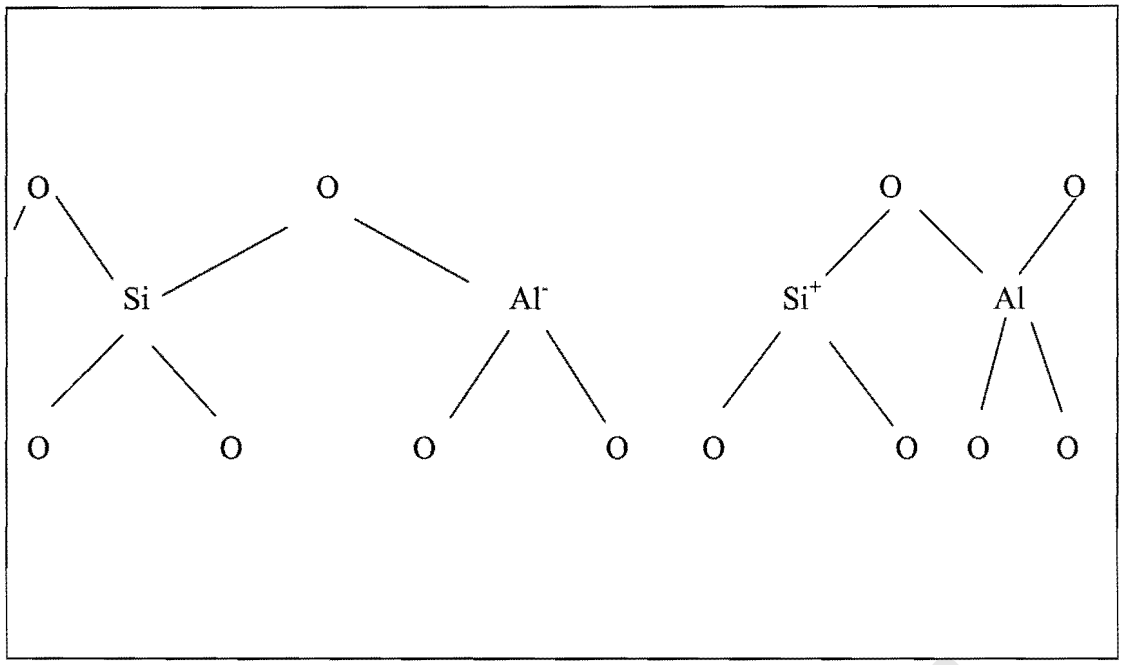

Figure 1.7 Lewis acid site (From Humphries et al., 1993)

The build-up of coke, a carbonaceous deposit on the inside and outside of zeolite crystals, is mostly an unwanted side reaction that takes place during the conversion of hydrocarbons over zeolites. ZSM-5 and other second-generation shape selective catalysts (e.g. theta-1) show a much reduced rate of coking compared to other zeolites due to restricted transition-state selectivity. The pore system of ZSM-5 reduces the formation of bulky, coke precursor species such as naphtalenes and other polynuclear aromatics inside the pores (Thomas and Thomas, 1997).

1.1.3 Industrial use

Zeolites only became of industrial importance in the 1950's, with the availability of synthetic samples on industrial scale (Roland and Kleinschmidt, 1998). Zeolites as catalysts currently have a major share in the petroleum refining market segment. Other applications are found in the chemical processing and emission control markets (SRI report, 1996).

ZSM-5 is the preferred octane enhancing additive in fluid catalytic cracking (FCC) catalysts (Horsley and Derouane, 1995). Other petrochemical applications of ZSM-5 include: synthesis of petrol (gasoline) from methanol (MTG process), alkylation of mono-nuclear aromatic hydrocarbons and their derivatives, ethylbenzene production, hydrocracking,

isomerisation of xylenes, toluene disproportionation, transalkylation of toluene, aromatisation of LPG, production of para-substituted aromatic compounds, isomerisation of C_5/C_6 n-alkanes and dewaxing of distillates and lubricants (SRI report, 1996, Horsley and Derouane, 1995, Thomas et al., 1997).

1.2 Isomerisation

Isomerisation reactions of olefins (mono-alkenes) can be classified into five types, with different ease of reaction. The types are listed in Table 1.1 below, in order of difficulty of reaction (Condon, 1958).

Table 1.1 Classification of isomerisation reactions

Classification	Description	Example
Type I	cis-trans isomerisation	cis-2-butene to t-2-butene without formation of 1-butene
Type II	double bond shift at a chain branch	interconversion of 2,4,4-trimethylpentenes
Type III	double bond shift in a linear chain	1-butene to 2-butenes, without isobutylene formation
Type IV	skeletal isomerisation without change in maximum chain length	interconversion of dimethylbutenes
Type V	skeletal isomerisation with change in maximum chain length	straight chain to branched chain

For the purposes of this discussion, the focus will be on double bond isomerisation and skeletal isomerisation .

1.2.1 Double-bond isomerisation

In the context of linear olefins, double-bond isomerisation refers to the conversion of alpha olefins to internal olefins without structural change, e.g. the conversion of 1-olefins to 2-olefins (Brooks, 1955). Industrially, double-bond isomerisation is an unwanted side-reaction which converts high-value alpha-olefins (1-olefins) to internal olefins. One process where double-bond isomerisation is required, is the Shell higher olefin process (SHOP).

The double-bond shift takes place readily due to the higher stability of the internal olefins. The stability of the alkene increases with increasing number of alkyl groups attached to the double bond. The stability of alkenes is:

$R_2C{=}CR_2 > R_2C{=}CHR > R_2C{=}CH_2$, $RHC{=}CHR > RHC{=}CH_2 > H_2C{=}CH_2$.

Thus 2-pentenes (RHC=CHR) are more stable than 1-pentene ($RHC{=}CH_2$). Of the 2-pentene isomers, trans-2-pentene is most stable. The heats of hydrogenation indicate the relative stabilities of the isomers 1-pentene (125.9 kJ/mol), c-2-pentene (119.7 kJ/mol) and t-2-pentene (115.5 kJ/mol kJ/mol) (Morrison and Boyd, 1987).

1.2.1.1 Mechanism of double-bond isomerisation (Type III)

As in the case of other acid-catalysed reactions, isomerisation of n-pentenes proceeds via a carbocation intermediate (Oblad et al., 1947). In the case of alkenes, the carbocation (carbenium ion) is formed by addition of a proton from the acid catalyst (Figure 1.8). If the reactant molecule is an alkane, either a combination of dehydrogenation and proton addition, or abstraction of a hydride ion, leads to the formation of a carbocation (Sie, 1997).

Carbocation rearrangement takes place so that a more stable carbocation is formed. The relative stabilities of carbocations is: tertiary > secondary > primary. This rearrangement takes place via a 1,2-hydride shift (Figure 1.9). A hydride shift is the migration of a hydrogen atom with a pair of electrons from an adjacent carbon to the carbon with the positive charge. The carbon losing the migrating group then acquires the positive charge (Morrison and Boyd, 1987).

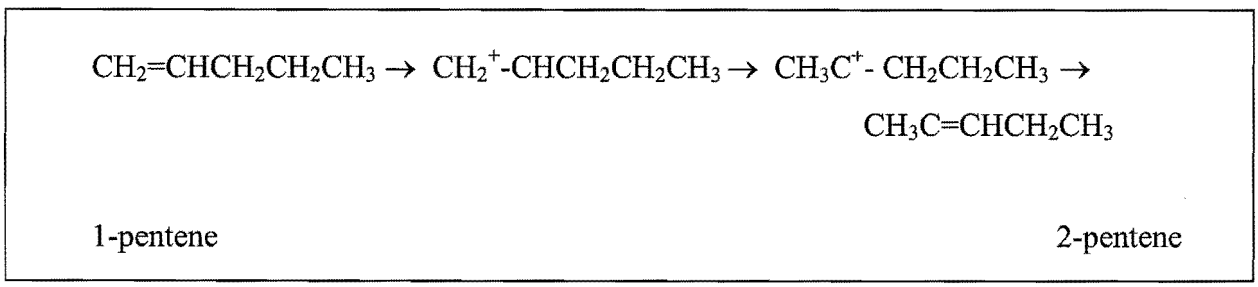

Figure 1.8 Mechanism of pentene double-bond isomerisation

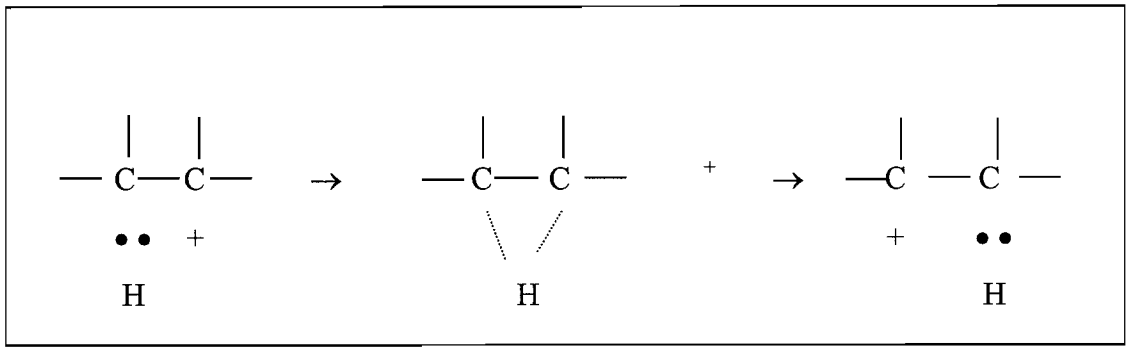

Figure 1.9 1,2-hydride shift

Thermodynamics for double-bond isomerisation of 1-pentene to t-2-pentene, for example, in the temperature range 150°C- 450°C range from –11.8 to -8.8 kJ/mol ΔH and -12.5 to -10.1 kJ/mol ΔG (HSC Chemistry Ver. 2.03). Thermodynamic tables are in Appendix I.

1.2.2 Skeletal isomerisation

Skeletal isomerisation (or structural isomerisation) of aliphatic compounds involves the rearrangement of the carbon skeleton by the breaking and formation of C-C single bonds (Hölderich and van Bekkum, 1991). Thus branched olefins are formed from straight-chain olefins. Branched olefins are important as feedstock for the formation of ethers, e.g. methyl-t-butyl-ether (MTBE) from isobutene and tertiary-amyl-methyl-ether (TAME) from isopentenes. These ethers are used to increase the octane of unleaded petrol. The research octane numbers (RON) of MTBE and TAME are 118 and 112, respectively. The use of MTBE is declining due to environmental concerns, as it is water-soluble. As mentioned in Section 1.2, two types of skeletal isomerisation are distinguished. The interconversion of the branched pentene isomers leaves the maximum chain length unchanged (type IV), while the conversion of n-pentenes to iso-pentenes involves a change in maximum chain length (type V).

1.2.2.1 Mechanism for the interconversion of iso-olefins (Type IV)

The interconversion of branched olefins can be seen as a 1,2-methyl shift (Figure 1.10; R represents an alkyl group) similar to the 1,2-hydride-shift in Figure 1.9.

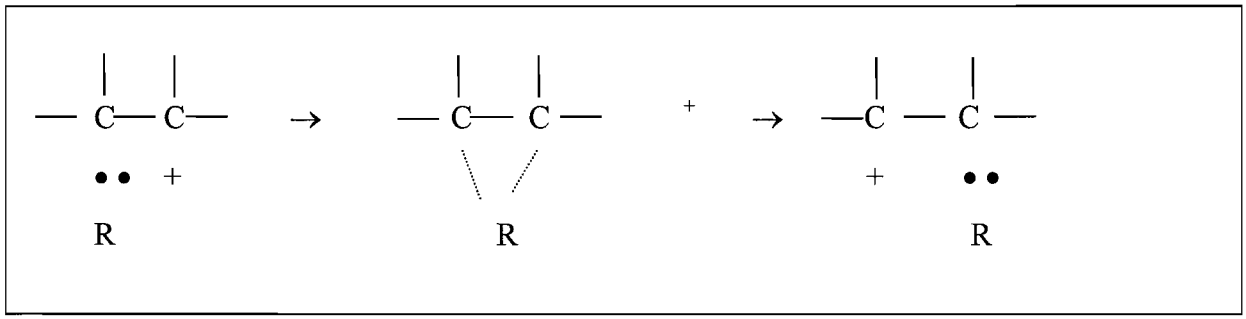

Figure 1.10 1,2-alkyl shift

The mechanism of this type of isomerisation involves 1,2-hydride shifts and a protonated cyclopropane (PCP) intermediate, as illustrated in Figure 1.11 (Jacobs and Martens, 1991).

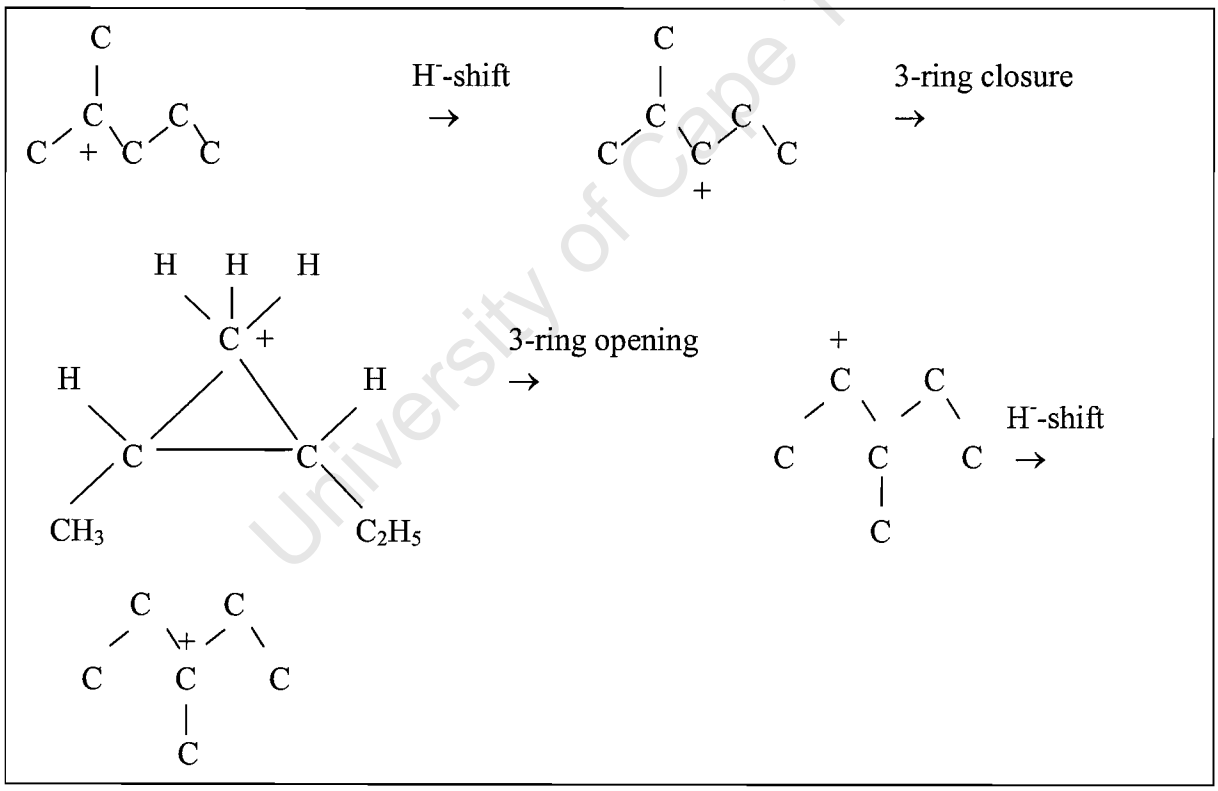

Figure 1.11 Isomerisation of 2-methyl-2-pentyl cation to 3-methyl-3-pentyl cation (Jacobs and Martens, 1991)

1.2.2.2 Mechanism for the conversion of n-pentenes to iso-pentenes (Type V)

The mechanism for isomerisation of normal olefins involves carbonium ions. It is likely that the skeletal isomerisation mechanism involves rearrangement of the classical secondary carbenium ion into a non-classical ion, namely a protonated dialkylcyclopropane (Sie, 1997, Höchtl et al., 2001). Alkanes and alkenes follow the same mechanism, the only difference being that with alkenes the hydrogenation/dehydrogenation step is not necessary. Transformation of the classical secondary carbenium ion will not involve a high energy barrier since it can be considered to be a hybrid of resonance structures. This resonance will contribute to the stability of the cyclopropane species and will compensate for the inherent strain of the three-membered ring (Sie, 1997). The carbon with the positive charge reacts with the carbon in the beta position to form the ring. At the same time, the H-atom on the beta carbon becomes a proton, which can move around the ring via the sides and edges. This mechanism is depicted in Figure 1.12. The difference in mechanism between (iv) and (v) is the additional step in (v) in which corner-to-corner jump of a proton on the cyclopropane ring takes place (Jacobs and Martens, 1991).

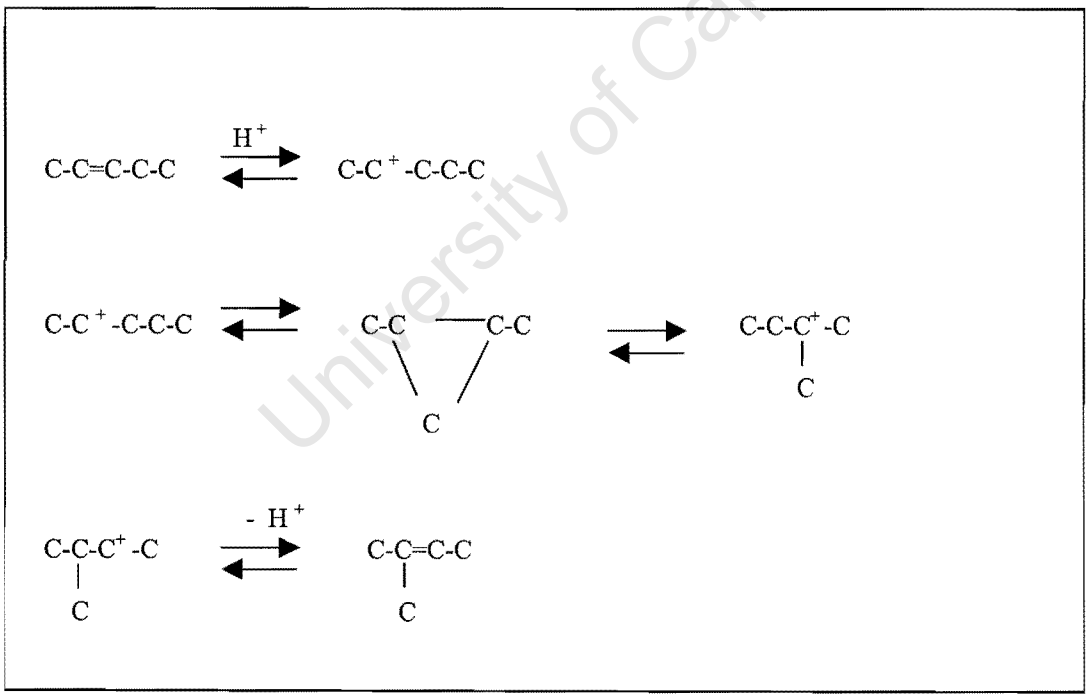

Figure 1.12 Mechanism for skeletal isomerisation of n-pentenes

Thermodynamics for skeletal isomerisation of 1-pentene to 2-methyl-1-butene, for example, in the temperature range 150°C- 450°C range from –15.7 to –15. 3 kJ/mol ΔH and –14.1 to -13.1 kJ/mol ΔG (HSC Chemistry Ver. 2.03). Thermodynamic tables are in Appendix I.

1.3 Oligomerisation

One of the addition reactions that alkenes can undergo is the addition of another alkene. (Morrison and Boyd, 1987). Polymerisation is the repeated addition of simple molecules (monomers) to form molecules with a high molecular weight, e.g. the repeated addition of ethylene molecules to give polyethylene. Oligomerisation generally refers to the addition of only a few monomers (Shaheen, 1983).

When two of the same alkenes are added and the product contains exactly twice the number of carbon and hydrogen atoms as the reactant molecule, the products are known as dimers. The reaction is called dimerisation. The formation of dimers is favoured at low temperature (Horsley, 1993).

1.3.1 Mechanism

Oligomerisation can be catalysed by acids. The mechanism of oligomerisation follows three basic steps: initiation, propagation and termination. The mechanism will be discussed using the dimerisation of isobutylene as example (see Figure 1.13) (Morrison and Boyd, 1987).

The first step is the protonation of the double bond to form a carbocation, with preference for the tertiary carbocation, which is most stable. In the second step, addition of the tert-butyl cation to a molecule of isobutylene takes place in such a way that the most stable tertiary cation is formed. The electron-rich carbon-carbon double bond completes the octet of the positively charged carbon atom. Depending on the reaction conditions, the third step can either lead to termination of the reaction, or further addition of another isobutylene molecule can take place. In the case of dimerisation, the carbocation loses a hydrogen ion yielding a dimer.

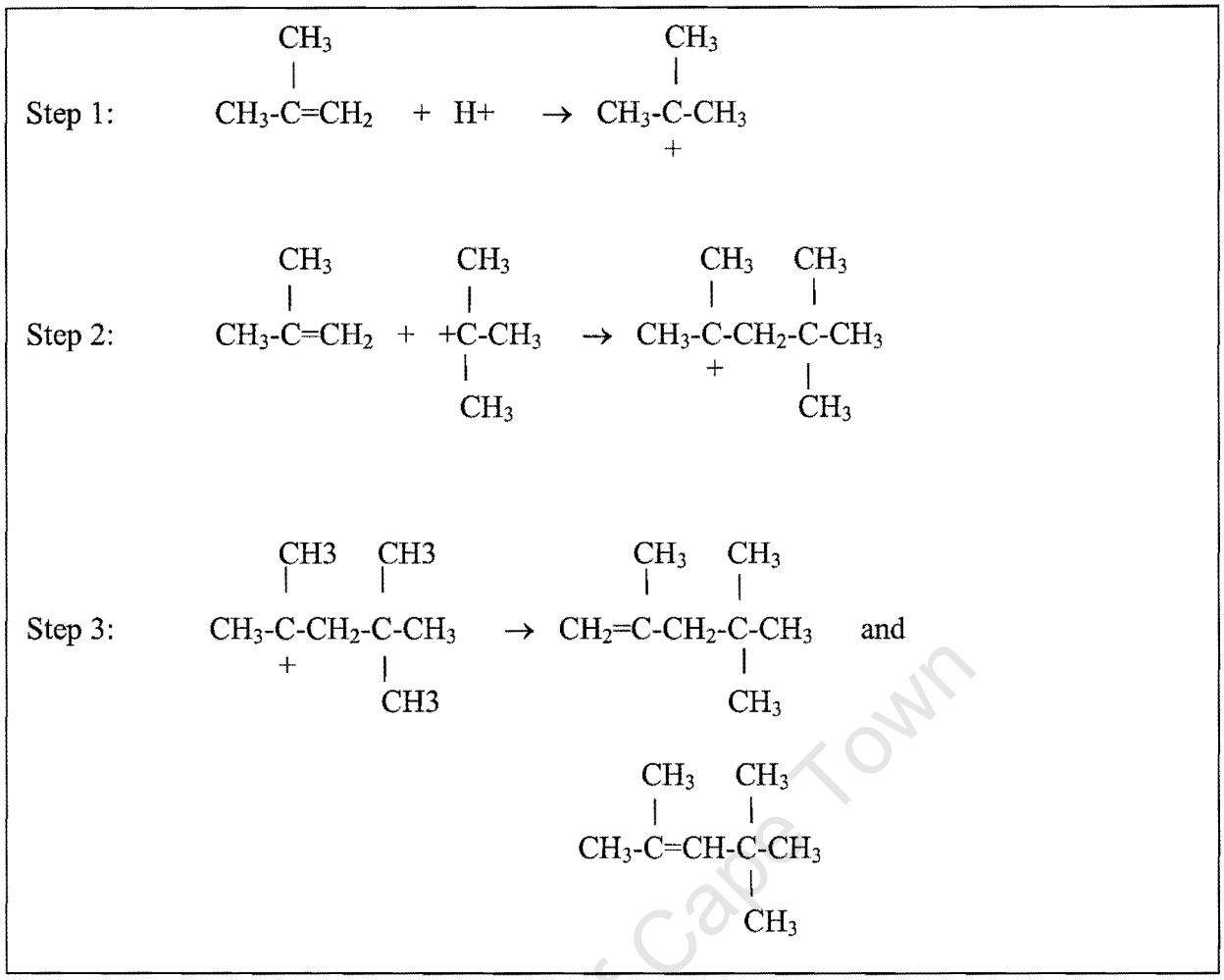

Figure 1.13 Dimerisation of isobutylene

The following steps were observed in a fast FTIR study of the oligomerisation of propylene with ZSM-5: (Thomas and Thomas, 1997)

(1) interaction of the alkene with Brønsted acid sites (the bridging hydroxyls) to form short-lived hydrogen bonded precursors

(2) protonation (rate-determining step)

(3) chain growth.

These steps are depicted in Figure 1.14.

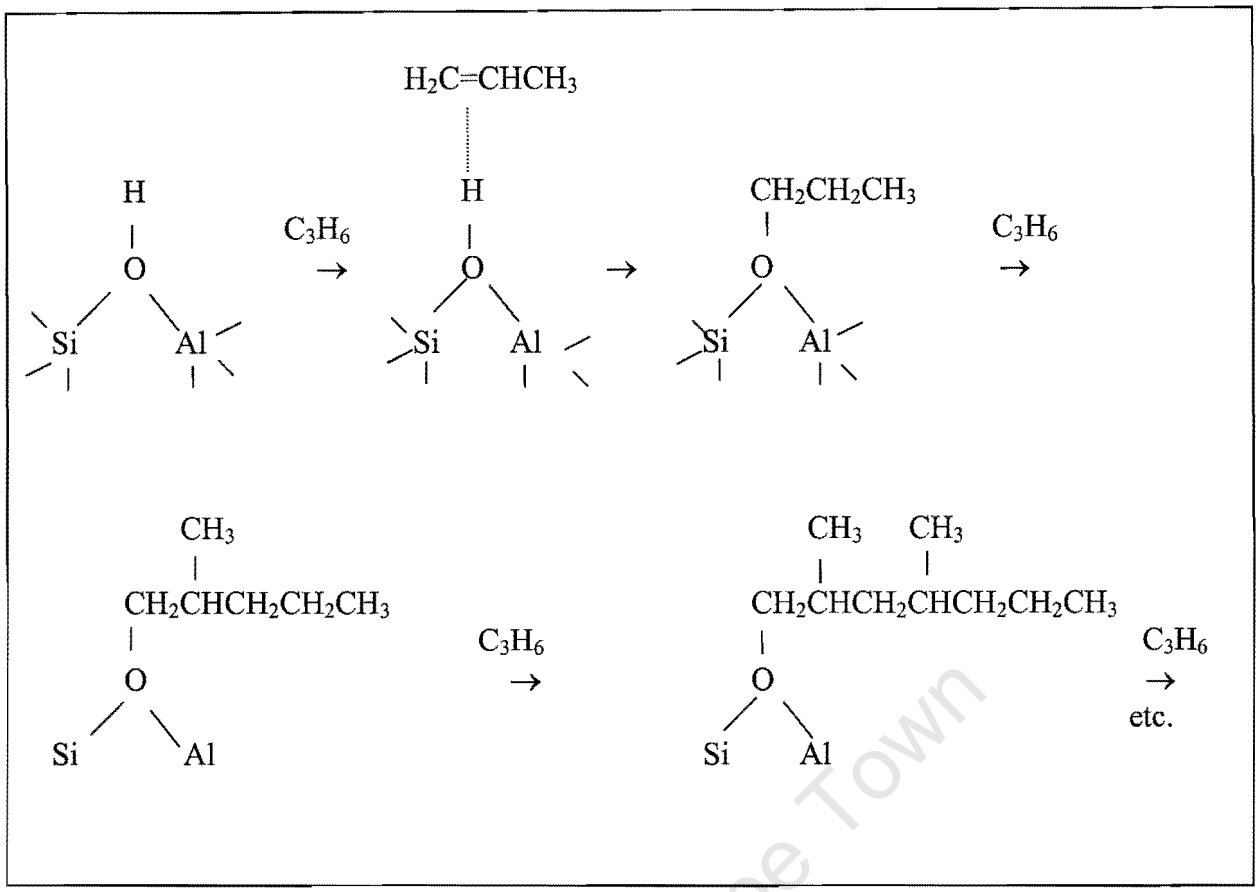

Figure 1.14 Oligomerisation of propylene

Thermodynamics for dimerisation of t-2-pentene to 1-decene, for example, in the temperature range 150°C- 450°C range from -57.6 to -53. 7 kJ/mol ΔH and 0.9 to 41.3 kJ/mol ΔG (HSC Chemistry Ver. 2.03). Thermodynamic tables are in Appendix I.

1.4 Cracking

Cracking is the breaking of carbon-carbon bonds to obtain molecules with a shorter chain–length. There are three major cracking processes: Thermal cracking, catalytic cracking and hydrocracking (Shaheen, 1983).

Thermal cracking, where alkanes are passed through a chamber heated to a high temperature, yields predominantly ethylene and some other small molecules.

Steam cracking is a modification of thermal cracking. In steam cracking the hydrocarbon feed is diluted with steam, heated for a fraction of a second to 700-900°C, and rapidly cooled.

The products, including ethylene, propylene, butadiene, isoprene and cyclopentadiene, are used mainly as chemicals.

Hydrocracking is carried out in the presence of a catalyst and hydrogen at high pressure and temperature of 250-450°C. The products are smaller hydrocarbons. Hydrocracking is used for the production of fuels.

In the process of catalytic cracking, high-molecular-weight molecules in gas oils (which cannot be directly reformed) are broken down to low-molecular-weight molecules, which can be blended with reformer products (Thomas and Thomas, 1997). Besides improving the yield of gasoline by cleavage of the large molecules, alkanes and alkenes with the highly branched structures desired in gasoline, are obtained (Morrison and Boyd, 1987).

1.4.1 Mechanism of catalytic cracking

Hydrocarbon cracking over solid acid catalysts involves several reactions. Primary reactions, such as paraffin cracking to olefins and smaller paraffins, olefin cracking to smaller olefins, dealkylation of alkyl aromatics, and cracking of cycloparaffins to olefins can take place. Secondary reactions include olefin oligomerisation, transalkylation of alkyl aromatics, and hydrogen transfer.

The classical, generally accepted mechanism for catalytic cracking involves carbenium ion formation, olefin adsorption/desorption steps, isomerisation, rupture of the carbon-carbon bond in a secondary position to the charge (ß-scission) and hydride ion transfer. Oligomerisation can take place prior to beta-scission if the substrate is a C_2 or C_3 hydrocarbon (Cortright et al., 1997, Thomas and Thomas, 1997, Jacobs and Martens, 1991, von Ballmoos et al., 1997).

In the case of a secondary carbenium ion formed from a straight carbon chain, there are however energetic considerations from which beta scission seems unlikely. This has led to the proposal of another mechanism. In this mechanism a non-classical carbonium ion, namely a protonated dialkyl cyclopropane species, is assumed to be the reaction intermediate in acid catalysed cracking. Cracking will occur if the hydrocarbon has seven or more

carbons. This is determined by energetic considerations, dictating that C-H dissociation in primary carbon atoms will be avoided (Sie, 1997; Sie, 1992; Condon, 1958) (Figure 1.15).

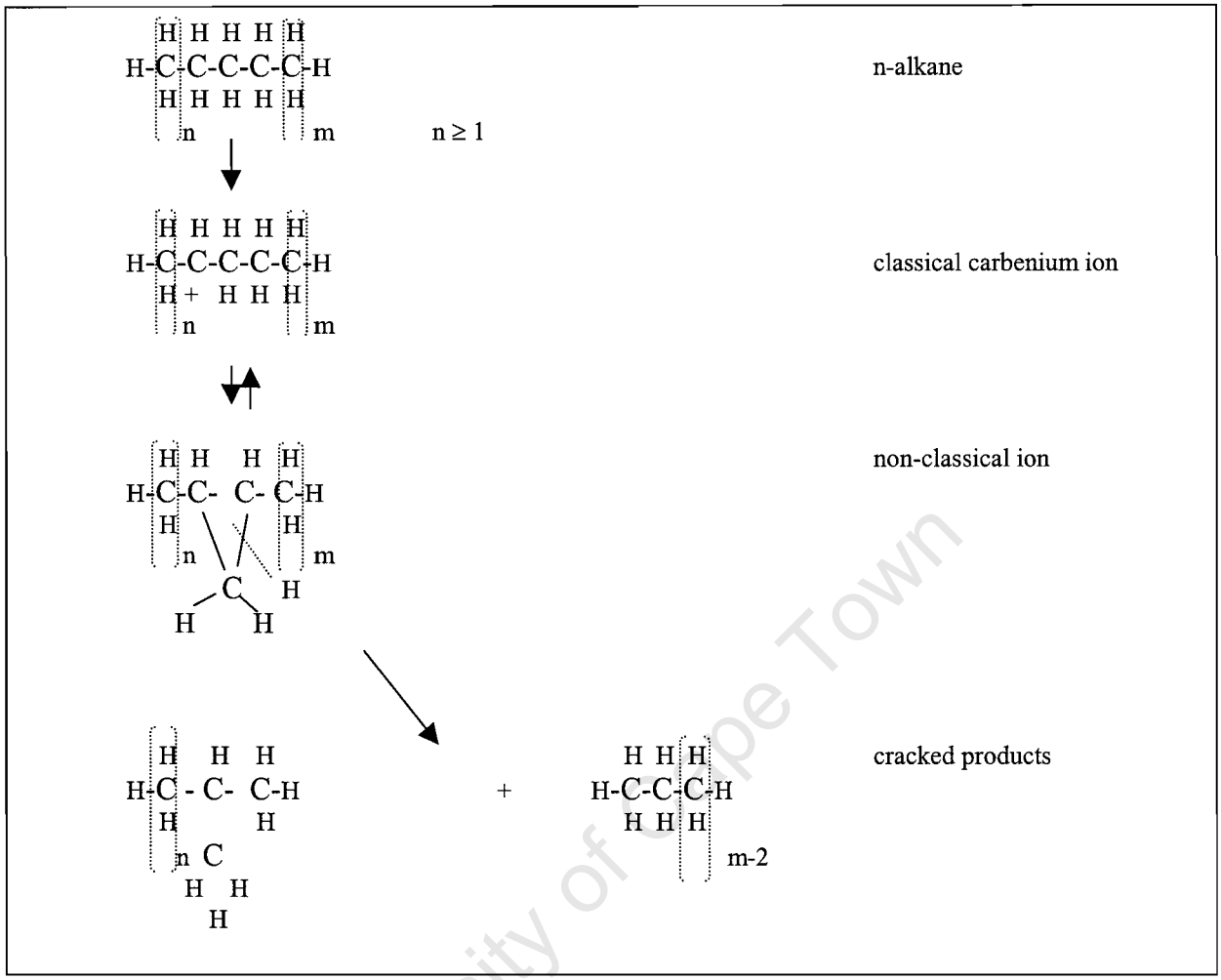

Figure 1.15 Cracking mechanism with protonated cyclopropane (PCP) species as intermediate

Thermodynamics for cracking of 1-decene to 2-methyl-1-butene, for example, in the temperature range 150°C- 450°C range from 49.8 to 48.1 kJ/mol ΔH and -8.8 to -49.91 kJ/mol Δ G (HSC Chemistry Ver. 2.03). Thermodynamic tables are in Appendix I.

1.5 Aromatisation

Aromatic compounds contain cyclic clouds of delocalised π-electrons above and below the plane of the molecule. The number of electrons in the pi-clouds must follow the Hückel-rule, i.e. contain a total of (4n+2) π-electrons (Morrison and Boyd, 1987). Aromatisation is the conversion of non-aromatic hydrocarbons into aromatic hydrocarbons. Three of the major reactions in catalytic reforming are aromatisation reactions: (i) dehydrogenation of cyclohexanes to aromatics, (ii) dehydroisomerisation of alkylcyclopentanes to aromatics, and (iii) dehydrocyclisation of alkanes to aromatics (Sinfelt, 1997). Light aromatics are used as feedstock for a wide variety of petrochemicals. Benzene, toluene and xylenes (the BTX aromatics) are also important components to increase the octane of petrol (O'Connor, 1997). Strict environmental legislation poses a limit on the use of aromatics in petrol, especially benzene. The South African limit for benzene in petrol is currently (2000) 1%, while total aromatics may amount to about 30% (Personal communication with Sasol Oil Research and Development).

Aromatisation catalysts can be divided into three groups, namely non-acidic catalysts, acidic catalysts, and bifunctional catalysts. An example of non-acidic catalysts is PtBa/KL, which contains highly dispersed platinum clusters in barium-exchanged potassium zeolite L. The aromatisation properties of this catalyst are attributed to a combination of the platinum clusters and the shape-selective properties of the zeolite (Maxwell and Stork, 1991).

H-ZSM-5 is used as an acidic catalyst for aromatisation. The restricted transition-state selectivity of the catalyst inhibits alkene polymerisation and thereby coke formation. (Horsley and Derouane, 1995). The hydrogen transfer properties of H-ZSM-5 facilitate aromatisation (Nash, 1994). In bi-functional catalysts the metal hydrogenation/ dehydrogenation function is combined with a catalyst that has acidic properties, e.g. Ga/HZSM-5 and Pt/HZSM-5.

1.5.1 Mechanism of aromatisation

The mechanism of aromatisation depends on the type of catalyst employed. The mechanisms for all three types of catalysts mentioned above will be discussed.

1.5.2 Aromatisation mechanism over acid catalysts

The net reaction converts alkenes into alkanes and naphtenes (cyclic alkanes) into aromatics. The first step is the formation of a carbenium ion. After cyclisation of the carbenium ion, β-elimination (elimination of H^+ in a beta position to the positive charge) and/or hydride transfer reactions can follow to form an aromatic compound (Figure 1.16). The R^+ species are derived from the addition of alkenes to the proton acid sites (Santilli and Gates, 1997).

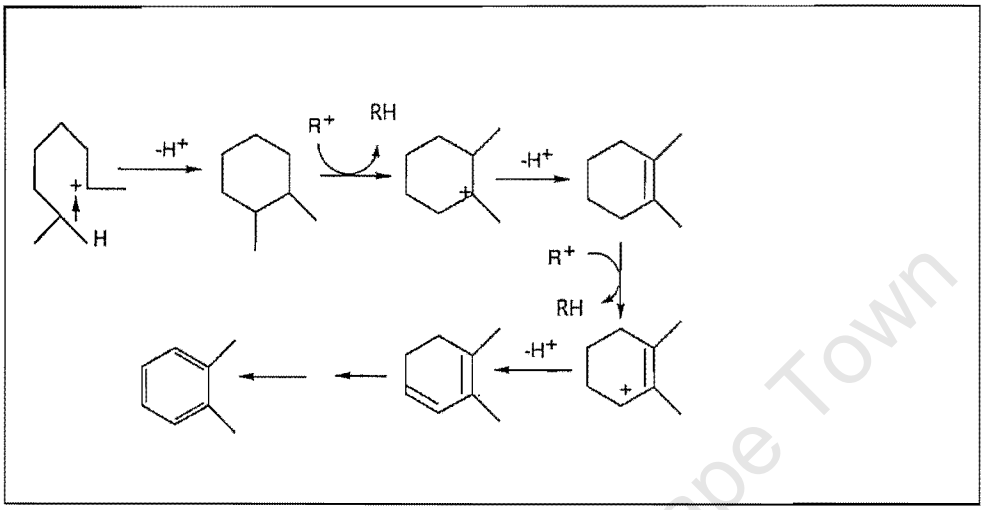

Figure 1.16 Aromatisation mechanism over an acid catalyst

1.5.3 Aromatisation mechanism : Bifunctional catalyst Ga/HZSM-5

In the bifunctional catalyst, there is the added dehydrogenation/hydrogenation function of the metal to be taken into consideration. A proposed mechanism for the aromatisation of propane is presented in Figure 1.17.

In the first step, propane is activated by transformation to propene via a $C_3H_7^+$ carbenium ion on the gallium sites.

In the second step, a pool of intermediate C_2-C_8 alkenes is expected. Oligomerisation of C_2-C_5 alkenes can lead to formation of dimers and trimers. Decomposition of the protonated pseudocyclopropane intermediate leads to the formation of carbenium ions CH_3^+, $C_2H_5^+$, and $C_3H_7^+$, which can react with alkanes and alkenes. Molecular dihydrogen is released via the Ga^{3+}, O^{2-} pair.

In the third step, dehydrogenation of the C_6-C_8 aliphatics on the gallium sites can lead to formation of diolefins. Cyclisation of the diolefins on protonic sites form naphtenes. Further dehydrogenation on the gallium sites leads to the formation of aromatics.

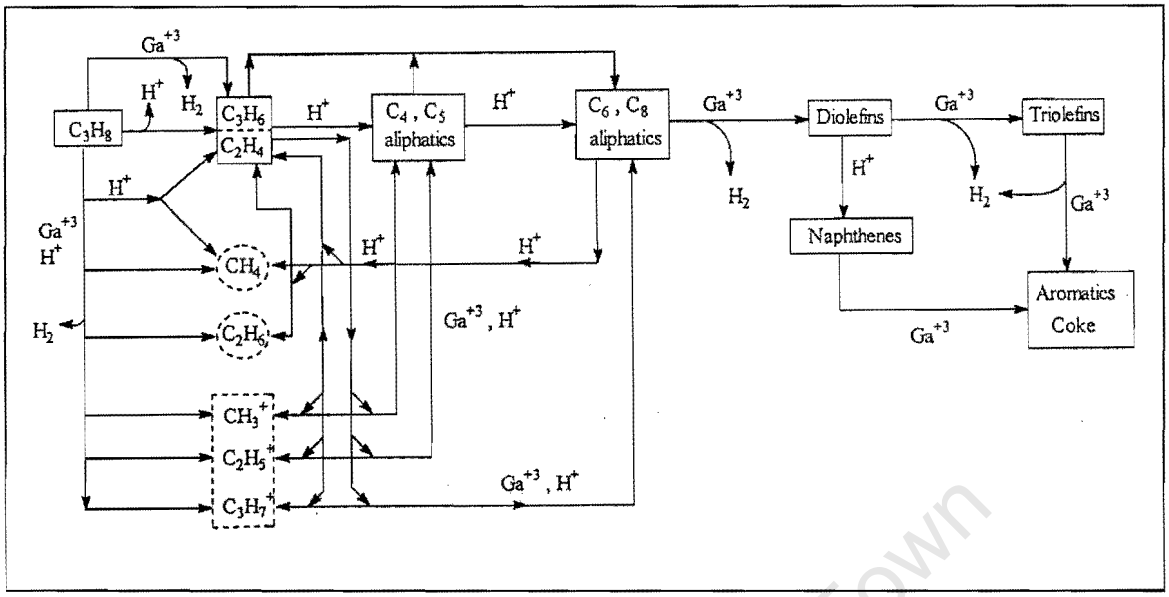

Figure 1.17 Proposed mechanism for propane aromatisation over Ga/HZSM-5 (O'Connor, 1997)

1.5.4 Aromatisation mechanism over non-acidic catalysts

In mono-functional metal catalysts, such as platinum on the non-acidic support BaK/L, dehydrocyclisation is catalysed by the platinum alone (Tamm, et al., 1988). Over platinum on a non-acidic support, the preferred route for aromatisation of alkanes with six or more carbon atoms in a straight chain, is direct 1,6-ring closure. Ring closure is followed by rapid dehydrogenation to form the aromatic compound (Derouane and Vanderveken, 1988, Tamm et al., 1988). Ring formation by 1,5-closure requires ring enlargement of the C_5-ring to a C_6-ring, a reaction which is generally slower over a monofunctional metal catalyst than a bifunctional catalyst containing metal and acid sites (Mériaudeau and Naccache, 1997). The reaction network for hexane aromatisation with AROMAX™ catalyst is represented in Figure 1.18.

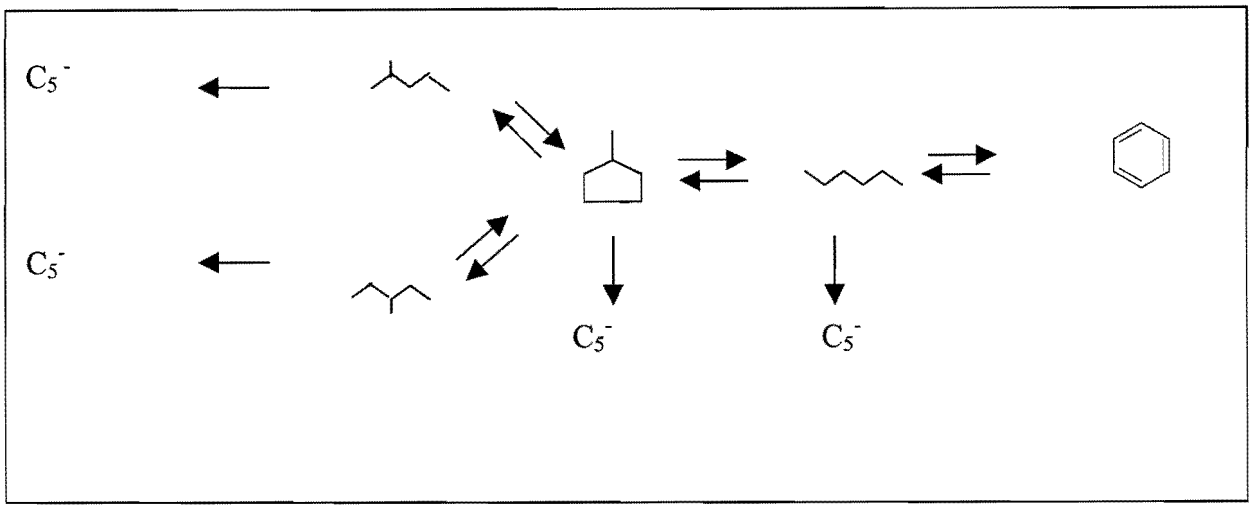

Figure 1.18 Reaction network for hexane aromatisation (Tamm, et al., 1988, Derouane and Vanderveken, 1988)

Thermodynamics for aromatisation of t-2-pentene to benzene, for example, in the temperature range 150°C- 450°C range from 127.1 to 134.8 kJ/mol ΔH and 14.5 to -67.9 kJ/mol ΔG (HSC Chemistry Ver. 2.03). Thermodynamic tables are in Appendix I.

1.6 Reaction pathway of olefin transformation.

Höchtl et al. (2001) suggested a reaction network based on the product distribution obtained from their studies of 1-pentene conversion over H-ZSM-5 (Si/Al ratio of 26) and several molecular sieves. The five main reactions are: double-bond isomerisation, skeletal isomerisation, direct cracking of pentene, dimerisation and oligomerisation, and hydride transfer. In the temperature range 250°C to 550°C the temperature dependence of these pathways showed a decrease in skeletal isomerisation with increase in temperature from the maximum at 250°C. Dimerisation increased from 250°C to a maximum at 350°C and then decreased. Cracking increased sharply above 400°C from where it was the dominant reaction. At 400°C, dimerisation and skeletal isomerisation still had a higher yield than cracking products. Hydride transfer remained constant throughout the temperature range studied.

Garwood (1983) gave evidence for the following steps in oligomerisation: Oligomerisation (formation of dimers, trimers, etc.) is followed by isomerisation and cracking of the oligomers to a mixture of intermediate carbon numbers. Thereafter copolymerisation of the

intermediate mixture of olefins occurs. Gnep et al. (1991) suggested a similar reaction pathway: Oligomerisation (formation of dimers, trimers, etc.) is followed by cracking and then alkylation of the cracking products. Tabak et al. (1986) described the oligomerisation of propene in four steps: Oligmerisation to form distinct oligomers is followed by isomerisation and then cracking to form a range of light olefins. Lastly, repolymerisation to an equilibrium (or pseudo-equilibrium) distribution of heavier olefins occurs.

The rates of acid-catalysed reactions over H-ZSM-5 vary as follows (Cortright et al., 1997 referring to work by Haag): double-bond shift of 1-hexene > skeletal isomerisation of 1-hexene > polymerisation of propene > isomerisation of m-xylene > cracking of hexane.

Viswanadham et al. (1996) suggested the following reaction pathway for aromatisation of paraffins over H-ZSM-5: Olefins crack to smaller olefins, small olefins oligomerise to C_6-C_8 oligomers, oligomers undergo cyclisation and hydrogen transfer to C_6-C_8 aromatics. The oligomers can also continue oligomerising to higher oligomers (C_9^+), which then undergo cyclisation and hydrogen transfer to form higher aromatics (C_9^+). Naphtenes can undergo cracking to small olefins.

Chen et al. (1986) proposed that the reaction products are independent of feed composition and are formed in a consecutive reaction pathway via cracking and hydrogen transfer reactions. The yield of aromatics is subject to the stoichiometric constraint of the carbon/hydrogen ratio.

1.7 Aims of the project

Reactions where pentene is used as feed are not widely documented. The reason for this is probably that C_5 and C_7 products are products unique to the Fisher-Tropsch process used by Sasol. The aim of the work is to investigate the effects of

a) temperature
b) weight hourly space velocity (WHSV)
c) pressure and
d) carrier gas

on the products formed when 1-pentene is reacted over H-ZSM5.

Chapter 2 Experimental

2.1 Flowsheet

The experiments were performed in a fixed-bed reactor equipped with a central thermowell to take temperature measurements inside the catalyst bed. A back-pressure regulator was used to obtain the required reaction pressure of 2-5 atm. The product pot was kept cool with a chiller (using isopropanol as coolant) set at 6°C. The 1-pentene feed was kept in a cylinder under 3 bar nitrogen pressure, from where it was fed into the reactor via a HPLC pump (piston pump). To ensure a liquid feed through the pump, the feed line between the pump and reactor was equipped with a load valve set at 14 bar. The heated GC sampling valve was connected to a point between the back-pressure regulator and product pot by steam-heated (ca. 140°C) lines to ensure that the sample taken for GC-analysis remained a gas. Any product that was not condensated in the chilled product pot, escaped to the vent-line via a wet product gas meter. The product gas was routed via the GC sampling line but the option to analyse the off-gas was not used. A schematic presentation of the experimental apparatus is given in Figure 2.1.

2.1.1 Reactor

The reactor was constructed of stainless steel and had an inner diameter of 14.0 mm. The temperature profile of the reactor was determined at 288°C when the reactor was filled with carborundum (SiC). The temperature profile is depicted in Figure 2.2. For each run, fresh catalyst was loaded and care was taken to position the catalyst bed in the isothermal zone. Carborundum (SiC) was used to fill the rest of the reactor, with glass wool in between as shown in Figure 2.2 .

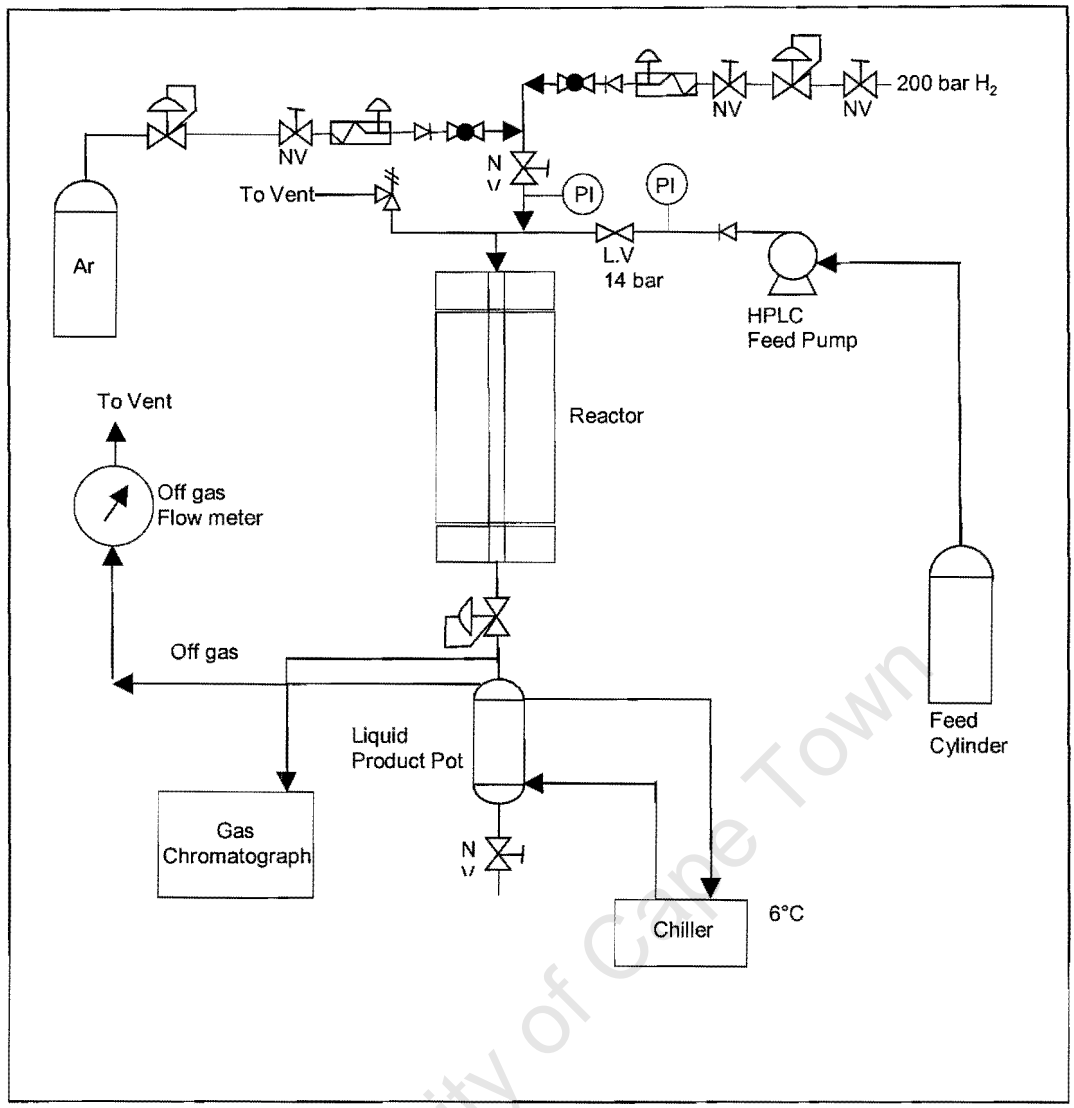

Figure 2.1 Schematic representation of reactor set-up

2.1.2 Leak test

The reactor was leak tested with argon at the start of run temperature (360°C for most runs). The back-pressure regulator was used to set the reactor pressure at 5 bar. If the pressure stayed constant (± 0.1 bar) for 30 minutes after the gas flow to the reactor had been shut off, it was accepted that the system was leak-free.

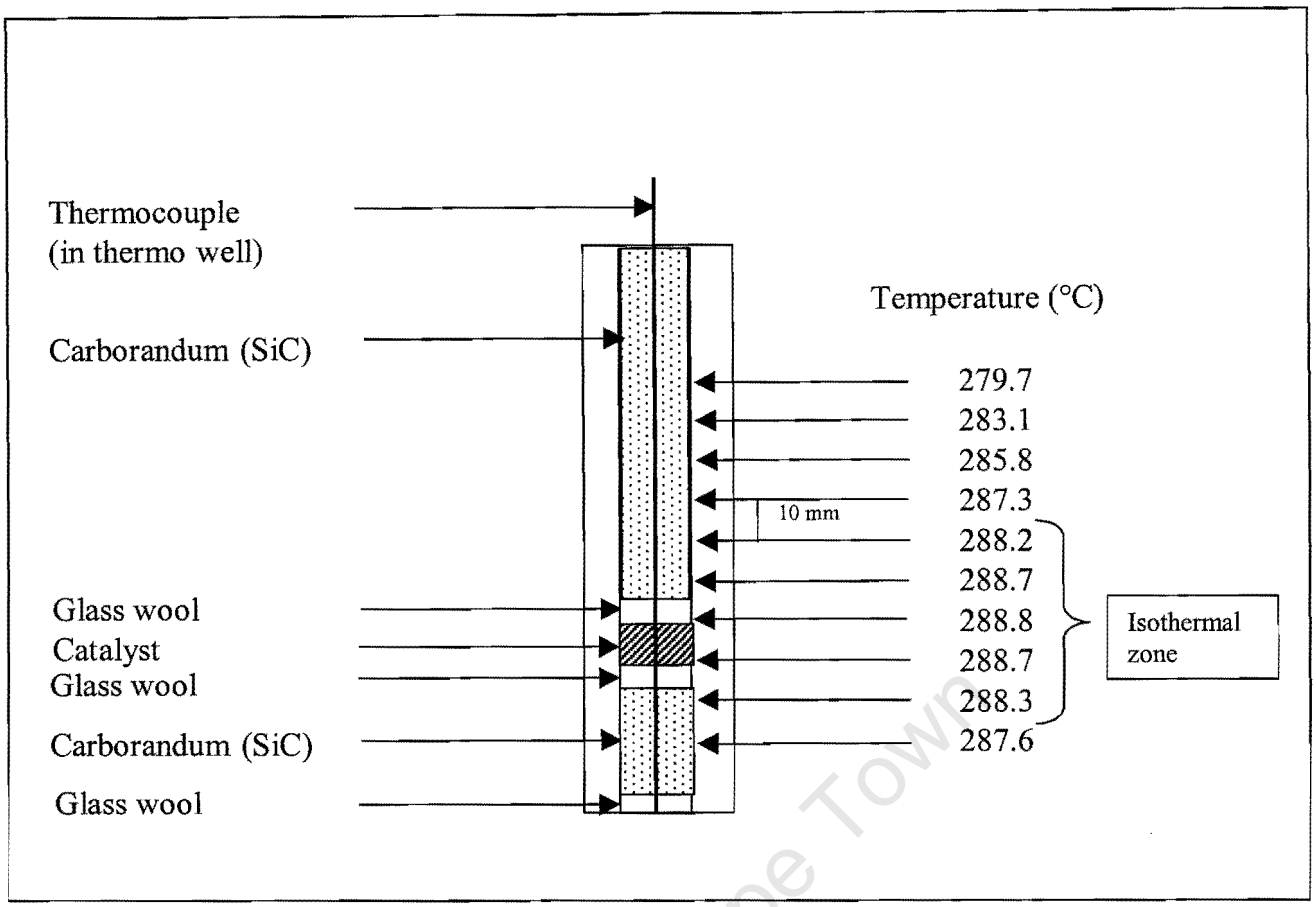

Figure 2.2 Temperature profile and catalyst loading

2.1.3 Calibration

2.1.3.1 Feed pump calibration

The feed pump was not calibrated. The flow rate as given was accepted.

2.1.3.2 Calibration of mass flow controllers

Brooks mass flow controllers were used to introduce either argon or hydrogen to the reactor. The mass flow meters were calibrated by setting the flow meter at different flow rates and measuring the off gas flow of the reactor with a bubble flow meter (argon) and water gas flow meter (hydrogen). The mass flow meter used for argon had a range of 0-2 $l_n h^{-1}$ and the mass flow meter used for hydrogen had a range of 0-30 $l_n h^{-1}$. Corrections were made for temperature and pressure. The calibration graphs are attached in Appendix II.

2.1.4 Mass balance

Mass balances were not calculated for each run. Mass balances for the blank run as well as the run at 153°C gave poor results (<35%). Since there were no leaks on the reactor or the feed line to the reactor, it was suspected that the mass loss had to be related to the off gas measurement. During some of the runs with catalyst, some product condensation was observed in the lines to the off gas meter. These lines could not be heated and therefore it was decided not to calculate mass balances for each run. (A typical mass balance calculation is given in Appendix II.)

2.2 Feed

The pentene feed used for all the experiments was 99.3 % pure 1-pentene obtained from Sasol. The hydrocarbon composition of the pentene feed is given in Table 2.1. The density of the feed was given as 0.6410 kg/l and it contained 3 mg/kg water. The feed was not dried prior to use.

Table 2.1 Hydrocarbon composition of pentene feed

Component	Carbon mass %
3-methyl-1-butene	0.0010
isopentane	0.0452
1-pentene	99.2979
2-methyl-1-butene	0.3917
pentane	0.2229
t-2-pentene	0.0209
c-2-pentene	0.0034
2-methyl-2-butene	0.0170

2.3 Catalyst

2.3.1 Characterisation

Commercial H-ZSM-5 powder was obtained from Syncat. The sample was screened to a size of 150-300 μm. The sample was characterised by ammonia temperature programmed desorption (NH_3 TPD), BET, Inductive coupled plasma atomic emission spectroscopy (ICP-AES), Scanning electron microscopy (SEM) and X-ray diffraction (XRD).

2.3.1.1 NH_3 TPD

TPD analyses were performed with a Micromeritics AutoChem 2910.

The uncalcined catalyst sample (0.1413 g) was calcined in situ at 500°C for 12 h with air as carrier gas. After calcination, the sample was cooled to 100°C under helium flow. The adsorbent gas (NH_3) was allowed to adsorb at a temperature of 100°C over a period of one hour. After the baseline determination, the desorption step followed. For the desorption step, the temperature was increased from 100°C to750°C at a rate of 10°C/min.

2.3.1.2 BET

BET analyses were performed on a Micromeritics Tristar 3000.

The sample was degassed overnight at a temperature of 200°C. Nitrogen was used as the adsorbate at liquid nitrogen temperature of 77K.

2.3.1.3 ICP-AES

ICP-AES analyses were performed on a VARIAN Vista AX CCD Simultaneous ICP-AES.

For the determination of aluminium, the VARIAN ICP 10 method was used. A wavelength of 396.152 nm was used, with a power setting of 1.0 kW and plasma flow of 22.5 litres/min. SiO_2 was determined gravimetrically by the SCI method 3.I.R1.

2.3.1.4 SEM

A LEO 1430 scanning electron microscope was used to obtain photographs of the catalyst.

The sample was mounted on an aluminum stub with double-sided carbon tape and covered with a gold layer. An electron beam of 15 kV was used to bombard the sample.

2.3.1.5 XRD

The calcined catalyst sample was analysed with a Siemens XRD. A qualitative diffractogram was recorded to identify the catalyst. Thereafter the crystallite size was determined. Three different sample packings were analysed. The external standard silicon was recorded using the same diffractometer settings as for the crystallite size determination. Table 2.2 shows the conditions that were used for the identification and crystallite size determination.

Table 2.2 Conditions for XRD

Variable	Identification	Crystallite size
Voltage	40 kV	40 kV
Amperage	25 mA	25 mA
Divergance slit	1 °	1 °
Receiver slit	0.15 °	0.15 °
Scan from	5 °2θ	26 °2θ
Scan to	105 °2θ	29 °2θ
Step size	0.05 ° 2θ	0.05 ° 2θ
Counting time	2 seconds	4 seconds

2.3.1.6 TEM analysis

The H-ZSM-5 sample was also viewed by a transmission electron microscope (TEM).

A Philips CM200 electron microscope fitted with a Gatan image filter was used to obtain photographs after directing an electron beam of 200 kV at the sample. An elemental scan

was obtained with by energy dispersive X-ray spectroscopy (EDS) using an Oxford EDS with 136 eV resolution.

The sample was prepared by crushing it to a fine powder in a mortar and pestle. A copper grid covered with a thin carbon layer was then dipped into the powder to allow particles to attach to the carbon film.

2.3.1.7 C,H determination

The analyses for carbon and hydrogen content of the spent catalyst were done by the SCI laboratories according to their analytical method 3.41/88. A short description of this gravimetric method is given below:

The sample, crushed to a particle size of less than 250 μm, was decomposed at 800°C in an oxygen flow of 300 ml/min. Over copper oxide all the carbon was converted to carbon dioxide and all the hydrogen to water. Carbon dioxide and water were determined gravimetrically after absorption over ascharite and magnesium perchlorate, respectively.

2.3.2 Calcination

The catalyst was calcined in a synthetic air atmosphere at atmospheric pressure. The air flow into the calcination tube was about 1 litre/min. Uncalcined catalyst was placed in the calcination tube and heated from room temperature to 500°C at a rate of 2.78°C/min. Once the temperature had reached 500°C, it was held there for 12h before allowing the reactor to cool down to room temperature.

The catalyst used for the runs was calcined in two batches. Runs 3z-15z were done with the first batch (HZSM5-1) and Runs 16z-20z with the second batch (HZSM5-2).

2.4 Product analysis

2.4.1 GC

On-line GC analysis of the product was performed. The total product prior to cooling and phase separation was analysed. Samples were analysed at intervals of 1.5 hours during the

six-hour duration of each run. The product from the reactor was analysed on-line with a Shimadzu GC 17A Gas Chromatograph equipped with a flame ionisation detector (FID). Integration was performed with Class VP software. A Pona column (length 60m, inner diameter (ID) 0.25 mm and film thickness 0.25 μm) was used. Hydrogen was used as carrier gas and nitrogen as make-up gas. The flame ionisation detector (FID) used hydrogen and synthetic air. The specification of the gases is given in Table 2.3 and the analysis conditions of the GC are given in Table 2.4.

Table 2.3 Gases used for GC

Gas	Specification
Hydrogen 5.0	CnHm ≤ 0.5 ppm, H_2O ≤ 2.0 ppm, O_2 ≤ 3.0 ppm
Nitrogen 5.0	CnHm ≤ 1.0 ppm, H_2O ≤ 2.0 ppm, O_2 ≤ 2.0 ppm, CO_2 ≤ 1.0 ppm
Synthetic air	CnHm ≤ 4 ppm, H_2O ≤ 4.0 ppm, O_2 19-23 %

Table 2.4 GC temperature program and conditions

Start temperature	30°C
Hold time	5 min
Ramp	2°C/min
Temperature 1	120°C
Hold time	1 min
Ramp	15°C/min
Temperature 2	250°C/min
Hold time	7 min
Injector temperature	150°C
Detector temperature	280°C
Injector 2 (GC valve)	150°C
Split ratio	100:1
Split flow	160 ml/min
Velocity	34 cm/s
Column flow	1.6 ml/min
Total flow	165 ml/min
Detector range	1 (medium sensitivity)

2.4.2 GC-MS

The liquid product of every run was analysed with a Hewlett-Packard 5972 gas-chromatograph-mass spectrometer equipped with a Pona column. The same conditions as for the on-line GC analysis were used. The results obtained by the GC-MS analysis were used for identification of compounds on the on-line GC trace.

2.5 Experimental procedure

The same experimental procedure was followed for all runs.

1. The catalyst was calcined and kept in a desiccator until use.
2. One gram of undiluted catalyst was loaded into the isothermal zone of the reactor. The catalyst was not diluted because carbon and hydrogen analyses were done on the spent catalyst.
3. The reactor inner diameter was 14.0 mm and the height of the bed ca. 1 cm.
4. The rest of the reactor was loaded with carborundum and glass wool plugs.
5. The catalyst was then heated to 400°C at a heating rate of 50°C/h under hydrogen flow and kept at 400°C for 3 hours before allowing the reactor to cool down under argon flow to the reaction temperature for the run. This step was done to remove all adsorbed moisture from the catalyst.
6. After setting the appropriate gas flows (argon or argon/hydrogen), the feed was introduced from a cylinder kept under 3 bar pressure with nitrogen. The feed was pumped at the rate required to obtain each of the space velocities in Table 2.5.
7. The total reactor product was analysed by on-line GC at time intervals of 1.5 h.
8. The liquid sample (obtained from the product pot at 6°C) was analysed by GC-MS.
9. The duration of each run was 6 h.
10. The reactor and lines to the GC were flushed with hydrogen while the reactor was cooling down.
11. The catalyst was unloaded at room temperature and stored in a desiccator for later carbon analysis.

2.6 Experimental programme

The runs performed are listed in Table 2.5 and have been grouped according to the effect of temperature (runs 5z-8z, 13z, 15z, 16z, 20z); WHSV (runs 3-5z, 8z, 14z, 16z, 17z, 18z); and pressure and diluent (runs 5z, 8-10z, 12z, 16, 19z.). Run 21z was a blank run without catalyst.

Table 2.5 Experimental programme

Run name	Ar flow ($l_n h^{-1}$)	Feed:Ar Mol/mol	H_2 flow H_2:feed (molar)	T_{set} * (°C)	P (bar)	Mass catalyst (g)	WHSV (h^{-1})
Blank							
z21	0.64			360	2		-
Effect of temperature							
z5	0.64	11.4		360	2	1.037	22
z6	0.64	11.8		300	2	1.024	23
z7	0.64	11.7		250	2	1.022	23
z8	0.64	11.8		360	2	1.024	23
z13	0.64	11.7		400	2	1.022	23
z15	0.64	11.7		200	2	1.020	23
z16	0.64	11.8		360	2	1.025	23
z20	0.64	11.8		150	2	1.026	23
Effect of WHSV							
z3	0.64	34.6		360	2	1.019	68
z4	0.64	22.9		360	2	1.020	45
z5	0.64	11.4		360	2	1.037	22
z8	0.64	11.8		360	2	1.024	23
z14	0.64	57.7		360	2	1.022	113
z16	0.64	11.8		360	2	1.025	23
z17	0.64	23.0		360	2	1.022	45
z18	0.64	34.8		360	2	1.024	68
Effect of pressure and diluent							
z5	0.64	11.4		360	2	1.037	22
z8	0.64	11.8		360	2	1.024	23
z9	0.64	11.8		360	5	1.025	23
z10	0.64	11.7	1:1	360	2	1.022	23
z12	0.64	11.8	1:1	360	5	1.024	23
z16	0.64	11.8		360	2	1.025	23
z19	0.64	11.7	1:1	360	5	1.022	23

* T_{actual} observed during the experiments are given in Chapter 3.

Note: Runs z1 and z2 were preliminary runs and are not reported.

Run 11z was aborted after 1.5 h and is therefore not reported.

Chapter 3 Results

This chapter is a summary of the results obtained. It is divided into two sections, characterisation of the catalyst before and after reaction (Section 3.1) and reaction analyses (Section 3.2).

3.1 Catalyst characterisation

3.1.1 NH_3 TPD

The TPD results in Figure 3.1 show the presence of weak (< 300°C) and medium (300-500°C) acid sites. The weak acid sites (0.137 mmol NH_3/g catalyst) and medium strength acid sites (0.197 mmol NH_3/g catalyst) give a total acidity of 0.334 mmol NH_3/g catalyst. This value is in line with the acidity (0.324 mmol/g H-ZSM-5) that is theoretically expected from H-ZSM-5 with a Si:Al atom ratio of 48.

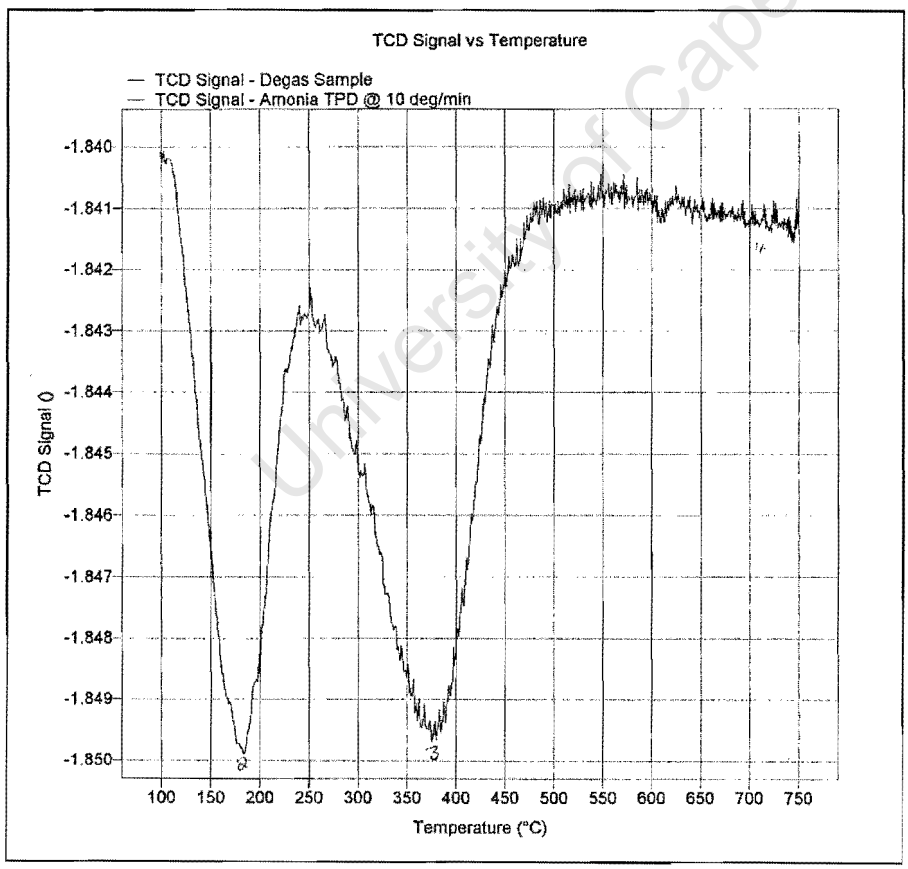

Figure 3.1 Ammonia TPD trace of H-ZSM-5

3.1.2 N_2-BET

Table 3.1 BET analysis

Sample[1]	HZSM5-1	HZSM5-2	HZSM5-3
BET surface area m^2/g	420 ± 10	410 ± 10	390 ± 10
BJH Avg. pore diameter (nm)	16.9	12.2	27.9
Micropore volume (cm^3/g)	0.134	0.133	0.00645

[1]HZSM5-1 and HZSM5-2 denote the two different batches of calcined catalyst used for runs 3z-15z and 16z-20z respectively. HZSM5-3 is the uncalcined catalyst.

The results in Table 3.1 indicate that the three samples have similar BET areas. Typically, BET areas for H-ZSM-5 range from 400-500 m^2/g. BET areas of 423 and 425 m^2/g have been reported by Bhattacharya and Sivasanker (1996) and Viswanadham et al. (1996) respectively. The uncalcined sample (HZSM5-3) and calcined samlpes (HZSM5-2 ans HZSM5-3) have pore diameters in the meso pore range. It can be noted that calcination led to an increase in micropore volume, which decreased the BJH average pore diameter.

IUPAC pore size definitions are as follows:
Macro pores: >50 nm (500 Å)
Meso pores: 2-50 nm (20-500 Å)
Micro pores: < 2 nm (20 Å)

3.1.3 ICP-AES

Analysis of the H-ZSM-5 powder gave an aluminium content of 0.86 mass % Al. The gravimetric analysis gave a SiO_2 content of 88.20 mass %. This gives a Si:Al atom ratio of 48:1. The Si:Al ratio indicated by the suppliers was 40:1.

3.1.4 SEM

The cystallite size of the ZSM-5 catalyst could not be determined by SEM analysis. A SEM photograph is shown in Figure 3.2.

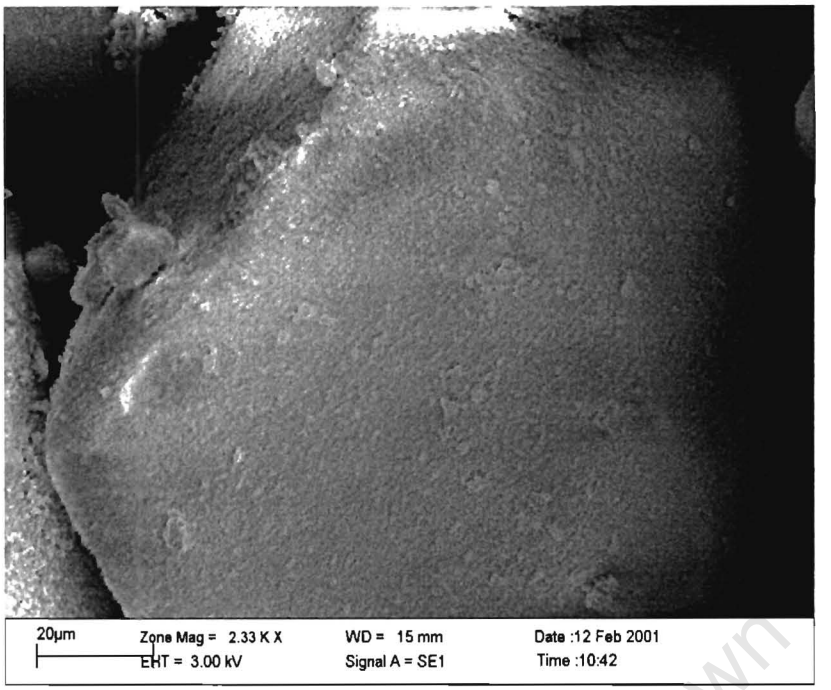

Figure 3.2 SEM photograph at 2.33K X magnification

3.1.5 XRD

The XRD pattern of the sample and the best database match are shown in Figure 3.3.

The method of XRD only detects the elements incorporated in the crystalline structure of the zeolite. If the aluminium ions in the sample are not part of this structure, it will lead to a higher Si:Al ratio than expected. This might explain the difference in Si:Al ratio between the XRD results and the ICP results. The sharp peaks also indicate the presence of crystallites. The exact crystallite size could not be determined by XRD. The high baseline obtained could be indicative of small crystallites.

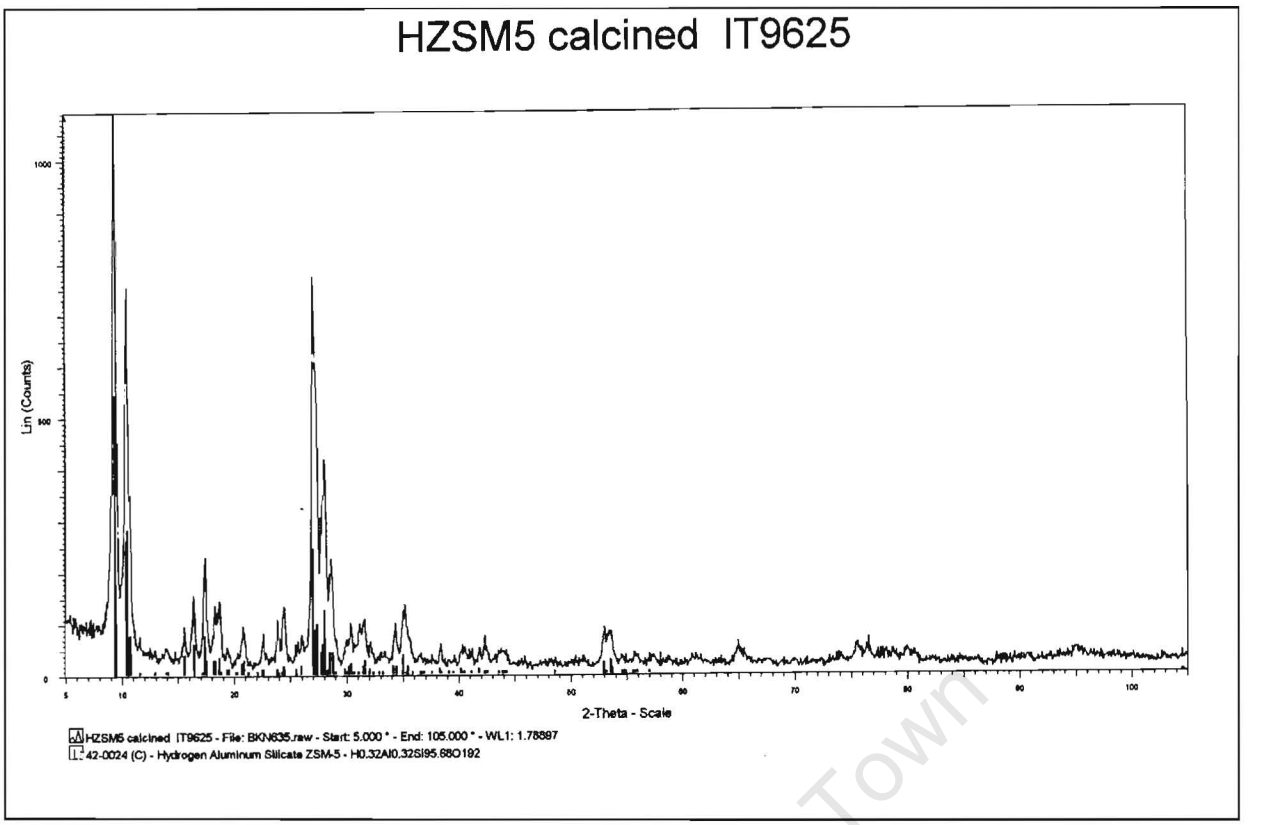

Figure 3.3 XRD pattern for calcined H-ZSM-5

3.1.6 TEM analysis

The TEM photograph of the H-ZSM-5 sample is shown in Figure 3.4. Crystallite sizes ranging from about 25 nm to 30 nm (0.02-0.03 μm) were observed. The EDS scan (Figure 3.5) showed peaks for si.icon, oxygen and a small quantity of aluminium. The peaks for copper and carbon originate from the copper grid covered with a carbon layer.

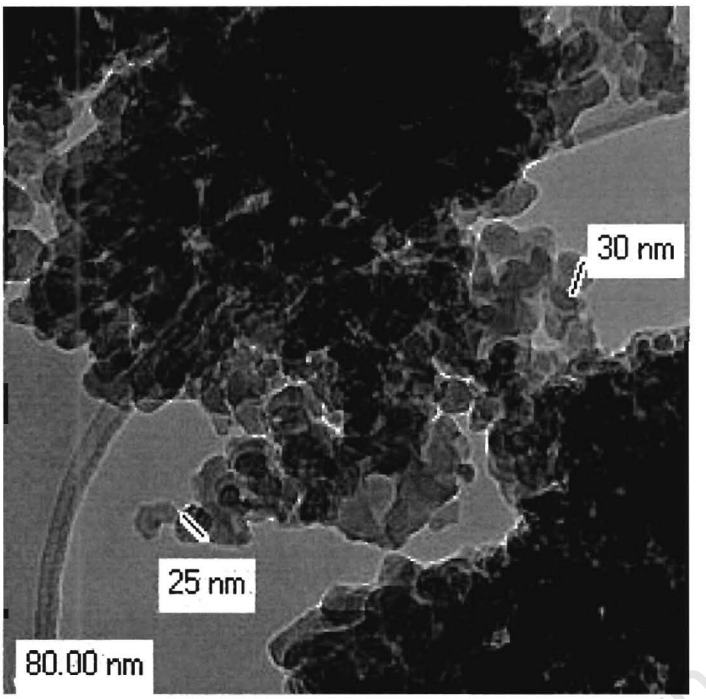

Figure 3.4 TEM photograph of H-ZSM-5 sample

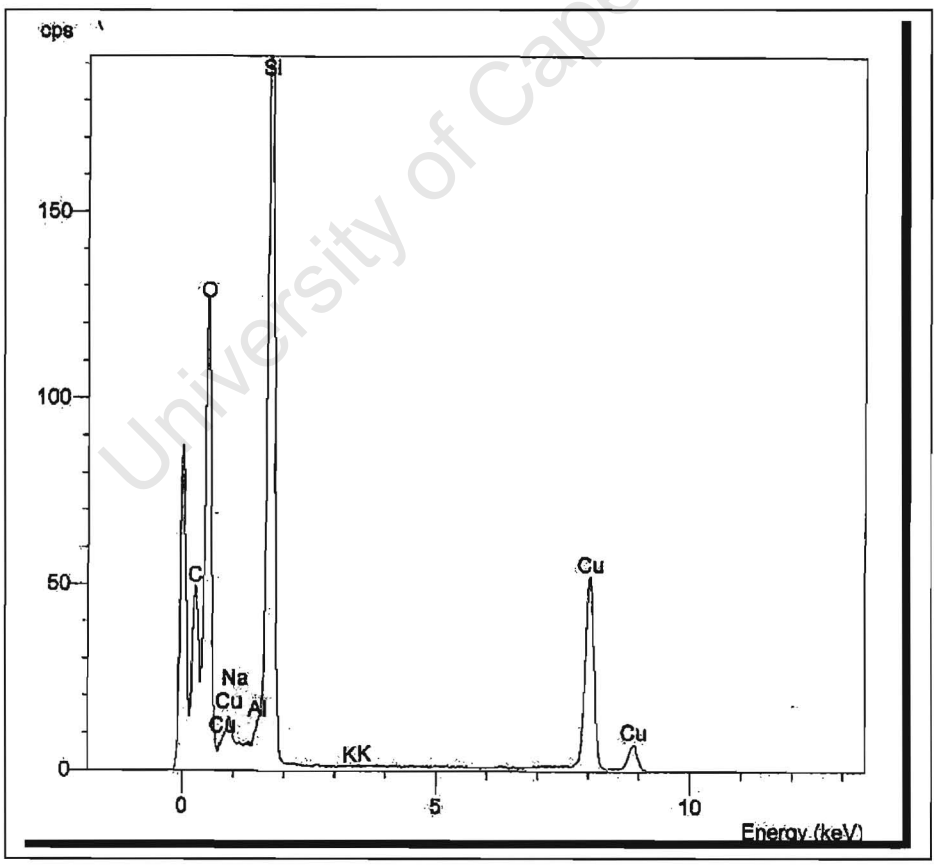

Figure 3.5 EDS scan of H-ZSM-5

3.1.7 Carbon and hydrogen analysis

The effects of temperature, WHSV and pressure on the carbon and hydrogen content of the spent catalyst are shown in Table 3.2, Table 3.3, and Table 3.4, respectively. The results are depicted graphically in Figures 3.6, 3.7 and 3.8.

Table 3.2 The effect of temperature on the carbon and hydrogen content of the spent catalyst at argon flow of 0.64 $l_n h^{-1}$

Run name	Ar flow ($l_n h^{-1}$)	H_2 flow H_2:feed (moles)	T (°C)	P (bar)	WHSV (h^{-1})	C (m%)	H (m%)	C:H (Mole ratio)	Colour of spent catalyst
z21	0.64	-	360	2	-	-			
z20	0.64	-	153	2	23	35.80	5.82	0.52	Orange- yellow
z15	0.64	-	201	2	23	31.56	4.86	0.54	Brown with light specks
z7	0.64	-	269	2	23	7.68	0.76	0.85	Yellow-grey
z6	0.64	-	321	2	23	4.13	0.36	0.96	Brown-black
z16	0.64	-	367	2	23	2.44	0.15	1.37	Dark grey
z8	0.64	-	377	2	23	2.67	0.16	1.40	Black
z5	0.64	-	364	2	22	2.45	0.10	1.87	Dark grey
z13	0.64	-	407	2	23	2.13	0.05	3.57	Dark grey

Increasing the temperature had mainly two effects:

a) The C:H ratio increased from approximately 0.5 to 4. Typically a C:H ratio of 0.5 represents an olefinic feed while a C:H ratio of 1 represents benzene-like structures. Considerably higher values such as 4 represent carbon that is approaching graphite in nature. Thus at low T the residual hydrocarbons are merely a strongly adsorbed long chain olefinic species. As the temperature increases the remaining species on the surface become more aromatic and ultimately graphitic. The formation of aromatics as well as more graphitic hydrocarbons is also indicated by the decrease in hydrogen content.

b) The amount of C deposited appears to decrease with an increase in temperature. This effect may be explained by noting that the low temperature samples contained a lot of olefinic material, which could not be desorbed at low temperature. The reason for using low temperature for pre-treatment of the sample is that increasing the temperature will cause the olefinic species to be converted to aromatic and graphitic species. The low temperature samples contained excesssive olefinic material and thus the carbon content values of the spent catalyst for these runs are unusually high. At high temperature, the HZSM-5 efficiently converts these olefinic species to smaller hydrocarbons, producing a small amount of carbon on the surface. In particular around 400°C, it is known that the coke content on ZSM-5 is at a minimum. (Zhao, 1991.)

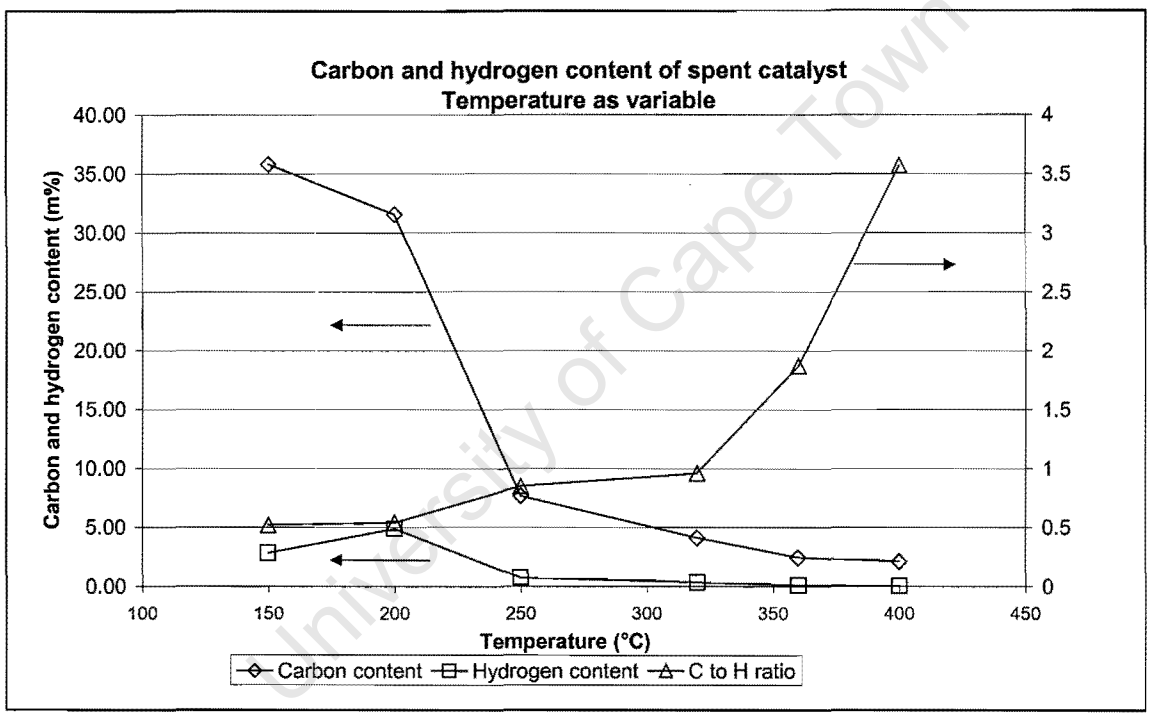

Figure 3.6 Effect of temperature on carbon deposits

Table 3.3 The effect of WHSV on the carbon and hydrogen content of the spent catalyst at argon flow of 0.64 $l_n h^{-1}$ and total pressure of 2 bar.

Run name	T (°C)	WHSV (h^{-1})	C m%	H m%	C:H Mole ratio	Colour of spent catalyst
z5	364	22	2.45	0.11	1.87	Dark grey
z8	377	23	2.67	0.16	1.40	Black
z16	367	23	2.44	0.15	1.37	Dark grey
z4	368	45	4.35	0.26	1.40	Brown-black
z17	395	45	5.26	0.40	1.10	Black darker than z1, z8
z3 (1)	371	68	5.42	0.27	1.68	Brown black
z18	421	68	7.84	0.46	1.43	Black, like z17
z14	431	113	8.04	0.51	1.32	Black, darker than z17
z11 (2)	360	339	2.64	0.05	4.43	Grey black

(1) The actual temperature for run z3 was higher than recorded due to incorrect placement of the thermocouple.

(2) The results for run z11 are after only 1.5 h on stream, whilst the other results were obtained after six hours on stream.

The data for run z11 (run stopped after 1.5 h) is not included in these trends because reaction time is a very important parameter, especially for product distribution and coke content. It can be noted, however, that at the high space velocity (339 h^{-1}) of run z11 the carbon content after just 1.5 h was already the same as the carbon content after 6 hours for the lower space velocity runs (23 h^{-1}).

Increasing the WHSV had mainly the following effects:

a) Increasing the WHSV has very little influence on the C:H ratio, which varies between 1.1 and 1.9. Although runs z18 and z14 have different WHSV, the temperatures were in the same range. The similarity of carbon and hydrogen content as well as C:H ratio suggests that the influence of temperature is much more pronounced than that of WHSV. The nature of the carbon deposits seems to be aromatic approaching graphitic in nature.

b) Increasing the WHSV led to an increase in carbon content of the spent catalyst. This may be explained as follows: The formation of coke may in many cases be related to the amount of fluid passed over the catalyst. Higher WHSV would therefore result in more coke being deposited. The highest amount of carbon (ca. 8 m%) was, however, much lower than the highest amount of carbon (32-36 m%) found in the temperature runs. Also, whereas the high carbon content deposits in the temperature runs were olefinic in nature, the high carbon content deposits in the WHSV runs were not olefinic in nature. This might be expected, since the high carbon content deposits of olefinic nature in the temperature runs, were performed at lower temperatures than any of the WHSV runs.

c) The high WHSV runs resulted in much higher reaction temperatures. The influence of changing WHSV is therefore not conclusive.

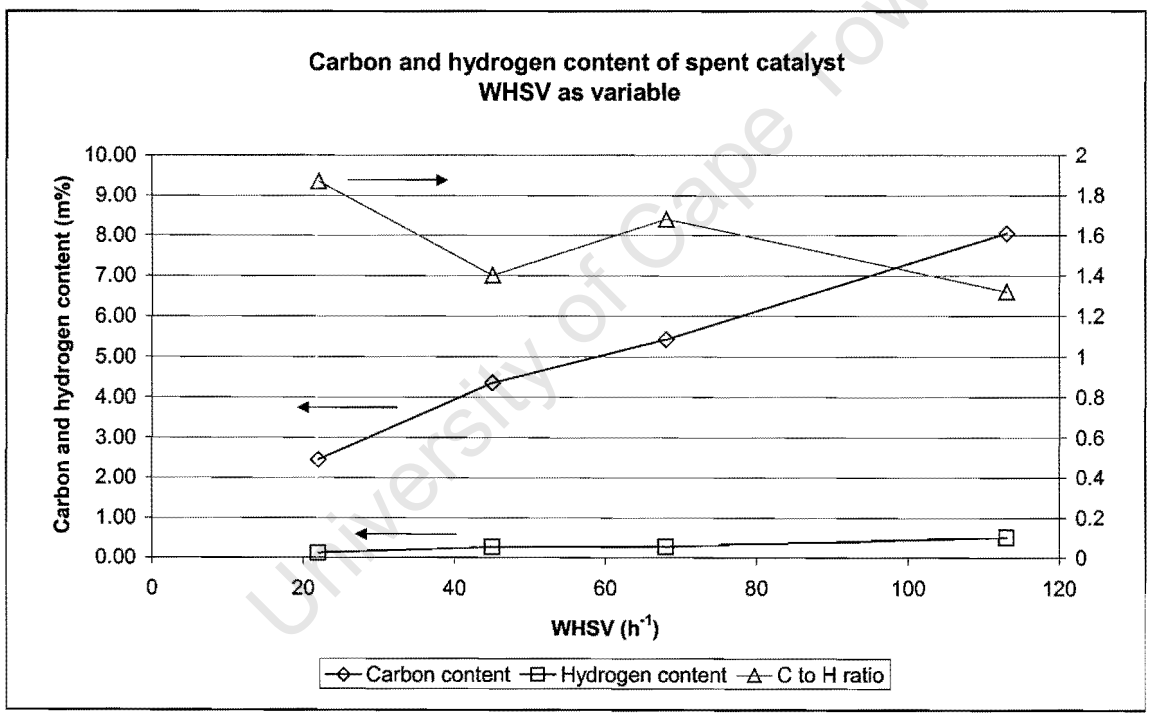

Figure 3.7 Effect of WHSV on carbon deposits

Table 3.4 The effect of pressure and H_2 on the carbon and hydrogen content of the spent catalyst at argon flow of 0.64 $l_n h^{-1}$ and WHSV=23 h^{-1}

Run name	H_2 flow H_2:feed (moles)	T (°C)	P (bar)	C (m%)	H (m%)	C:H (Mole ratio)	Colour of spent catalyst
z8	-	377	2	2.67	0.16	1.40	Black
z9	-	379	5	4.66	0.22	1.78	Brown black
z10	1:1	373	2	2.67	0	∞	Grey
z12	1:1	363	5	0.55	0	∞	Blue grey
z19	1:1	372	5	1.66	0.02	6.96	Grey

Increasing the pressure and adding hydrogen resulted in the following:

a) Increasing the pressure from 2 bar to 5 bar, resulted in the formation of more carbon (see z8 and z9).

b) Adding hydrogen had no effect on carbon content at low pressure but increased the C:H ratio (see z8 and z10).

c) The addition of H_2 and using higher pressure, favour the formation of less carbon deposits which are more graphitic in nature. This may be due to the H_2 being able to reduce the amount of aromatisation and thus reduce the probability of the formation of carbon, especially the formation of highly condensed aromatic rings.

d) The increase in C:H ratio, indicating the more graphitic nature of the carbon deposits, could be the result of hydrogen reacting with the deposited carbon. The residual carbon would then be much richer in carbon than in the absence of hydrogen.

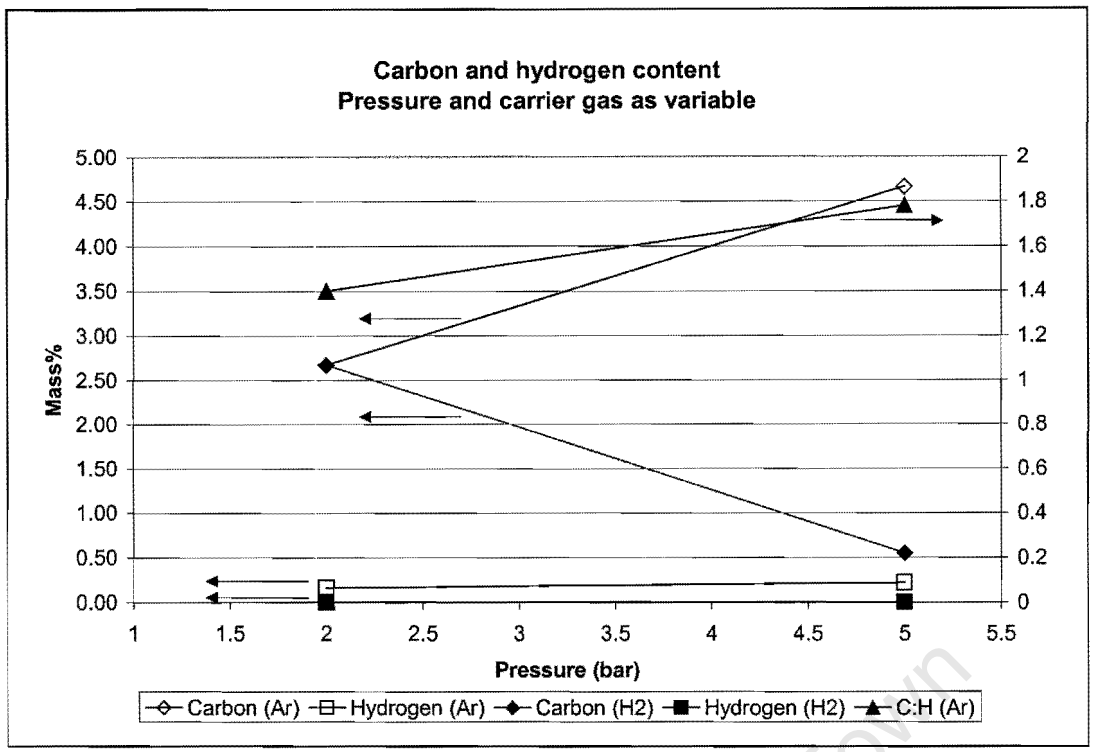

Figure 3.8 Effect of pressure and carrier on carbon deposits

3.2 Reaction Analyses

3.2.1 Assignment of product groups

The GC results and identification of peaks on the chromatograms are given in this section. A Pona column was used for both the GC analysis and GC-MS analysis. Since a Pona column separates compounds according to their boiling points, compounds with similar boiling points could not be separated well. At the higher temperatures, where several reactions took place in competition, very complex chromatograms were obtained. All the peaks could not be identified by GC-MS, especially in the range of the heavier compounds (C_{10} and higher). Depending on the temperature of the reaction, different product classes eluted in the same retention time areas.

Figures 3.9 and 3.10 represent sample chromatograms at both low and high temperature, respectively. In the case of the many isomers and higher aromatics obtained, especially at the higher temperatures, this has made analysis of the product spectrum complicated. Not even the use of a GC-MS could resolve the large number of compounds. Analysis therefore had to

resort to using a number of key peaks and looking for patterns in the spectra as a function of temperature.

Table 3.5 shows typical product compounds that were assigned in this work. At the low temperatures the species were essentially olefinic, while at the higher temperatures the spectrum became essentially aromatic. As these data are too complex to use for meaningful interpretation, these were grouped into the following broad classifications in an attempt to follow the reaction pathway as a function of temperature and WHSV (i.e. conversion), viz. olefins, paraffins, naphtenes (cyclic paraffins) and aromatics for each carbon number. The broad classifications for the chromatograms are shown in Table 3.5. The classifications for the other runs can be found in Appendix IV.

Assignment of the unknown compounds in the GC trace were made on the following basis:

1. At the lower carbon numbers (up to C_6) an unknown compound was not grouped as an olefin if all the olefinic isomers were already identified.
2. At the higher carbon numbers (C_9 and higher), unknown compounds were grouped mostly as aromatics, since at the temperatures employed, cracking of the olefins and paraffins would have taken place.

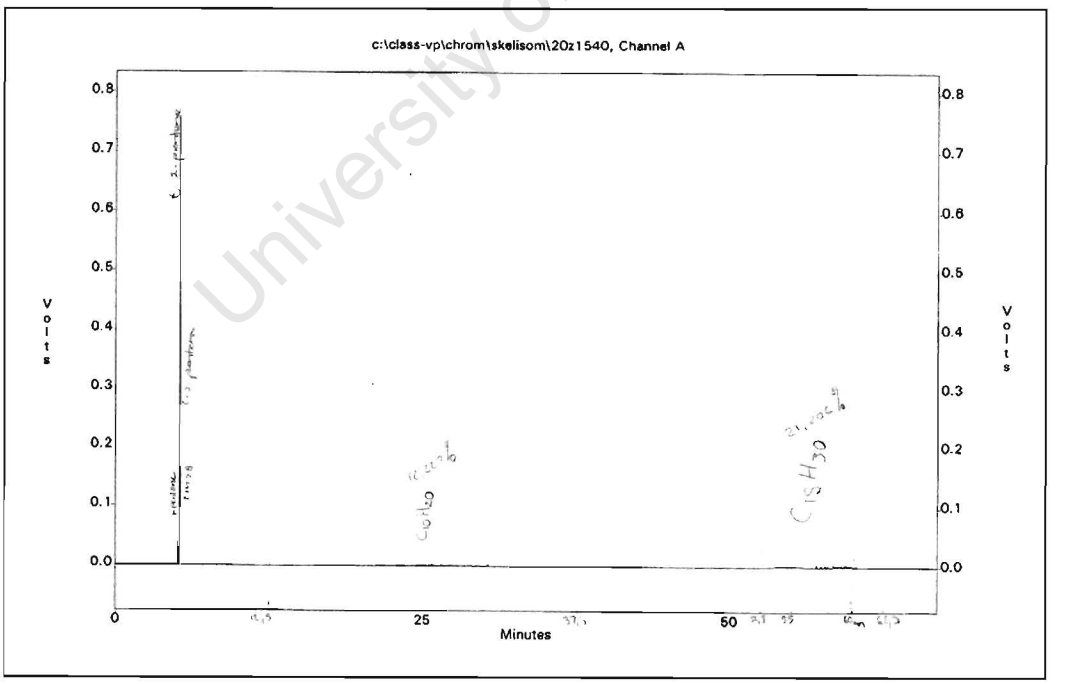

Figure 3.9 Gas chromatogram of pentene conversion at 153°C.

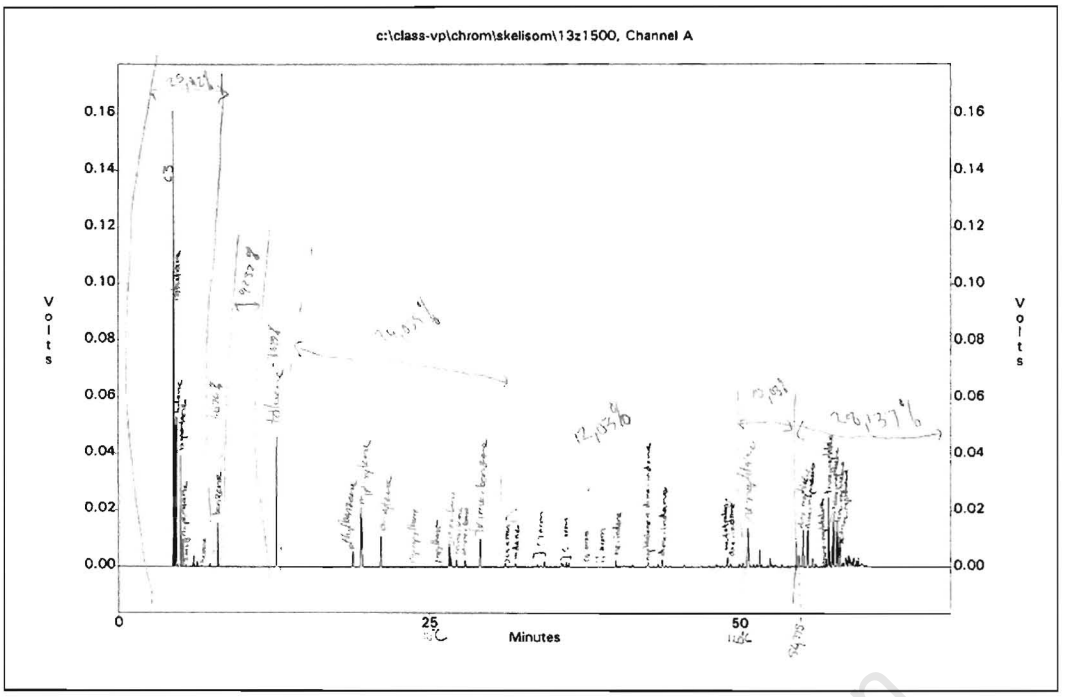

Figure 3.10 Gas chromatogram of pentene conversion at 407°C.

Table 3.5 Product distribution as a function of temperature. An example to show how assignment was carried out. (All data taken at 6 h on stream.)

	Temperature (°C)	153	362	407
		20z	5z	13z
C. no.	Component	C mass%	C mass%	C mass%
2	C2 HC	0.00	0.04	0.65
3	C3 HC	0.00	1.37	10.07
4	C4 HC	0.02	2.70	10.00
3	isopentanes	0.06	1.70	2.62
5	n-pentanes	0.00	0.67	0.66
5	isopentenes	1.08	0.06	0.11
5	n-pentenes	65.26	0.02	0.02
5	cyclopentane+2,3-dimethyl butane	0.00	0.15	0.14
6	olefins	0.08	0.05	0.03
6	paraffins	0.00	1.42	0.59
6	naphtenes	0.00	0.46	0.13
6	aromatics			
6	Benzene	0.00	2.08	1.67
7	Toluene	0.00	18.38	7.69
8	m,p-Xylene	0.00	15.33	6.48
8	o-xylene	0.00	4.42	2.08
8	eBz	0.00	3.61	0.99
	BTX + eBZ	0.00	43.83	18.90
7	olefins	0.04	0.00	0.00
7	paraffins	0.00	0.96	0.12
7	naphtenes	0.00	0.86	0.10
7	aromatics			
8	olefins	0.02	0.00	0.00
8	paraffins	0.00	0.38	0.02
8	naphtenes	0.00	0.86	0.03
8	aromatics			
9	olefins	0.00	0.00	0.00
9	paraffins	0.00	0.04	0.00
9	naphtenes	0.00	0.46	0.00
9	aromatics	0.00	14.91	5.98
10	olefins	12.24	0.00	0.00
10	paraffins	0.00	0.00	0.00
10	naphtenes	0.00	0.00	0.00
10	aromatics	0.00	8.98	5.39
11+	olefins	21.21	0.00	0.00
11+	paraffins	0.00	0.00	0.00
11+	naphtenes	0.00	0.00	0.00
11+	aromatics	0.00	20.08	44.44
	Total	100.00	100.00	100.00

3.2.2 Repeatability of data

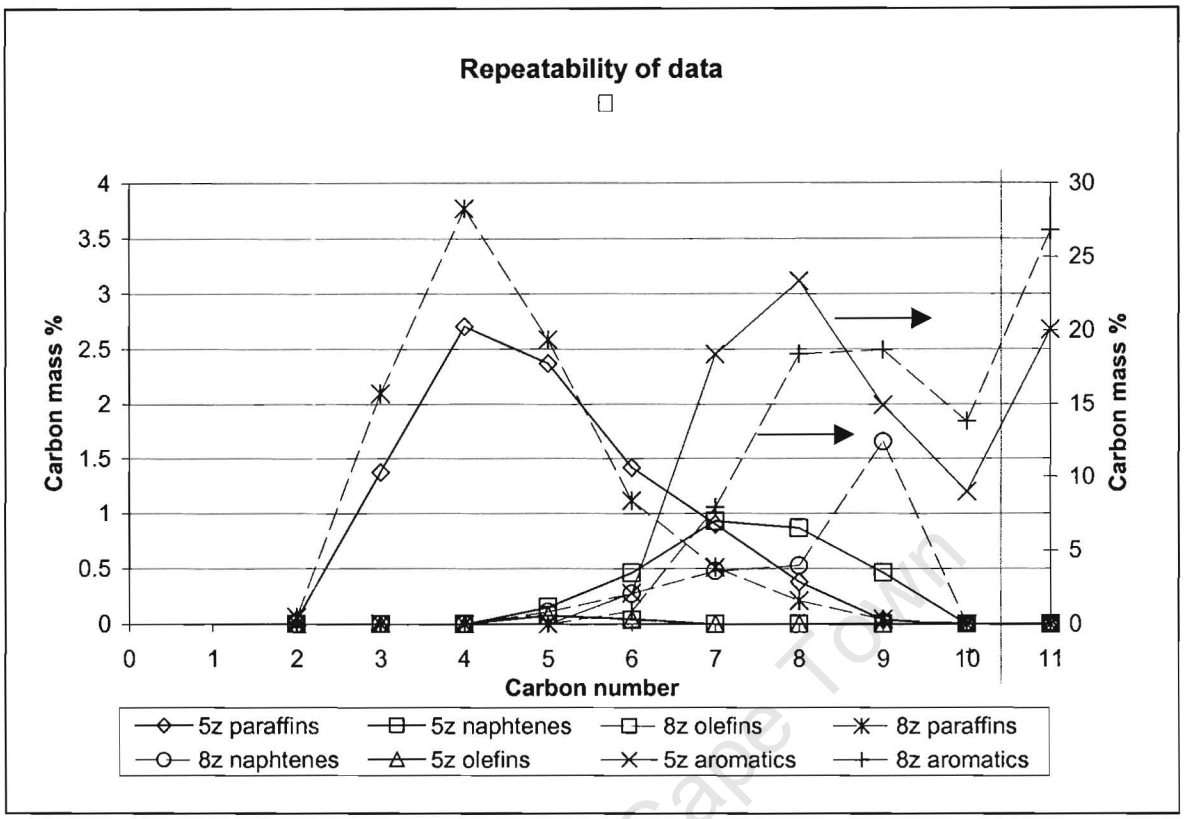

Figure 3.11 Repeatability of data illustrated by runs at 360°C and WHSV=23 h^{-1}

Both run 5z and 8z were performed at the same reaction conditions of T=360°C and WHSV=23 h^{-1}, with catalyst from the same calcined batch. At a first glance, the repeat runs show the same trend, namely that the main products at the reaction conditions are aromatics and some paraffins. Further inspection of Figure 3.11 reveals that although similar trends can be found at low carbon numbers (C_1-C_6), different trends are observed at higher carbon numbers (C_7+). Both runs show a maximum for paraffins at carbon number four. The aromatics distribution, however, differs. Double the amount of toluene was formed in Run 5z and more xylenes were formed as well, compared to Run 8z. The actual temperature in the catalyst bed for the repeat runs also varied, in spite of the same starting temperatures of 360°C before feed was introduced. The actual run temperature was 362°C for Run 5z and 377°C for Run 8z. The differences in aromatics distribution could possibly be attributed to slight differences in start-up in spite of following the same procedure. Packing of the catalyst bed could also have differed slightly for the two runs. Repeatability was thus not as good as desired due to the high sensitivity of the reaction to temperature and start-up conditions.

3.3 Effect of temperature on product distribution

3.3.1 Lumping groups as PONA (paraffins, olefins, naphtenes, aromatics)

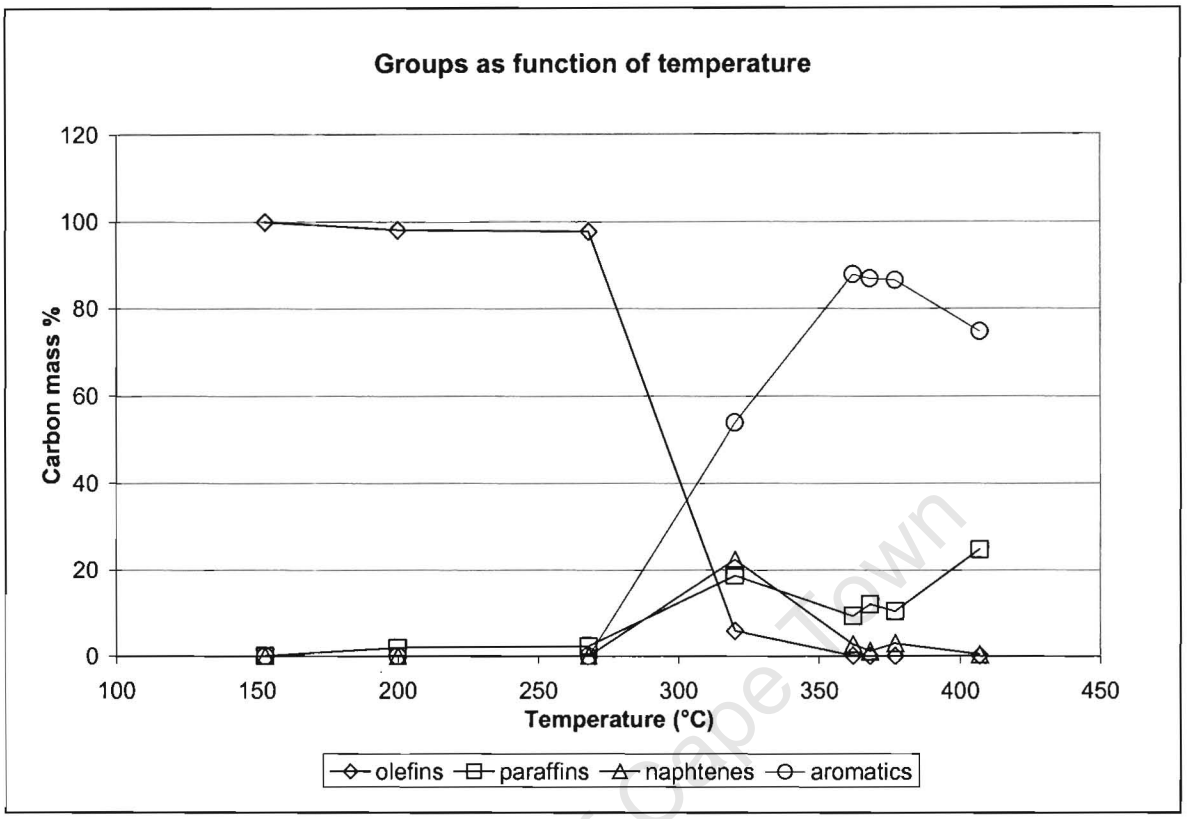

Figure 3.12 Product distribution as a function of temperature

In Figure 3.12 the distribution of lumped groups is given as a function of temperature. At the three temperatures below 320°C, viz. at 153°C, 200°C and 258°C, the main reaction products are olefins, while some paraffins are present. At 320°C and higher, the olefin content dropped sharply and the main products are aromatics. The formation of naphtenes and aromatics is observed at temperatures above 320°C. An increase of paraffins was also observed, as would be expected with the formation of aromatics. At the highest temperature of 407°C, the main products are aromatics and paraffins. The decrease in aromatics and increase in paraffins probably indicate cracking of the side chains on the higher aromatics. It could also be ascribed to the "paring" reaction, whereby methyl groups are removed to form benzene or toluene and light paraffins.

3.3.2 Carbon number distribution

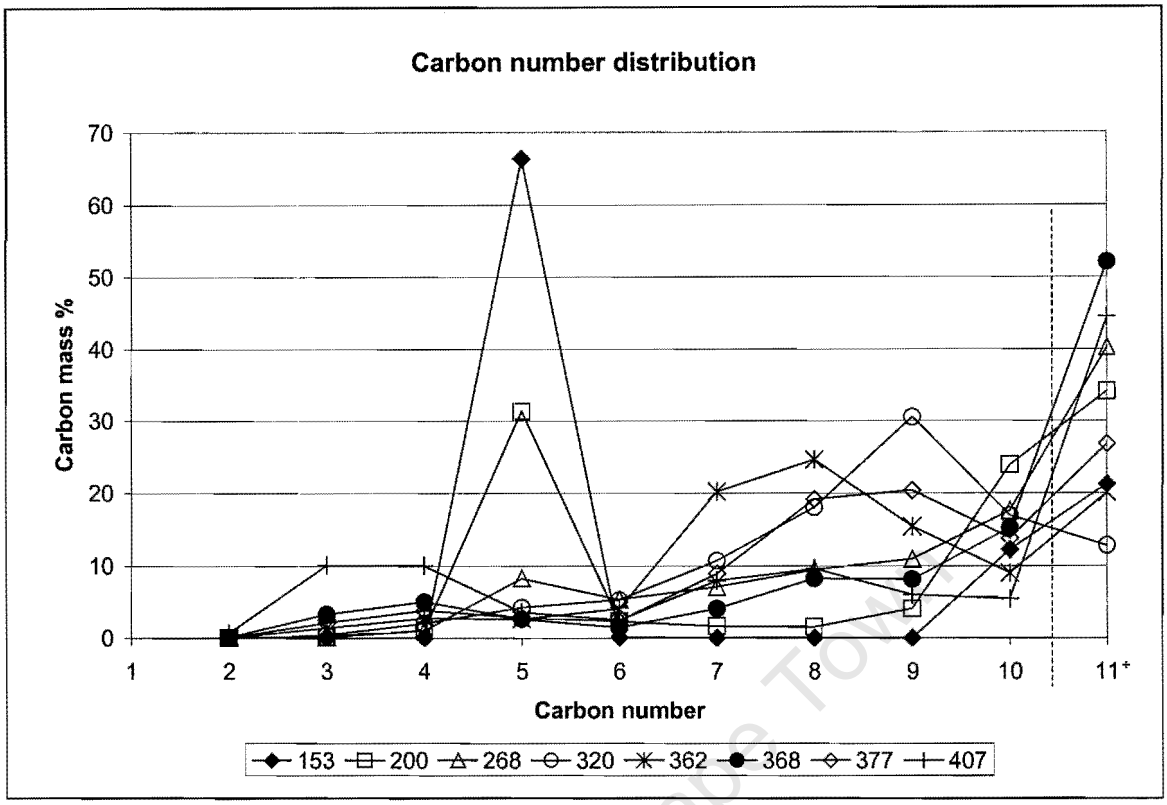

Figure 3.13 Carbon number distribution

Figure 3.13 shows that at the lowest temperature of 153°C, the product was mainly C_5 components and some C_{10} and C_{11+} (in this case C_{15}) hydrocarbons. Since the starting material was 1-pentene (C_5), and from the previous set of graphs it was seen that the products were mostly olefinic, it can be assumed that the main reactions at 153°C was double-bond isomerisation of the feed with some dimerisation to C_{10} compounds and trimerisation to C_{15} compounds. Increasing the temperature to 200°C led to a decrease in C_5 components and an increase in C_{10} and C_{15} components, indicating further dimerisation and trimerisation of the C_5 material. At 268°C the feed material was converted into products of a range of carbon numbers. These products are still mostly olefinic, indicating that the dimers and trimers formed are cracking to produce a mixture of hydrocarbons of different carbon numbers. At 320°C and higher, the carbon number distribution shifts to C_6 and higher, as would be expected from the formation of benzene (C_6), toluene (C_7), xylenes and ethylbenzene (C_8) and higher aromatics. An increase in the C_3 and C_4 paraffins is also observed for the higher temperatures.

In Figures 3.14, 3.15 and 3.16 respectively, the lumped groups as function of carbon number are given for a low (200°C), intermediate (320°C) and high (407°C) experimental temperature.

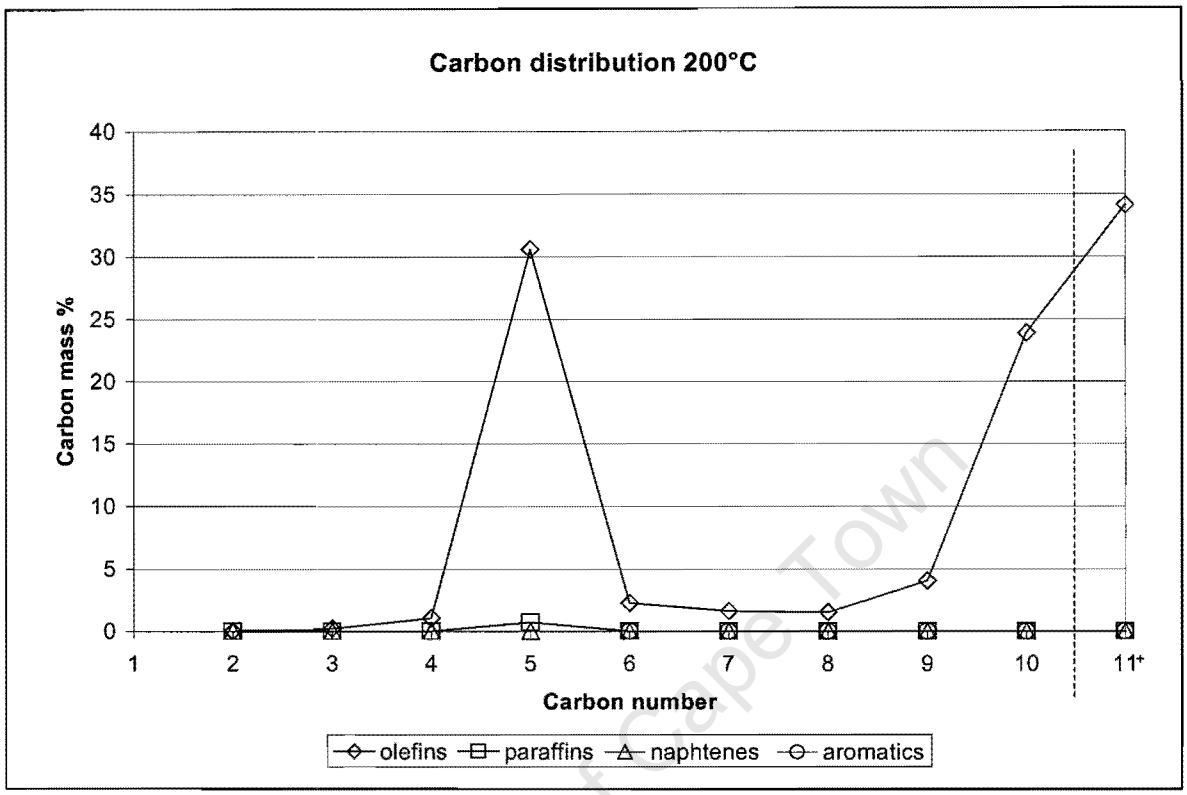

Figure 3.14 Lumped groups as a function of carbon number at 200°C.

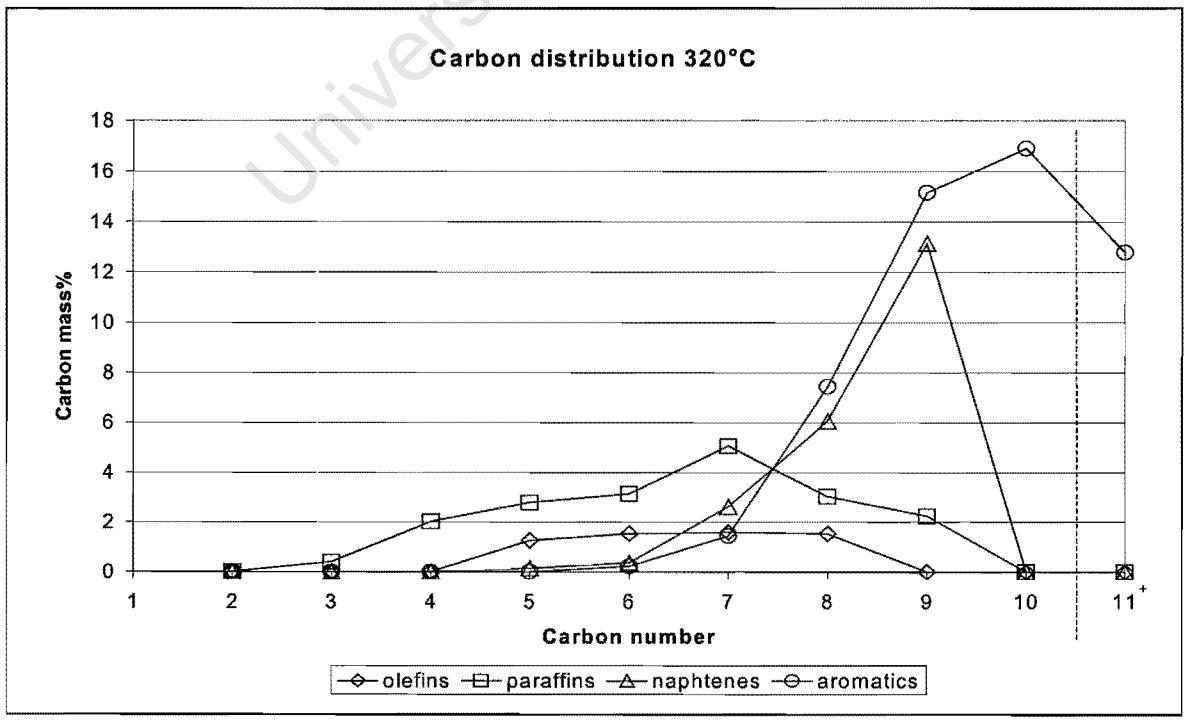

Figure 3.15 Lumped groups as a function of carbon number at 320°C

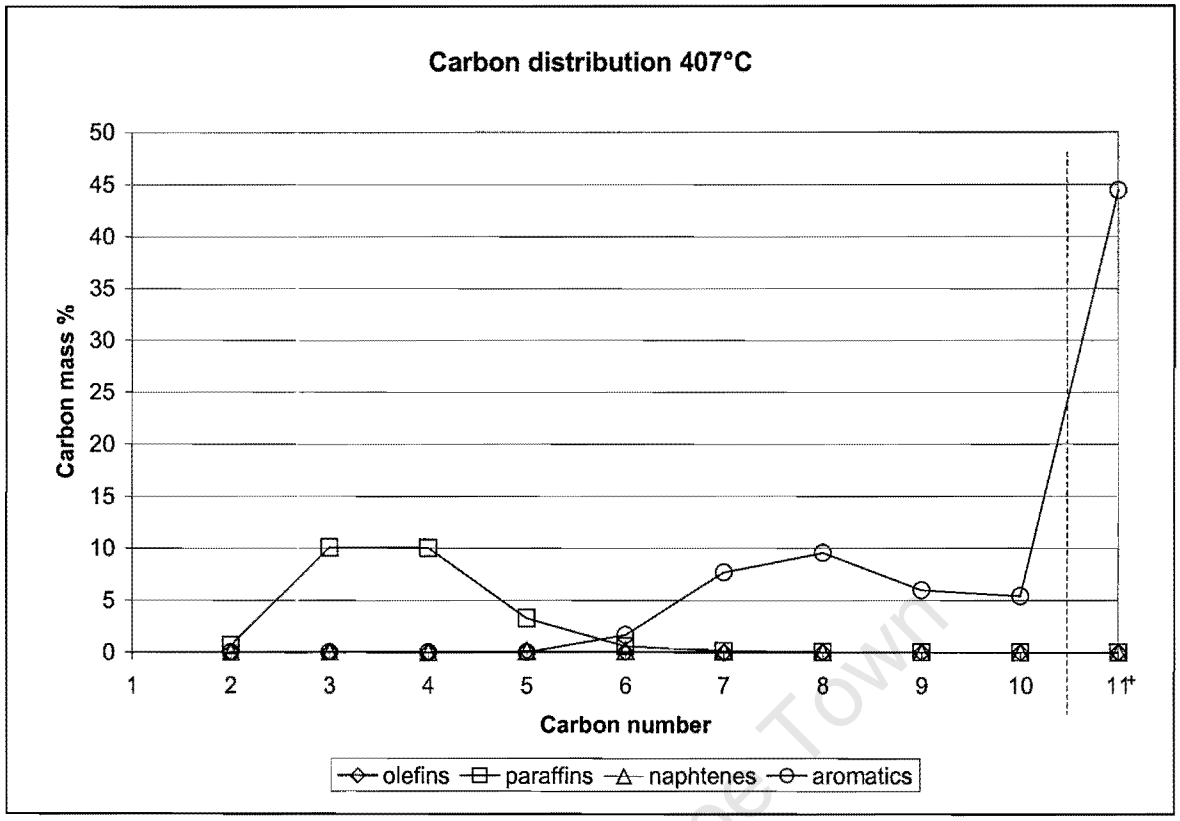

Figure 3.16 Lumped groups as a function of carbon number at 407°C

3.4 Effect of WHSV on the product distrubution

The results of the GC analyses of runs where WHSV was the variable, are summarised in Table 3.6.

Table 3.6 The effect of WHSV on the product distribution

	WHSV (h^{-1})	23	45	68	113
		5z6h	4z6h	3z6h	14z6h
	Actual Average bed temperature (°C)	364	368	372	431
	Set temperature (°C)	360	360	360	360
C no.	Component	C Mass%	C Mass%	C Mass%	C Mass%
2	C2 HC	0.04	0.05	0.11	0.08
3	C3 HC	1.37	1.10	1.78	0.96
4	C4 HC	2.70	2.17	3.49	1.69
5	isopentanes	1.70	1.32	1.99	0.76
5	n-pentanes	0.67	0.56	0.87	0.32
5	isopentenes	0.06	0.13	0.34	0.32
5	n-pentenes	0.02	0.04	0.12	0.12
5	cyclopentane+2,3-dimethyl butane	0.15	0.12	0.21	0.09
6	olefins	0.05	0.14	0.32	0.38
6	paraffins	1.42	1.12	1.64	0.60
6	naphtenes	0.46	0.41	064.	0.25
6	aromatics				
6	Benzene	2.08	1.01	1.39	0.44
7	Toluene	18.38	9.70	11.23	3.43
8	m,p-Xylene	15.33	13.29	17.02	7.95
8	o-xylene	4.42	4.08	5.27	2.70
8	eBz	3.61	2.93	3.47	1.43
	BTX + eBZ	43.83	31.01	38.37	15.95
7	olefins		0.12	0.25	0.43
7	paraffins	0.90	0.78	1.07	0.51
7	naphtenes	0.93	0.95	1.40	1.03
7	aromatics				
8	olefins				
8	paraffins	0.38	0.42	0.55	0.41
8	naphtenes	0.86	1.50	2.37	2.71
8	aromatics				
9	olefins	0.00	0.00	0.00	0.00
9	paraffins	0.04	0.00	0.00	0.27
9	naphtenes	0.46	1.63	1.82	3.80
9	aromatics	14.91	16.47	19.82	15.14
10	olefins	0.00	0.00	0.00	0.00
10	paraffins	0.00	0.00	0.00	0.00
10	naphtenes	0.00	0.00	0.00	0.00
10	aromatics	8.98	10.59	10.06	23.99
11+	olefins	0.00	0.00	0.00	0.00
11+	paraffins	0.00	0.00	0.00	0.00
11+	naphtenes	0.00	0.00	0.00	0.00
11+	aromatics	20.08	29.37	12.78	30.17
	Total	100.00	100.00	100.00	100.00

3.4.1 Lumping groups as PONA (paraffins, olefins, naphtenes, aromatics)

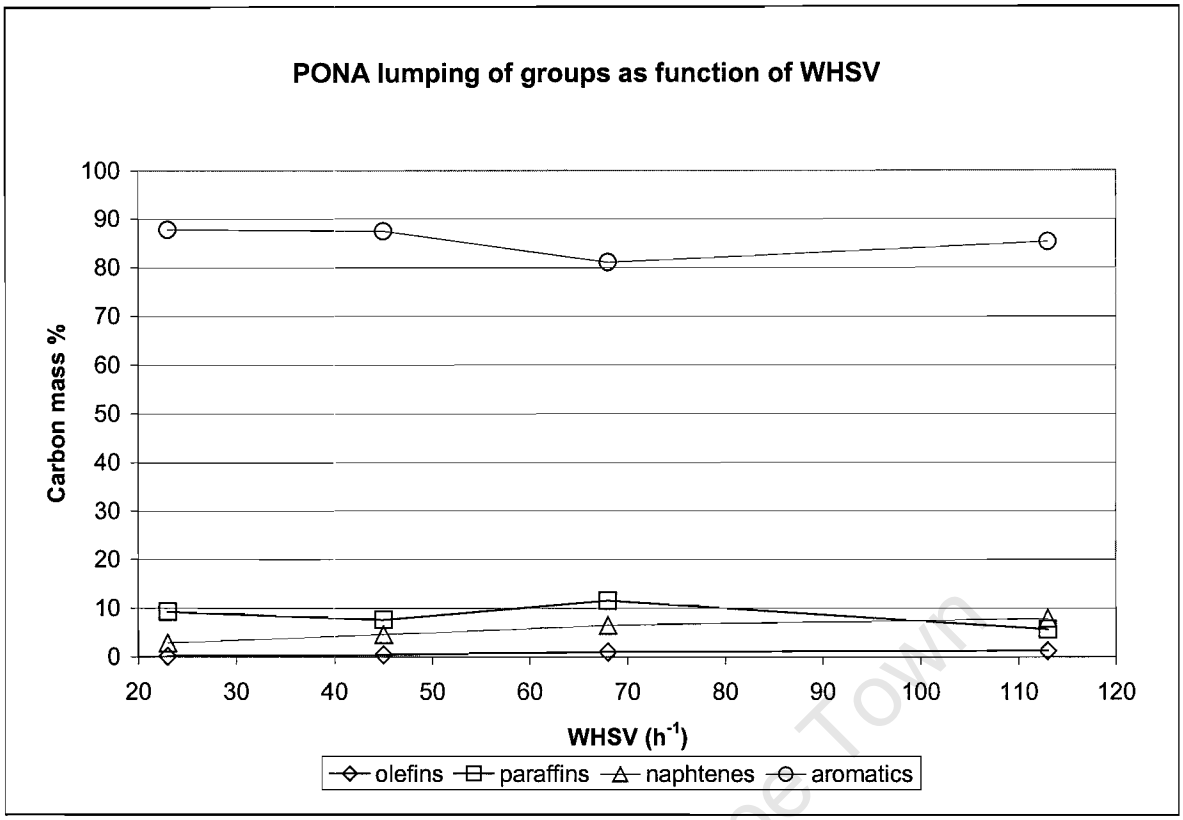

Figure 3.17 PONA lumping as a function of WHSV

Figure 3.17 shows that increasing the WHSV had almost no effect on the main groups of products formed (paraffins, olefins, naphtenes, aromatics). The main products at every WHSV were aromatics and paraffins, with aromatics by far the most abundant. Olefins and naphtenes increased with an increase in WHSV but were never the major products.

3.4.2 Carbon number distribution

Figure 3.18 shows that the formation of heavier compounds (C_7-C_{10}) were favoured at all the WHSV. The major product being aromatics, it can be assumed that the C_7 components are mainly toluene; C_8 components xylenes and ethylbenzene, C_9 components mainly higher aromatics. Figure 3.18 then seems to indicate a decrease in toluene formation with increasing WHSV, a decrease in xylenes and an increase in C_9 aromatics. At WHSV=68 h^{-1} an increase was observed. It is also interesting to see that the WHSV=113 h^{-1} data does not go through a maximum as in the cases of the other WHSV. This could be attributed to the high reaction temperature that was observed for the WHSV=113 h^{-1} run. It is expected that more BTX will

be produced at higher temperatures. The results, however, indicate less BTX, indicating that the WHSV dominates here, producing more high aromatics.

The decrease in BTX and EB with increasing WHSV (Figure 3.18) and increase in naphtenes with increasing WHSV (Figure 3.17) suggest that the formation of BTX and EB from 1-pentene proceeds via naphtenes. At the lower WHSV the reaction kinetics for the formation of BTX and EB is probably so fast that the naphtenes are not detected.

A decrease in BTX and EB with increasing WHSV (Figure 3.18) would be expected due to the shorter contact time. The increase in C9 and C10 products (mainly aromatics) with increasing WHSV can probably be attributed to less cracking reactions or paring reactions taking place at the shorter contact time.

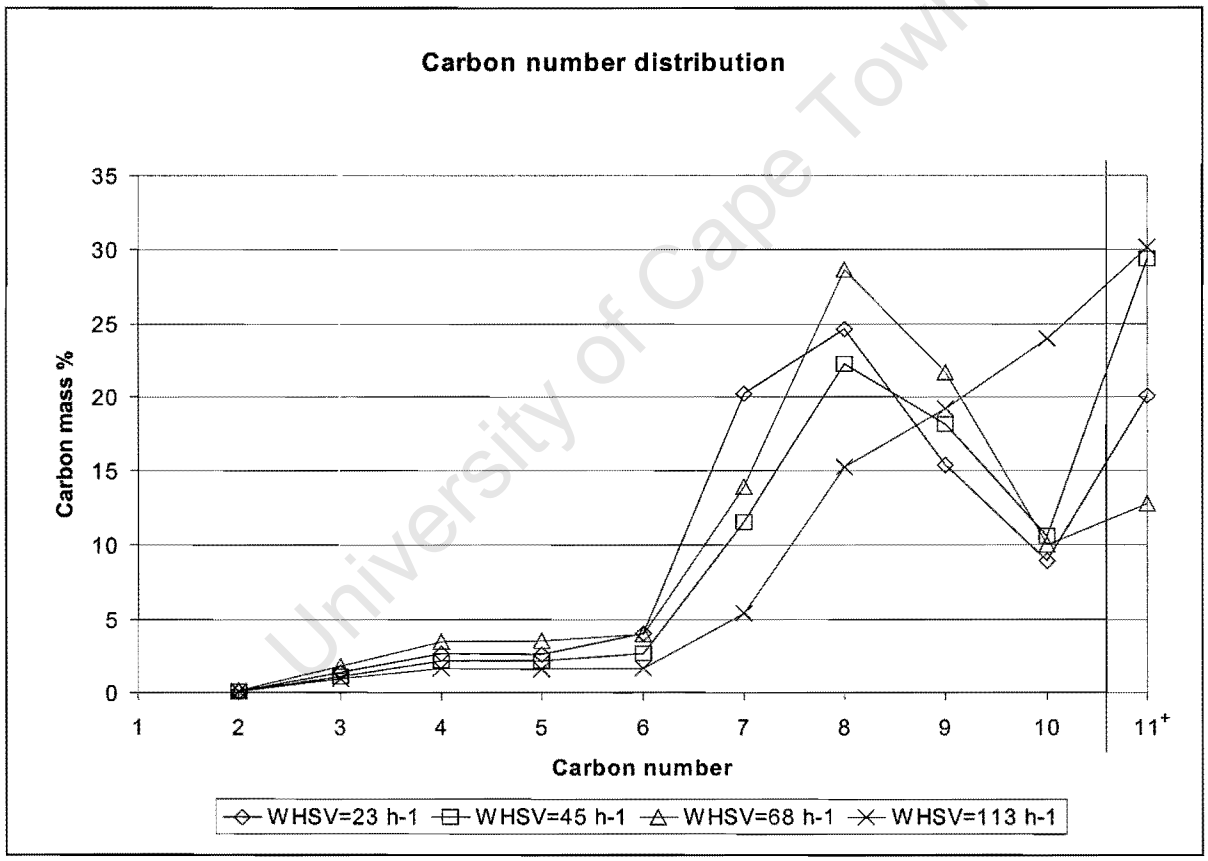

Figure 3.18 Carbon number distribution for WHSV runs

3.5 The effect of pressure and carrier gas on the product distribution.

The results of the GC analyses of runs where pressure/carrier was the variable, are summarised in Table 3.7.

Table 3.7 The effect of pressure and carrier gas on the product distribution

	Total pressure (bar)	2	2	5	2	5	5
	H_2 (H_2:feed molar ratio)	0	0	0	1	1	1
	Actual average bed temperature (°C)	364	367	379	373	363	372
	Set temperature (°C)	360	360	360	360	360	360
		5z	8z	9z	10z	12z	19z
C no.	Component	C Mass %	C Mass %	C Mass %	C Mass %	C Mass %	C Mass %
2	C2 HC	0.04	0.06	0.05	0.23	1.42	0.50
3	C3 HC	1.37	2.09	2.22	2.36	11.89	7.99
4	C4 HC	2.70	3.77	4.14	5.43	24.75	15.67
5	isopentanes	1.70	1.89	2.64	2.37	11.29	6.76
5	n-pentanes	0.67	0.69	1.02	1.01	4.96	2.35
5	isopentenes	0.06	0.06	0.06	0.29	0.40	0.27
5	n-pentenes	0.02	0.02	0.03	0.04	0.00	0.07
5	cyclopentane+2,3-dimethyl butane	0.15	0.11	0.17	0.19	1.01	0.45
6	olefins	0.05	0.03	0.05	0.15	0.03	0.13
6	paraffins	1.42	1.11	1.87	1.40	5.20	3.34
6	naphtenes	0.46	0.27	0.32	0.56	1.59	0.80
6	Benzene	2.08	0.88	1.45	0.41	0.89	0.73
7	Toluene	18.38	7.91	8.12	3.90	4.69	5.02
8	m,p-Xylene	15.33	11.86	10.18	7.74	4.28	6.41
8	o-xylene	4.42	3.86	3.42	2.60	1.26	1.98
8	eBz	3.61	2.69	2.29	1.77	0.94	1.55
	BTX + eBZ	43.83	27.20	25.46	16.42	12.07	15.68
7	olefins						
7	paraffins	0.90	0.51	0.72	0.68	1.80	1.30
7	naphtenes	0.93	0.48	0.62	1.37	2.68	1.54
7	aromatics						
8	olefins						
8	paraffins	0.38	0.21	0.24	0.38	0.79	0.56
8	naphtenes	0.86	0.53	0.52	1.64	1.16	1.36
8	aromatics						
9	olefins						
9	paraffins	0.04	0.04	0.00	0.02	0.00	0.08
9	naphtenes	0.46	1.65	0.48	1.94	0.10	0.56
9	aromatics	14.91	18.68	16.38	15.78	4.01	8.68
10	olefins						
10	paraffins						
10	naphtenes						
10	aromatics	8.98	13.79	15.75	13.82	1.92	5.19
11+	olefins						
11+	paraffins						
11+	naphtenes						
11+	aromatics	20.08	26.79	27.26	33.94	12.95	26.72
	Total	100.00	100.00	100.02	100.00	100.00	100.00

Note: The temperatures for all repeat runs were set to the same value at the start of the run. Differences in exotherms upon addition of the feed, led to different actual catalyst bed temperatures for these runs.

The base case for investigating the effect of carrier and pressure, were the runs with argon at a pressure of 2 bar, temperature of 360°C and WHSV of 23 h^{-1}. Four cases can be seen from the table:

1. Effect of increasing pressure from 2 bar to 5 bar with argon as diluent.
2. Effect of keeping pressure at 2 bar but using hydrogen as diluent, i.e. changing diluent at 2 bar pressure.
3. Effect of increasing pressure from 2 bar to 5 bar with hydrogen as diluent.
4. Effect of changing diluent at 5 bar pressure.

3.5.1 Carbon number distribution of PONA groups

The PONA (paraffin, olefin, naphtenes, aromatics) group distribution as a function of carbon number is depicted in Figures 3.19–3.22.

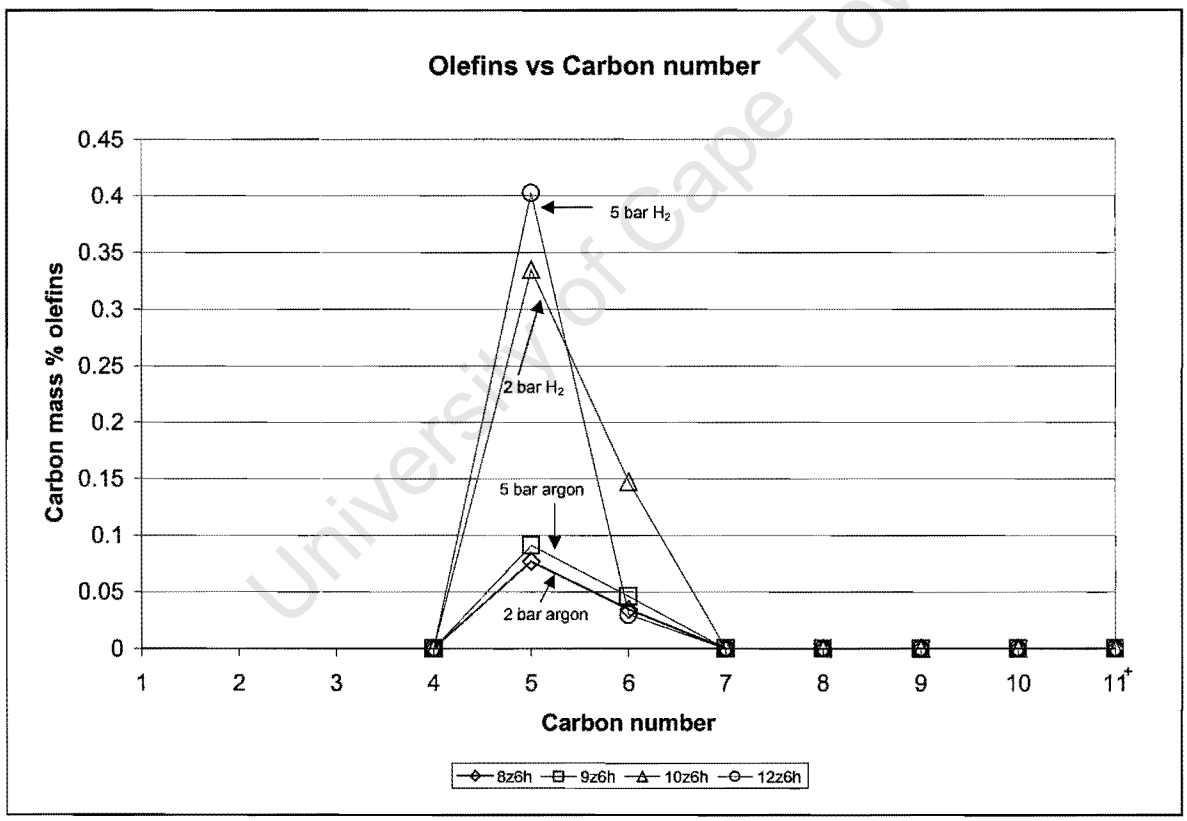

Figure 3.19 Olefins vs carbon number

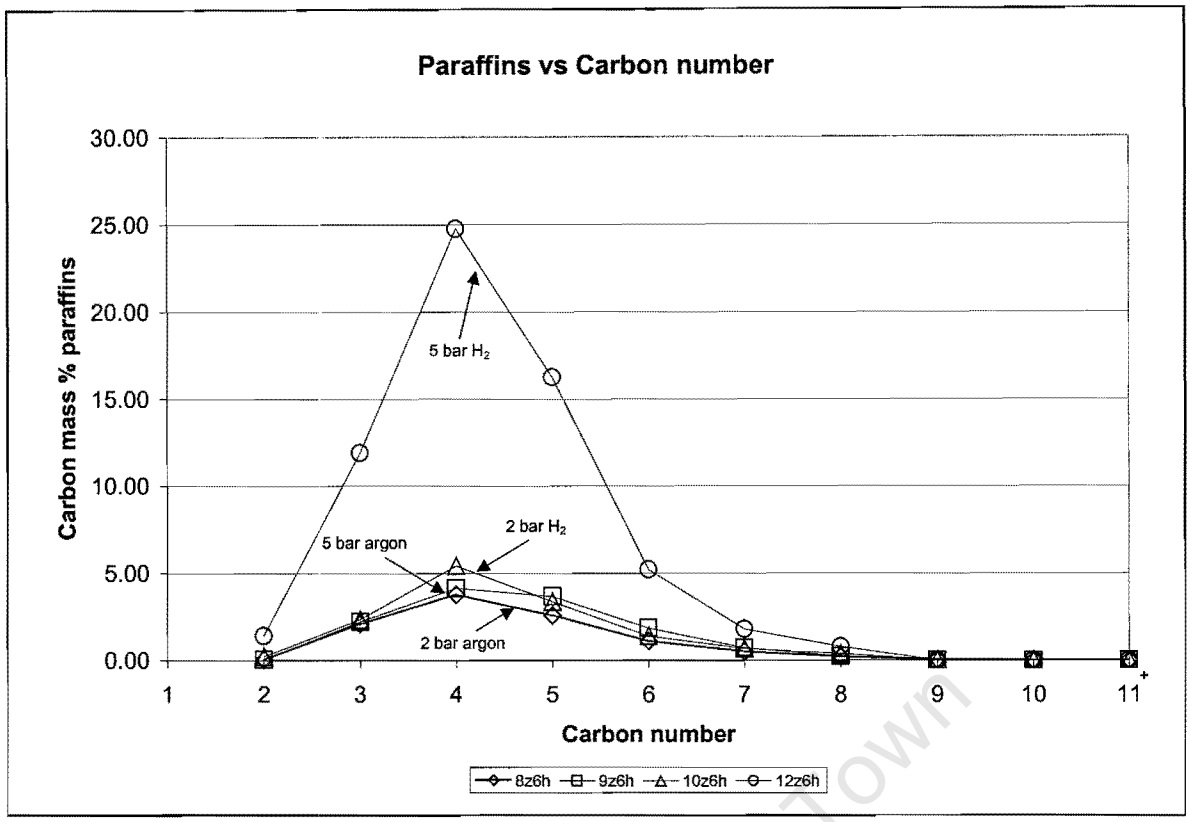

Figure 3.20 Paraffins vs carbon number

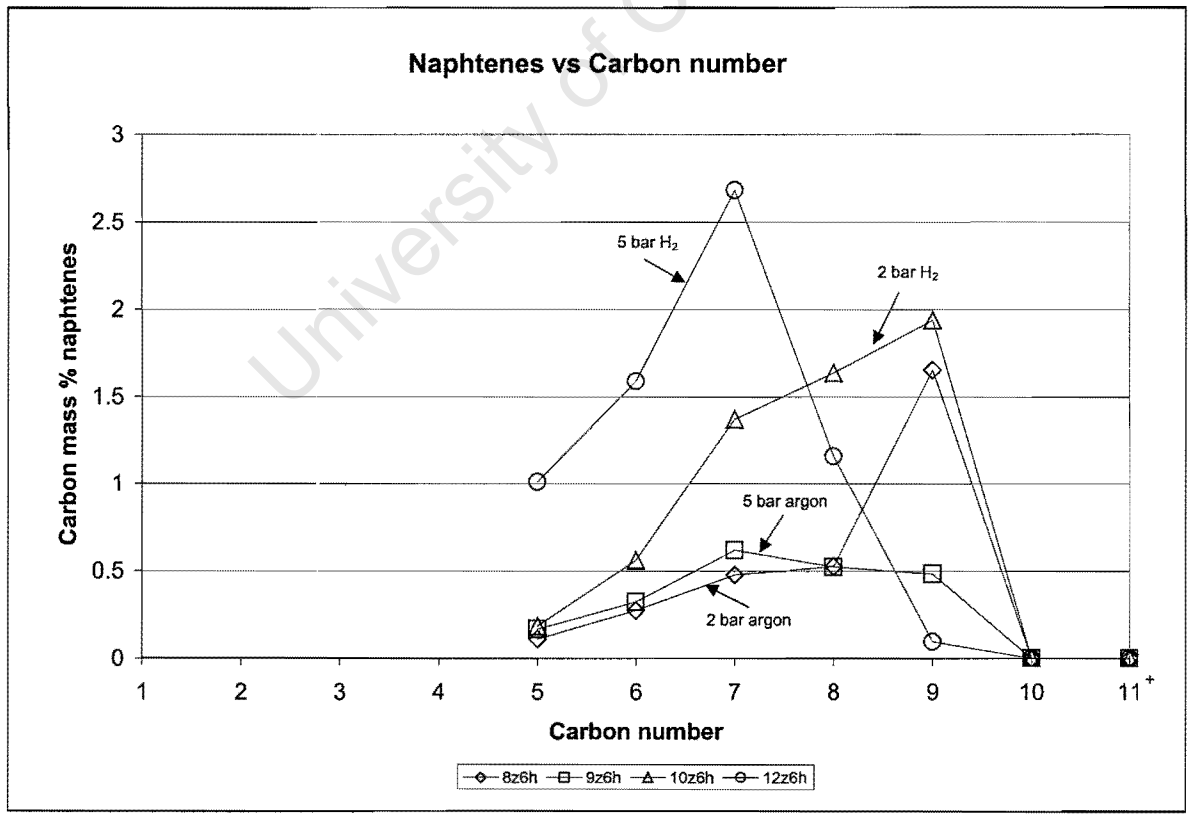

Figure 3.21 Naphtenes vs carbon number

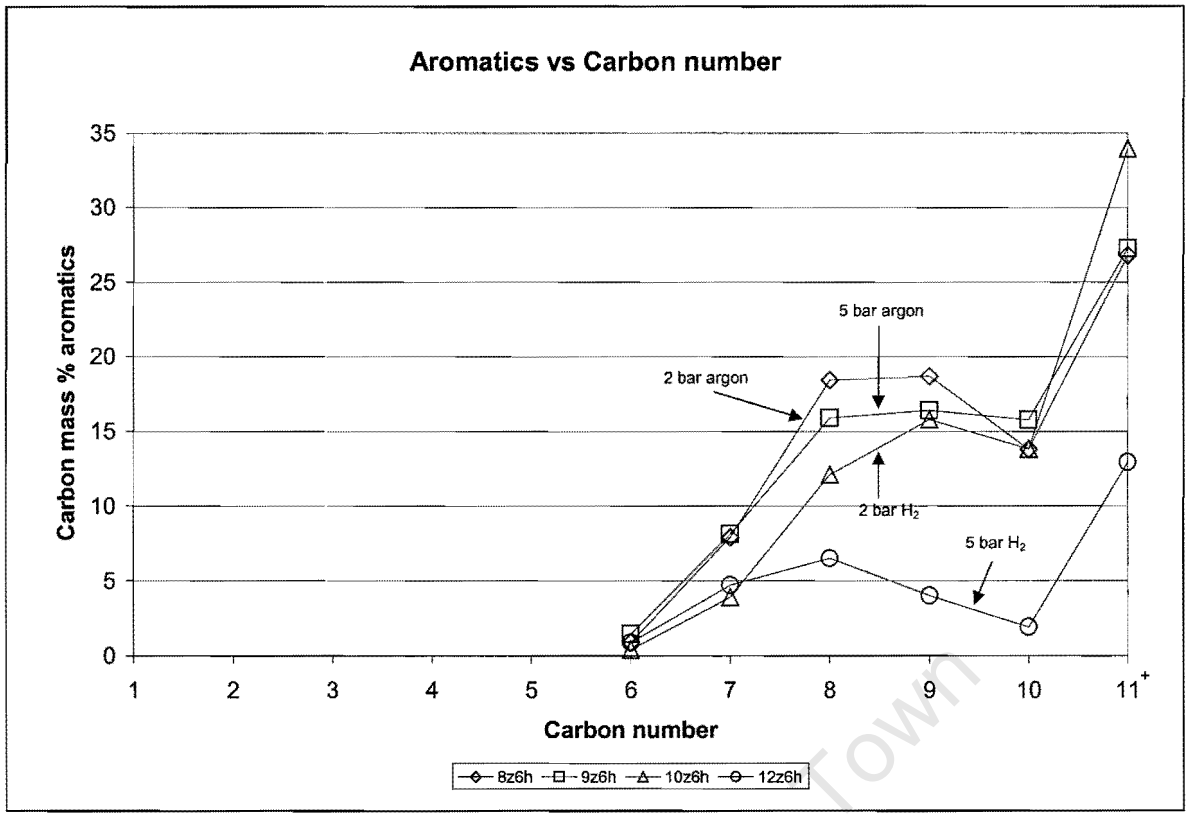

Figure 3.22 Aromatics vs carbon number

1. Effect of increasing pressure from 2 bar to 5 bar with argon as carrier:

Comparing base case 8z with 9z:

Only a small amount of olefins was detected in the product and only C_5 and C_6 olefins. Increasing the pressure with argon as carrier had no effect on the olefin content. (Figure 3.19.) Small increases in C_4-C_6 paraffins were observed. (Figure 3.20.) Naphtenes showed a slight increase in C_6-C_8 naphtenes and a decrease in C_9 naphtenes, although the amount of naphtenes in the product is low (Figure 3.21.) The benzene (C_6) content increased slightly and toluene (C_7) remained unchanged. C_8 and C_9 aromatics decreased slightly while a slight increase was observed for C_{10} aromatics. (Figure 3.22.) Overall thus, increasing the pressure with argon as carrier seems to have had no effect.

2. Effect of keeping pressure at 2 bar but adding hydrogen as carrier:

Comparing base case 8z with 10z:

A bigger increase in C_5 and C_6 olefins was observed than by increasing the pressure under argon flow, although the olefins are still in very small quantities (Figure 3.19). The C_4-C_6

paraffin increase is also slightly more than in the case of just increasing the pressure. A more marked increase in naphtenes was observed, although once again, the naphtenes make out a small part of the product. A clear decrease in C_6-C_9 aromatics (thus BTX+EB and C_9 aromatics) was observed, while C_{10} aromatics remained unchanged and C_{11+} aromatics inceased. The most visible effect of using hydrogen as carrier is thus to decrease BTX and EB as well as C_9 aromatics, while increasing heavier aromatics. Also, especially in the case of naphtenes and aromatics, the use of hydrogen had a much more pronounced effect than increasing the pressure without addition of hydrogen.

3. Effect of increasing pressure from 2 bar to 5 bar with hydrogen as diluent

Comparing 10z with 12z:

An increase in C_5 olefins but a decrease in C_6 olefins is observed. A marked increase in paraffins, especially C_3-C_6 was observed. It has been reported (Senger and Radom 2000, Sano et al. 1986, and Jacobs et al. 1992) that H-ZSM-5 (transition metal-free) is active as a hydrogenation catalyst. At low temperatures (350°C), Na^+ ions are thought to be the active sites while Brønsted acid sites are thought to be the active sites for hydrogenation at high temperature (450°C). C_5-C_7 naphtenes increased while C_8 and C_9 naphtenes decreased. A slight increase in benzene and toluene and a big decrease in xylenes and ethylbezene (C_8) and higher aromatics were observed. Thus overall there is an increase in non-aromatic compounds and a decrease in aromatic compounds. The same trends for olefins, paraffins, naphtenes and aromatics were observed when increasing the pressure with only argon as carrier (see point 1). The changes were, however, much more pronounced with the addition of hydrogen. This indicates a chemical effect and not just a physical effect due to the increase in pressure.

4. The effect of changing diluent at 5 bar pressure:

Comparing 12z (5 bar hydrogen) with 9z (5 bar argon)

Adding hydrogen at 5 bar pressure increased the C_5 olefins but decreased the C_6 olefins slightly. (The same trend was found when changing diluent at 2 bar pressure.) Paraffins increased markedly, especially C_3-C_6 paraffins. This gives clear evidence that hydrogen is being incorporated into the products. (This effect was not so pronounced at 2 bar pressure.) An increase in C_5-C_8 naphtenes but a decrease in C_9 naphtenes was observed. (An increase in

C_5-C_8 naphtenes was also observed at 2 bar.) A marked decrease in BTX+EB and heavier aromatics was observed. (The effect was more pronounced at 5 bar than at 2 bar.) The main effect of adding hydrogen was thus a marked increased in paraffins and a marked decrease in aromatics. This effect was more pronounced at 5 bar than at 2 bar.

In addition: increasing the pressure had more of an effect with hydrogen as carrier than with argon. Adding hydrogen had a more pronounced effect at the higher pressure of 5 bar than at 2 bar.

Chapter 4 Discussion and Conclusions

4.1 Influence of temperature

4.1.1 Conversion

Figure 4.1 shows that the conversion of 1-pentene is complete above 200°C. At 150°C the conversion of 1-pentene is mainly to double bond isomers, which is well known to be a rapid reaction over acid catalysts. However, due to this rapid reaction at low temperatures, it may be assumed that the pentene linear isomers are in equilibrium. This is shown in Figure 4.2. Thus, at temperatures above 150°C, the linear pentene group may be considered as the feed to the reactor. If this is done the complete conversion of the linear pentenes is achieved at around 250°C. These results are similar to those obtained by Oblad et al. (1947) and Mäurer and Kraushaar-Czarnetzki (1999). The pentene conversion to other hydrocarbons is very rapid at low T. It is clear that the slow step in these reactions must be due to sequential reaction steps.

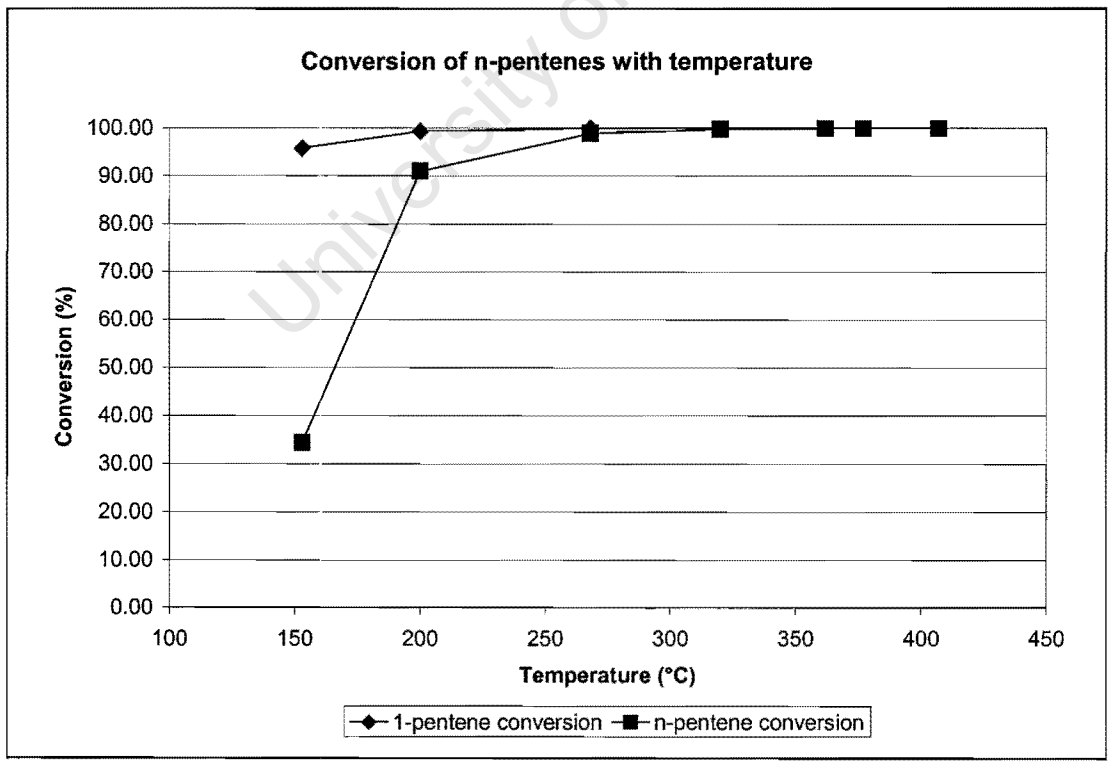

Figure 4.1 Conversion of n-pentenes as a function of temperature

The conversion of n-pentenes increased rapidly from about 34% (run at 153°C) to almost 100% conversion (runs at 268°C and higher), indicating that the 2-pentenes are also converted to other products rapidly at relatively low temperatures.

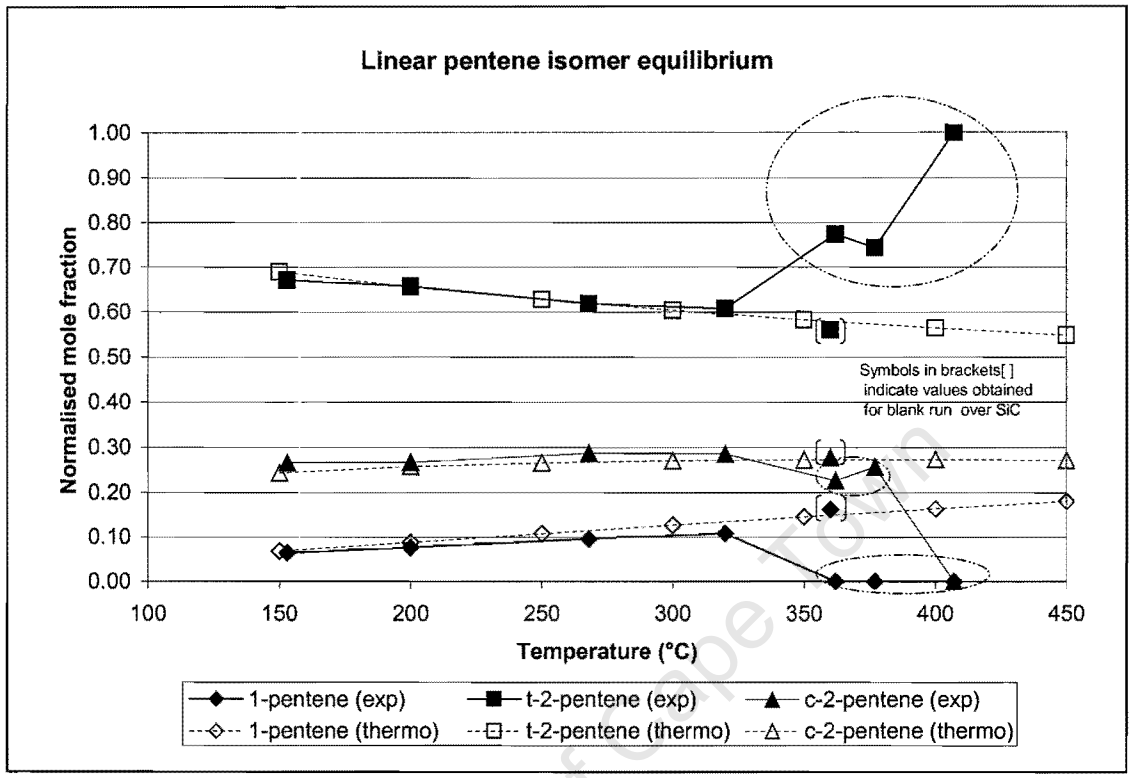

Figure 4.2 Linear pentene isomer equilibrium

The data circled in Figure 4.2 does not follow the normal equilibrium trend. Two factors may be contributing to this. Fast secondary reactions convert the 1-$C_5^=$ very rapidly and lead to the observed shift. It is, however, unlikely that these steps are faster than linear pentene conversion. It is more likely that an error in analysis has occurred due to the extremely low concentrations of $C_5^=$ species. Linear $C_5^=$ equilibrium is therefore assumed for the high temperatures. The SiC data (indicated by square brackets in Figure 4.2) shows that linear $C_5^=$ equilibrium is possible at the high temperatures.

4.1.2 Reaction types

4.1.2.1 Isomerisation

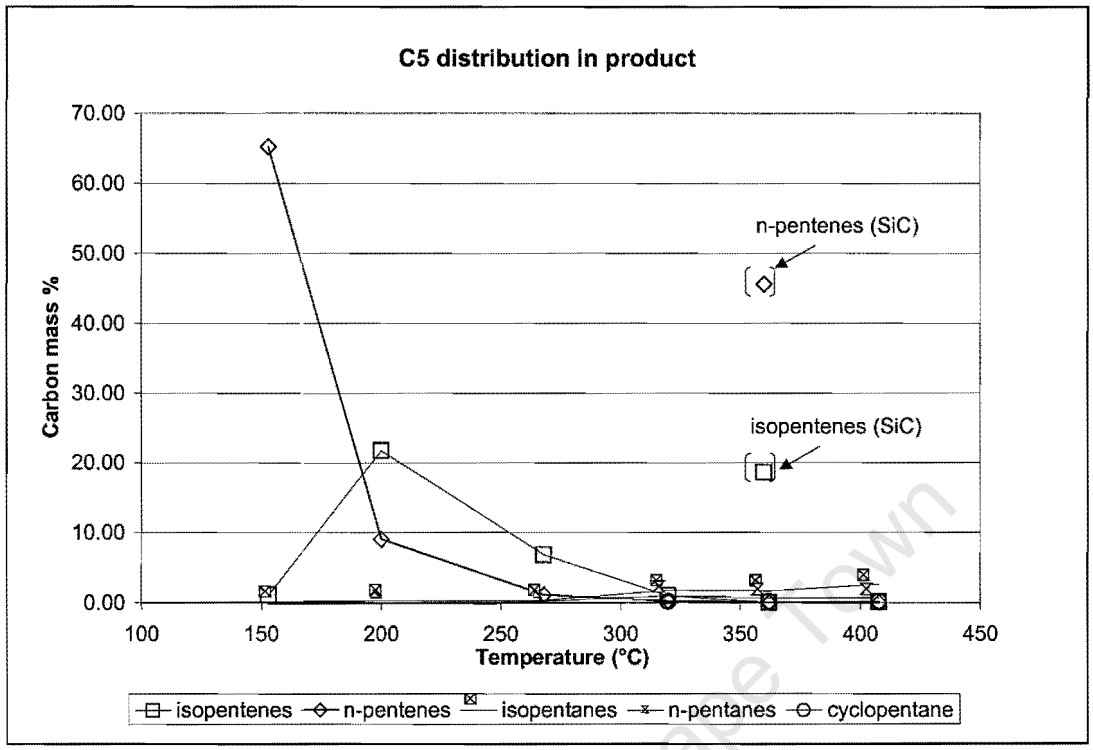

Figure 4.3 C_5 distribution in product

A breakdown of the C_5 components in the product is shown in Figure 4.3. Pentanes (linear, branched and cyclic) only contributed a small fraction to the total product. Cyclopentane formation was only detected at 320°C and higher. An increase in n-pentane and isopentane was observed with increasing temperature.

Double-bond isomerisation

Linear pentenes were the main product components at 153°C (66.40 carbon mass %) but declined sharply as the temperature was increased. Double-bond isomerisation of 1-pentene was the dominant reaction at 153°C. Over aluminas, Oblad et al. (1947) found that only double-bond isomerisation took place at temperatures below 250°C. As shown in Figure 4.2, the linear pentenes were in thermodynamic equilibrium below 320°C. At higer temperatures the experimental data points deviate from the thermodynamic data. This is because at the high temperatures, not all the C_5 isomers could be detected in the product and these calculations are thus based on incomplete data (the same holds for Figures 4.4-4.5). At high

temperature the $C_5^=$ species concentration is extremely low and difficult to measure and the error in analysis thus high. In Figures 4.2-4.5 the data points for the blank run with SiC at 360°C are indicated with square brackets.

Skeletal isomerisation

A small amount of isopentenes (1.08%) was detected at 153°C (Figure 4.3). As can be seen from the Figure 4.4 and Figure 4.5, this is well below the thermodynamic equilibrium value. At 200°C the highest value for skeletal isomers was obtained. Mäurer and Kraushaar-Czarnetzki (1999) found the maximum overall yield for 2-methyl-1-butene (2M1B) and 2-methyl-2-butene (2M2B) at 280°C in their experiments. As predicted by thermodynamics, skeletal isomerisation decreased with increasing temperature. Between 200°C and 268°C the branched isomers were in thermodynamic equilibrium. As mentioned previously, the experimental data for the skeletal isomers at higher temperatures is not in line with thermodynamic data due to difficulties in detecting the isomers accurately.

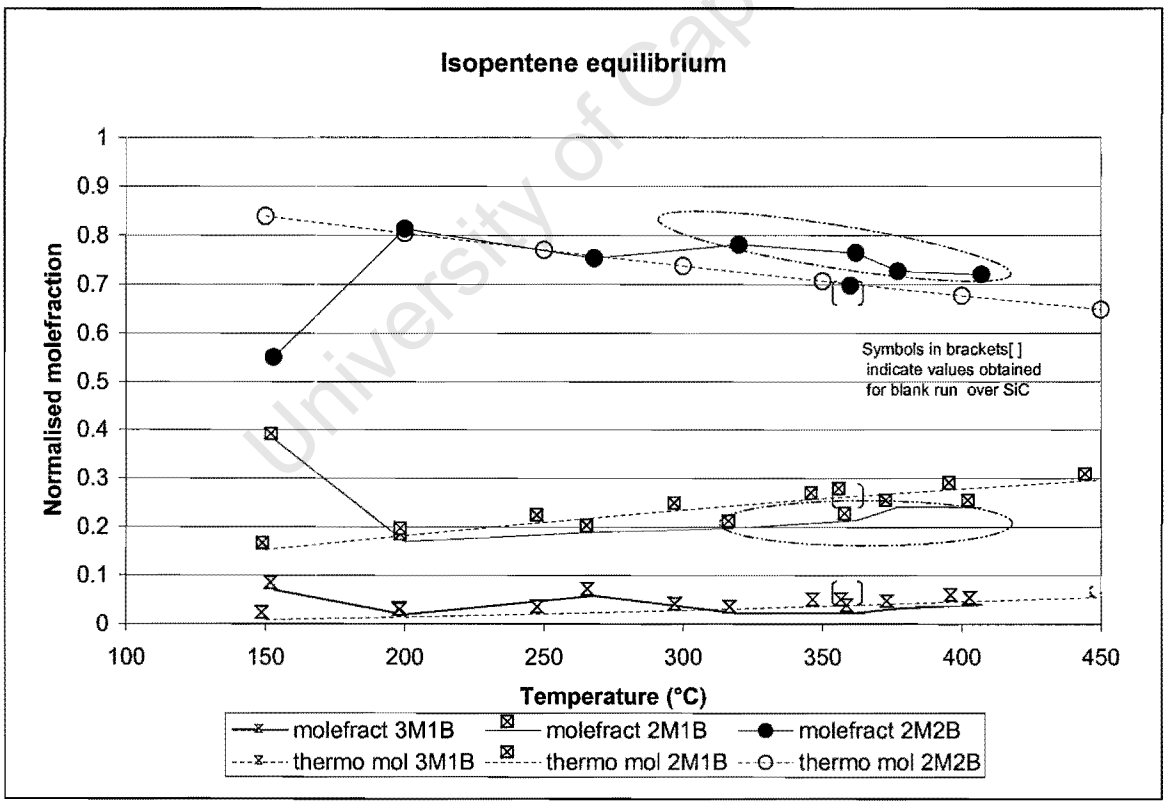

Figure 4.4 Isopentene equilibrium

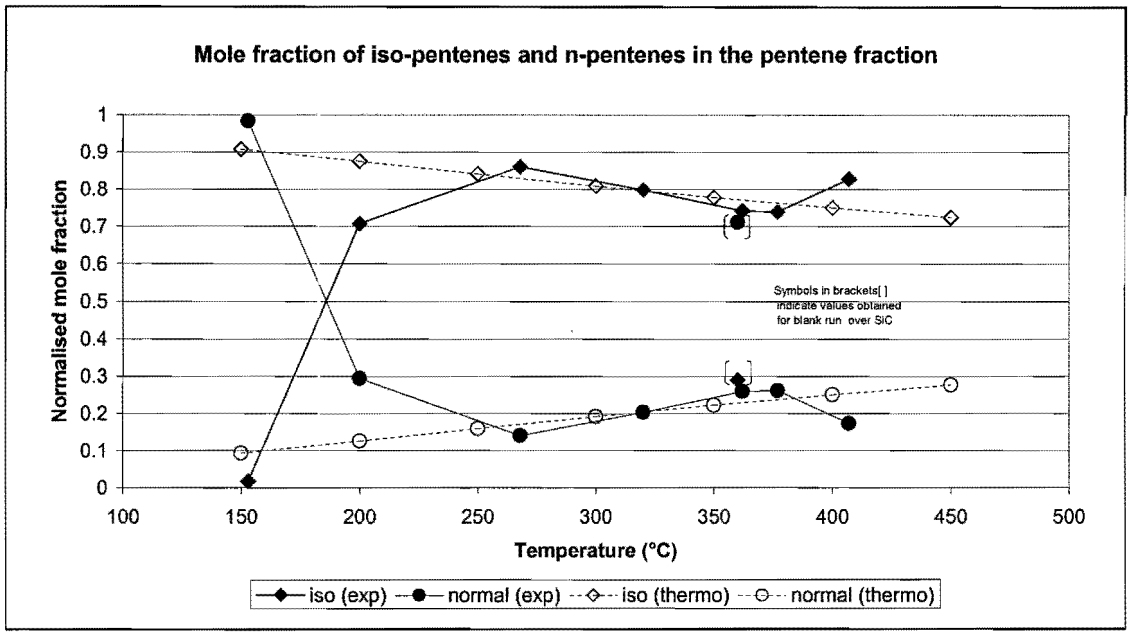

Figure 4.5 Total equilibrium in the pentene fraction

In Figure 4.5 the experimentally obtained mole fractions of iso-pentenes is compared with the thermodynamic data. From this comparison it is clear that the experimental data approached thermodynamic equilibrium in the temperature range between 250°C and 320°C. In their work, Ewell et al. (1941) reported equilibrium between 1-pentene and 2-pentene at temperatures ranging from 265°C to 365°C. The temperature range 250° C to 280°C was found by Mäurer and Kraushaar-Czarnetzki (1999) to be the range where skeletal isomerisation is kinetically controlled. Others (Höchtl et al., 2001) found skeletal isomerisation the prevailing reaction only at temperatures below 270°C. Otherwise dimerisation to higher alkenes and cracking were the main reactions. An equilibrium distribution can be maintained in this temperature range, despite continuous withdrawl of pentenes for other reactions, due to the sufficient rate of skeletal isomerisation (Höchtl et al., 2001). At 153°C, where mostly double-bond isomerisation and oligomerisation took place, the skeletal isomers are not in equilibrium. The experimental n-pentene values (0.06 1-pentene, 0.7 t-2-pentene, 0.27 c-2-pentene) are, however, in agreement with the thermodynamic data (0.07 1-pentene, 0.69 t-2-pentene, 0.24 c-2-pentene) for n-pentenes if only the n-pentenes are considered (Figure 4.2). The approach to equilibrium distribution depends on the strength of the acid sites, the pore dimensions and the structure of the catalyst (Höchtl et al., 2001). Although the highest skeletal isomer content (carbon mass %) was found at 200°C, the isomers were not in thermodynamic equilibrium here. This is probably due to the oligomerisation reactions being kinetically favoured. The skeletal isomerisation

reaction is also not fast enough to reach equilibrium at low temperature and requires longer residence times. The equilibrium distribution obtained over H-ZSM-5 is disturbed by the further reaction of the "pentene pool" by dimerisation and cracking (Höchtl et al., 2001, Mäurer et al., 1999).

The reason for obtaining the maximum isopentenes at a lower temperature (200°C) than the 280°C of Mäurer and Kraushaar-Czarnetzki (1999) might be ascribed to the difference in acidity of the zeolite catalysts used. Walendziewski and Pniak (1996) studied the influence of acidity of ZSM-5 catalysts on 1-pentene skeletal isomerisation activity. The ZSM-5 catalysts that were the most active for skeletal isomerisation reactions were those with medium or strong acidity, i.e. with a low or medium silica/alumina mole ratio (up to 50 mol/mol). Houzvicka et al. (1998) also found that catalysts of moderate acid strength have the highest selectivity for skeletal isomerisation. The Si/Al ratio of 48 implies a higher acidity than the Si/Al ratio of 59 of Mäurer and Kraushaar-Czarnetzki (1999), which could explain the higher activity and therefore lower temperature at which skeletal isomerisation was observed.

Isomerisation of carbon chains with lengths > C5

The many peaks in the chromatogram at higher temperatures indicate that isomerisation of carbon numbers higher than C_5 also took place. As the carbon chain length increases, not all isomers are formed due to shape selectivity of the H-ZSM-5 catalyst. Equilibrium ratios are therefore not observed. Determining theoretical equilibrium ratios for carbon numbers higher than C_6 (18 possible isomers) is also difficult because of the great number of possible isomers for the higher carbon numbers (895 possible isomers for C_{10}).

4.1.2.2 Oligomerisation

In Figure 4.6 the C_{10} and C_{15} olefins (oligomers of n-pentenes) are plotted as a function of temperature. Only data for the lower temperatures could be obtained. At temperatures above 268°C the C_{10} and C_{15} olefins (if any) could not be distinguished from the other C_{10} and C_{15} products and have been assumed to decrease. The presence of many C_2-C_4 and C_6-C_9 compounds indicate a significant degree of secondary reactions, i.e. cracking of the long chain olefins.

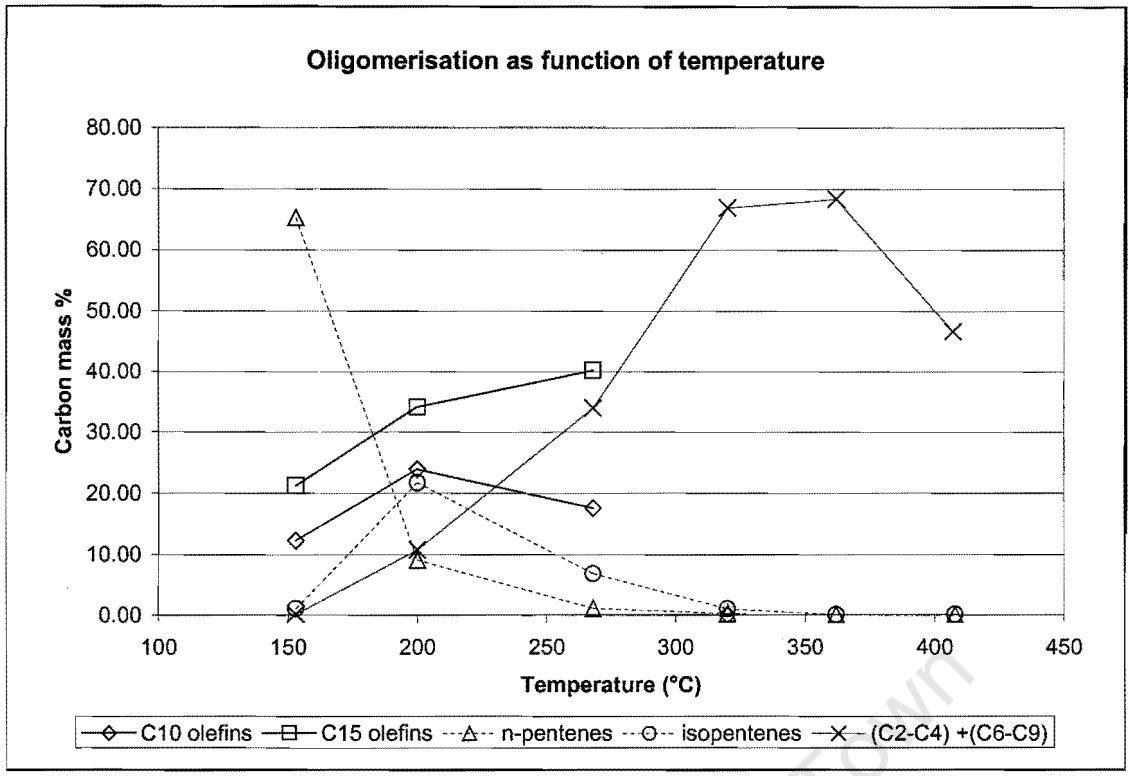

Figure 4.6 Oligomers and pentenes

4.1.2.3 Cracking

The formation of light products increased with increasing temperature (Figure 4.7). This coincided with a decrease in C10 olefins (dimers) and C15 olefins (trimers). C_2 hydrocarbons were first detected at 320°C, the same temperature at which aromatics formation started. It is interesting to note that the amount of light products for the blank run (SiC, 360°C) were very similar to those at 362°C using a catalyst. This seems to suggest that the temperature had a larger influence on cracking activity than the acidity of the catalyst.

Cracking is preceded by double-bond and skeletal isomerisation (Egloff et al., 1939, Buchanan et al., 1996). The secondary reactions of olefins, viz. isomerisation, hydrogen transfer, polymerisation and aromatisation, are important because they influence the products from catalytic cracking (Voge et al., 1946).

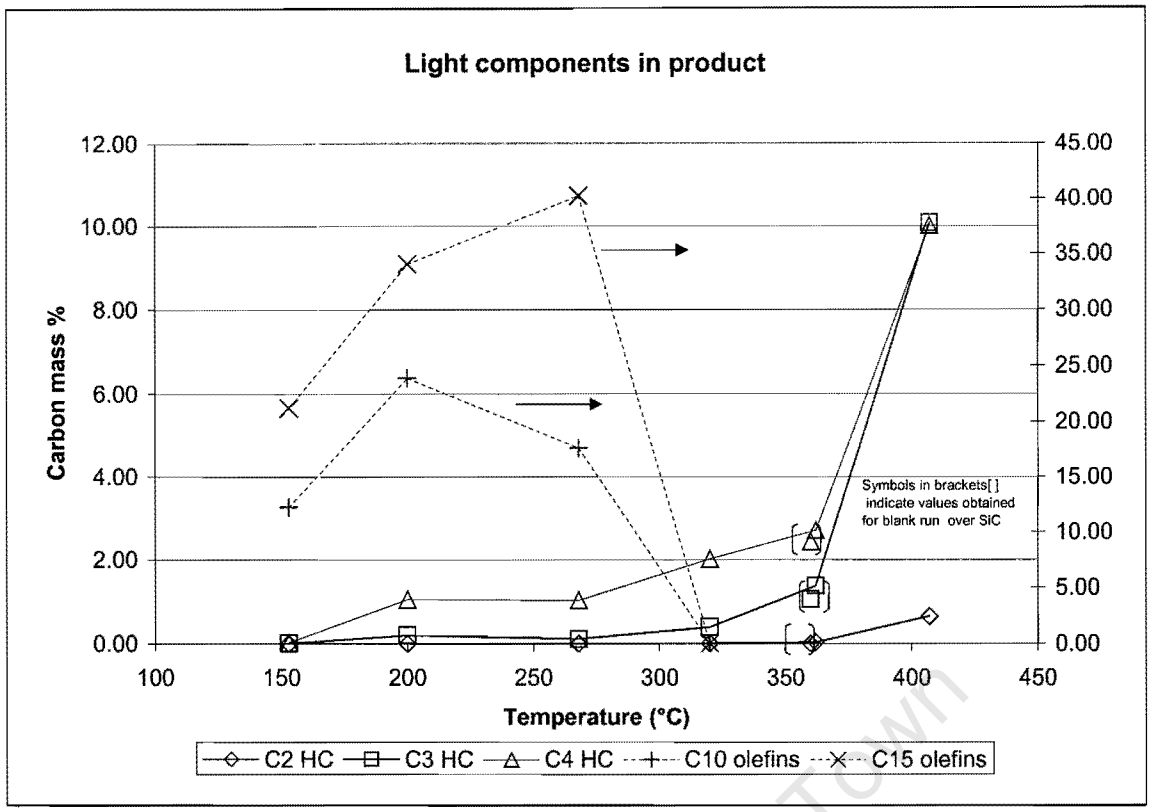

Figure 4.7 Light components in product

In Figure 4.8, the presence of C_4 and C_6 hydrocarbons and C_3 and C_7 hydrocarbons in the product obtained at 153°C (although extremely low quantities) indicate that cracking took place by the bimolecular mechanism (dimerisation of C_5 feed followed by cracking). Cracking of C_5 by the monomolecular mechanism would have yielded C_2 and C_3 products (Buchanan et al., 1996). At higher temperatures, the presence of C_2 could be due to cracking from other hydrocarbon chains, e.g. cracking of C_8 or higher. This makes it difficult to determine whether the monomolecular cracking mechanism was dominant for C_5 cracking at higher temperatures. For carbon numbers higher than C_5 the monomolecular mechanism increases in importance. Buchanan et al. (1996) found that the rate of olefin cracking increases dramatically as function of carbon number, especially for C_5 through C_8. Cracking of pentene would at some stage involve the formation of a primary carbocation, while octene cracking can proceed via tertiary carbocation intermediates. Dimerisation (a prerequisite for the bimolecular mechanism) becomes more difficult for longer-chain molecules due to diffusional limitations within the pore system as well as the lower probability of coincident reaction centres of the molecules (Quann et al., 1988). The observed maxima for C_7 and C_8 in Figure 4.8 indicate that secondary reactions, such as $C_3 + C_4$, $C_4 + C_4$, $C_3 + C_5$, etc. are taking place.

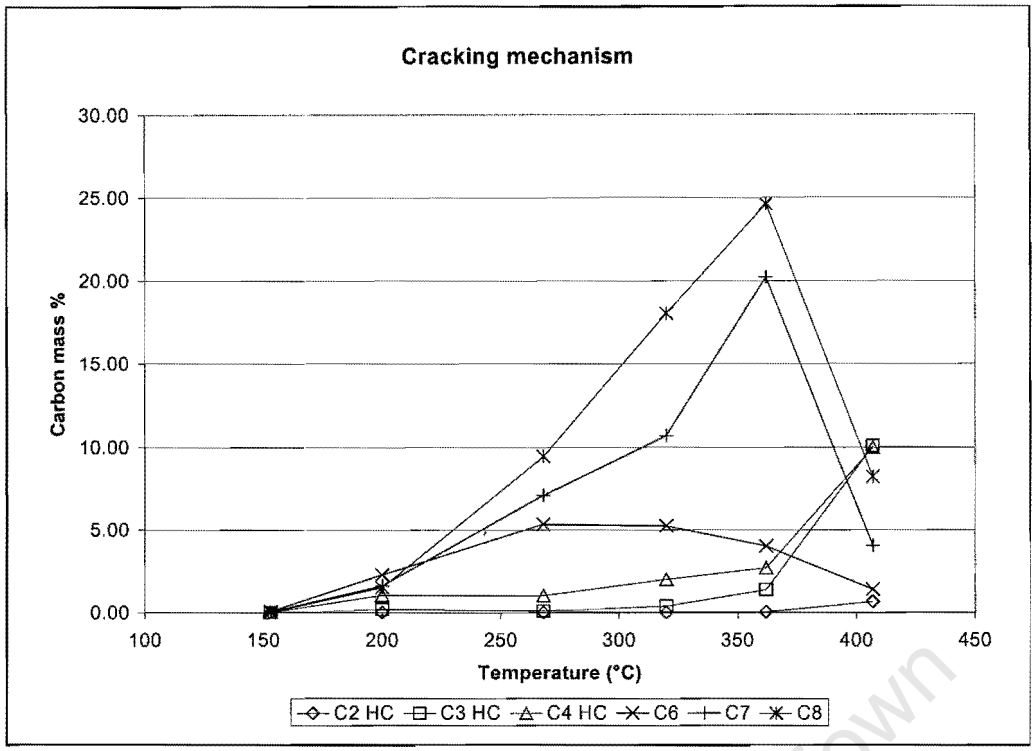

Figure 4.8 Cracking of C_5 via the bimolecular mechanism

4.1.2.4 Aromatisation

In the discussion on aromatics the main focus will be on BTX and EB, since these are the most important aromatics to industry. Aromatics were first detected at 320°C, the same temperature at which naphtenes were detected. At higher temperatures the kinetics of aromatisation is probably so rapid that no further naphtenes were detected. This gives evidence for the reaction pathway proceeding via naphtenes.

From Figure 4.9 it is clear that besides EB equilibrium at about 400°C, none of the BTX+EB aromatics are in equilibrium at any of the reaction temperatures. The reason for this is not clear. If the first point (320°C) is neglected, the benzene and toluene may also be approaching equilibrium. When the xylenes are normalised for the xylene fraction (Figure 4.10) it is clear that the xylenes are in equilibrium at the higher temperatures.

The formation of heavy aromatics is shown in Figure 4.11. Heavy aromatics were also first detected at 320°C. With a further increase in temperature, the C_9 and C_{10} aromatics decreased while the C_{11+} aromatics increased.

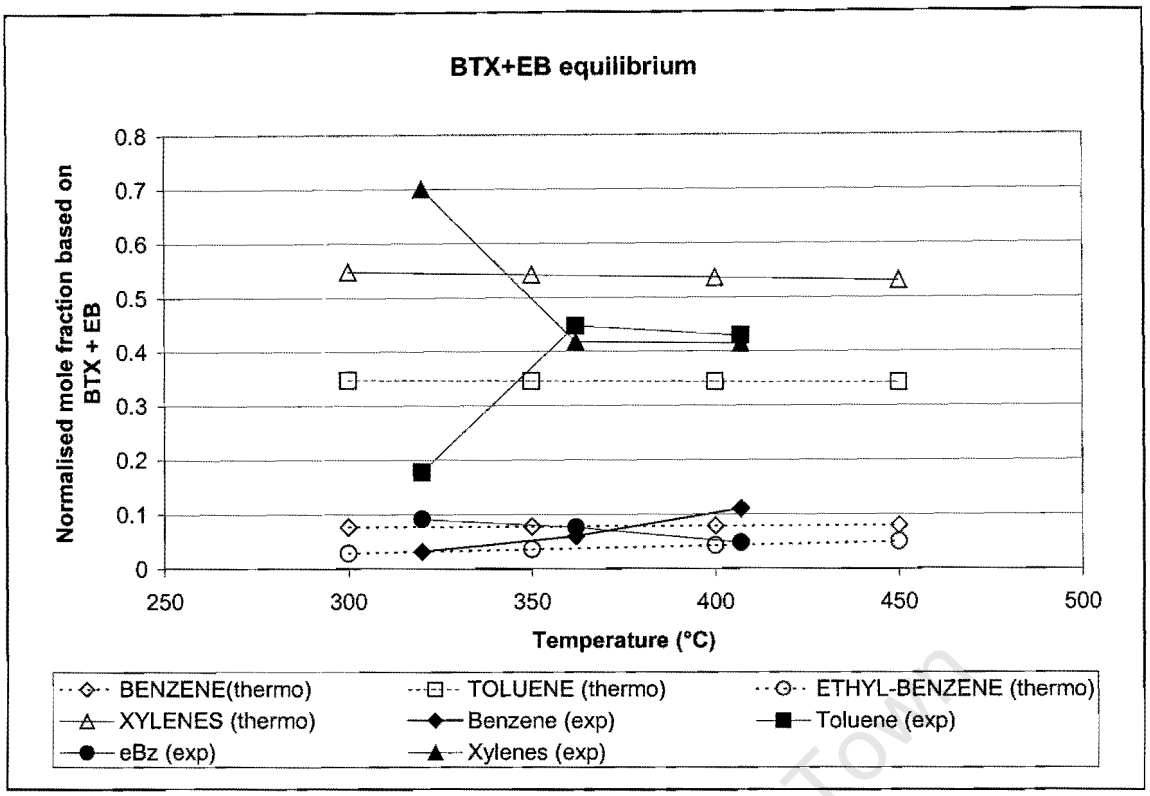

Figure 4.9 Benzene, toluene xylenes and ethylbenzene thermodynamic equilibrium

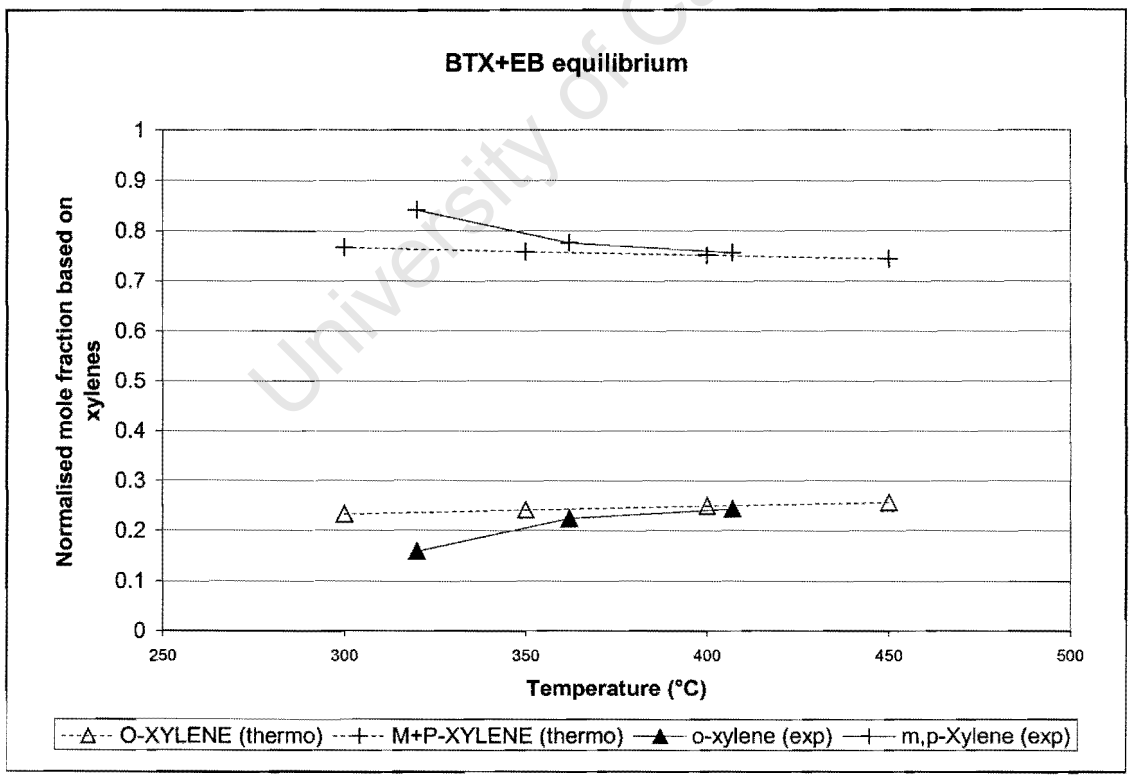

Figure 4.10 Xylenes thermodynamic equilibrium

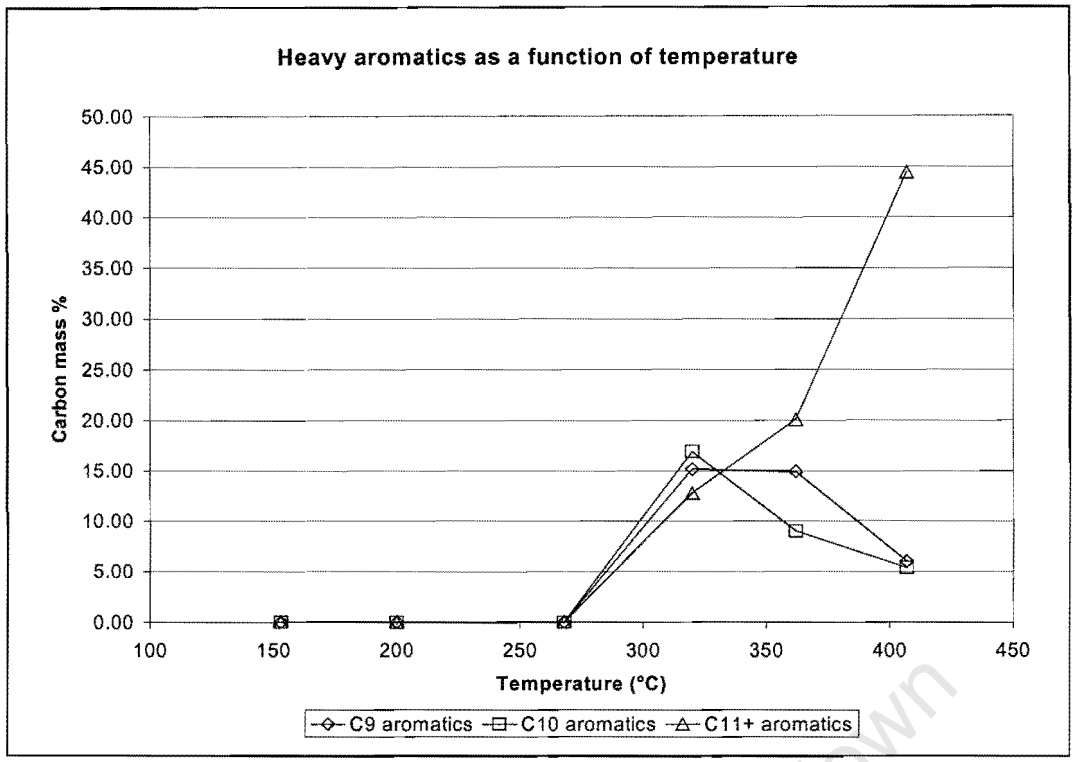

Figure 4.11 Heavy aromatics as a function of temperature

4.1.2.5 Coking

The effect of temperature on coking was discussed in Chapter 3, Section 3.1.7. The C:H mole ratios increased with increasing temperature, and the values indicate that the nature of the coke deposit became graphitic at the higher temperatures. As shown in Figure 4.12, the formation of coke that is more graphitic in nature coincided with the increase in C_{11+} aromatic content and C_3-C_4 compounds in the product. The formation of C_3 and C_4 paraffins could be the result of more hydrogen released by aromatics formation, as well as hydrogen transfer from coke to form more graphitic coke.

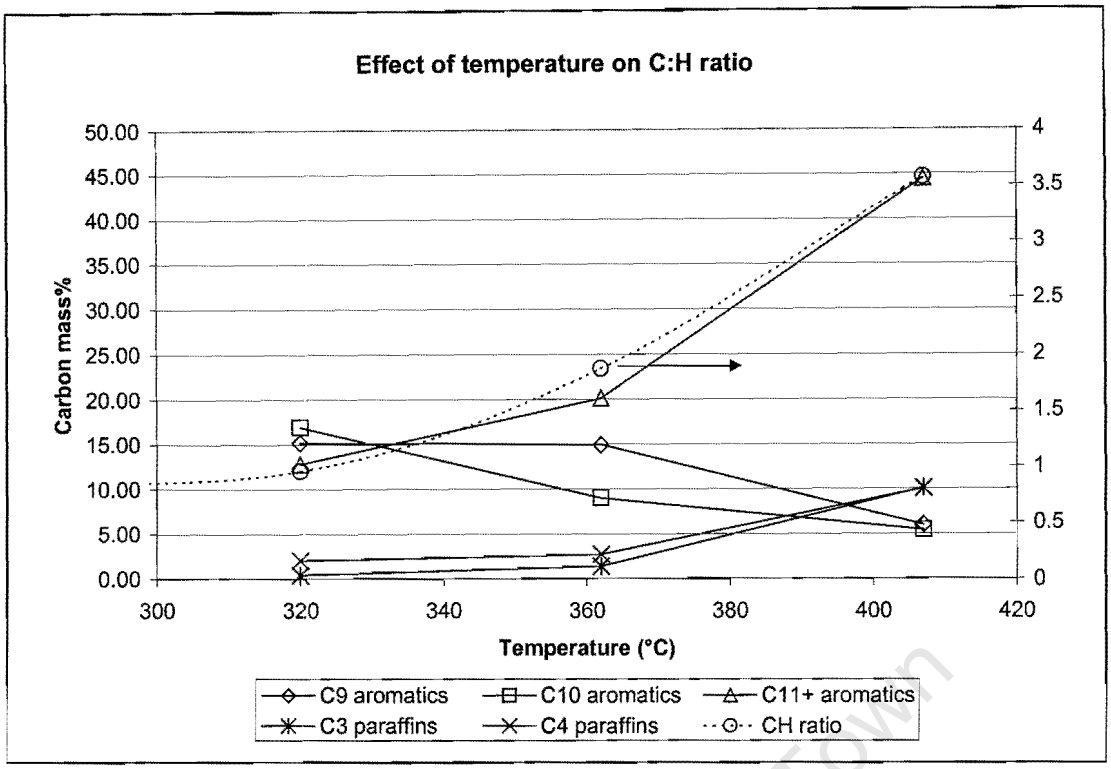

Figure 4.12 Effect of temperature on C:H ratio

4.2 Influence of WHSV

4.2.1 Conversion

The WHSV runs were performed at 360°C, and actual reaction temperatures ranged up to 430°C. As in the case of the temperature runs at 360°C and higher (Section 4.1, Figure 4.1), the conversion of pentene as a function of WHSV was complete for all the runs (see Figure 4.13). Increasing the WHSV from 23 h^{-1} to 113 h^{-1} therefore did not decrease the conversion, as would be expected for shorter contact times. This could indicate that at the reaction temperatures the reactions were sufficiently rapid to allow C_5 feed conversion even at very short contact times. It is also possible that the actual liquid feed rate was lower than expected, since the pump was not calibrated and mass balances were not very good. The increase in liquid products were, however, consistent with the increase in WHSV, i.e. doubling the WHSV resulted in approximately double the liquid product.

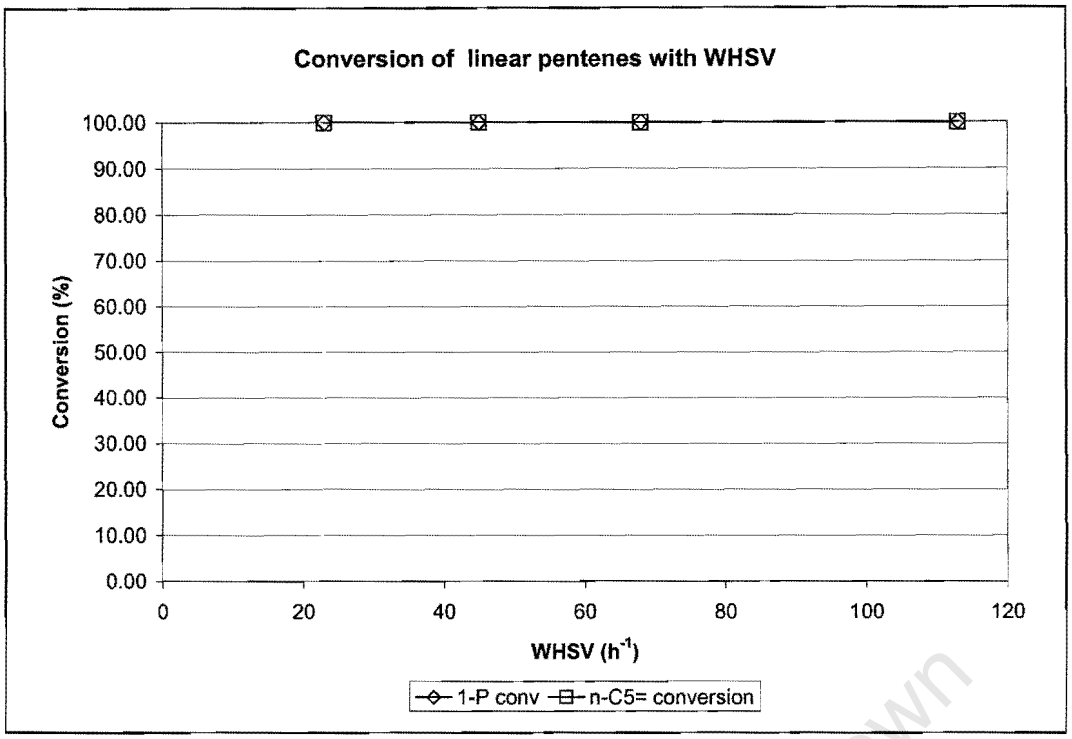

Figure 4.13 Conversion of linear pentenes as a function of WHSV

4.2.2 Reaction types

4.2.2.1 Isomerisation

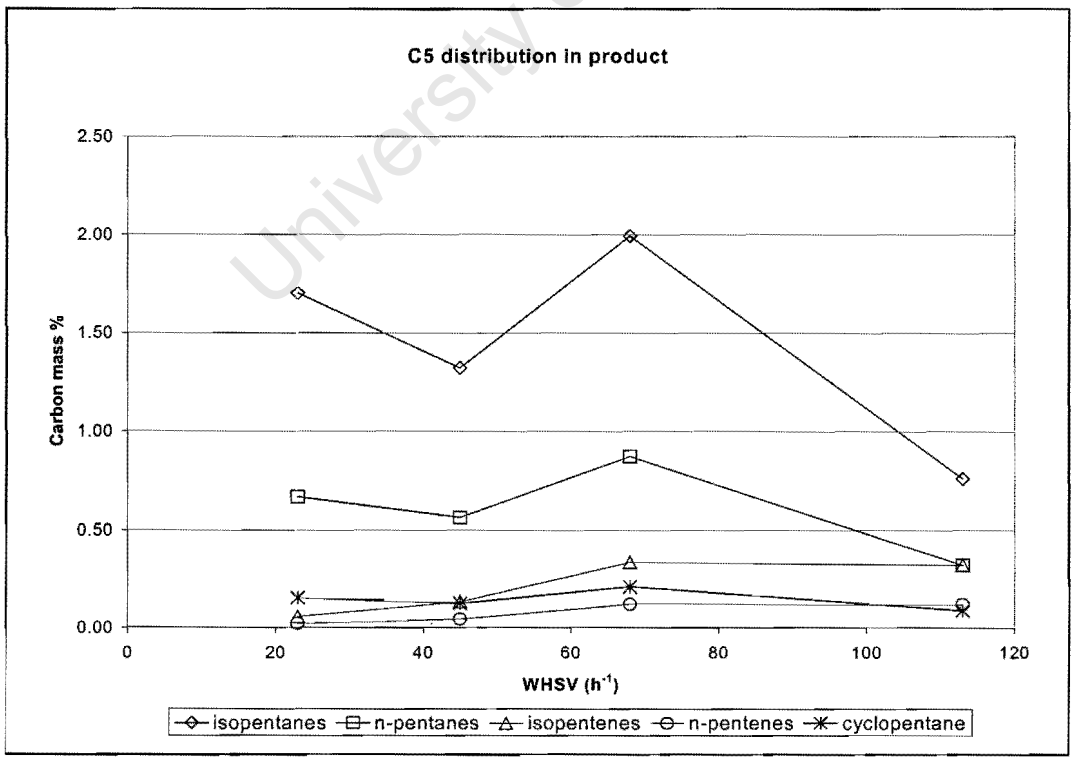

Figure 4.14 C_5 distribution in product

A breakdown of the C5 components in the product is depicted in Figure 4.14. Very little n-pentenes remained in the product as a result of the high conversion. The major C_5 components in the product are n-pentanes and isopentanes, although less than two carbon mass %.

Double-bond isomerisation

The thermodynamic equilibrium of the linear pentenes is depicted in Figure 4.15. The linear pentenes were close to equilibrium at higher space velocities. At the lower space velocities, the experimental data seems to be far from equilibrium because 1-pentene could not be measured accurately at the low concentrations.

Skeletal isomerisation

The pentene skeletal isomers were in equilibrium (see Figure 4.16). The deviation at WHSV 23 h^{-1} is ascribed to lack of data for 2-methyl-1-butene at this WHSV.

When lumping the linear isomers as a group and the branched isomers as a group (Figure 4.17), the experimental data matches the thermodynamic data well, except at the lowest WHSV, where some experimental data was not available. At the lower WHSV, secondary reactions dominate, consuming pentenes. The low concentrations of pentenes are difficult to measure, leading to experimental errors. At the high WHSV, secondary reactions are reduced and less pentenes are consumed.

Expressing the data as a ratio of experimental data to thermodynamic data allows the data to be plotted as a function of WHSV, as shown in Figure 4.18. The ratios for 1-pentene and 2-methyl-2-butene are close to unity at WHSV=68 h^{-1}, indicating equilibrium. The other pentenes seem to be approachinig equilibrium at WHSV=68 h^{-1}.

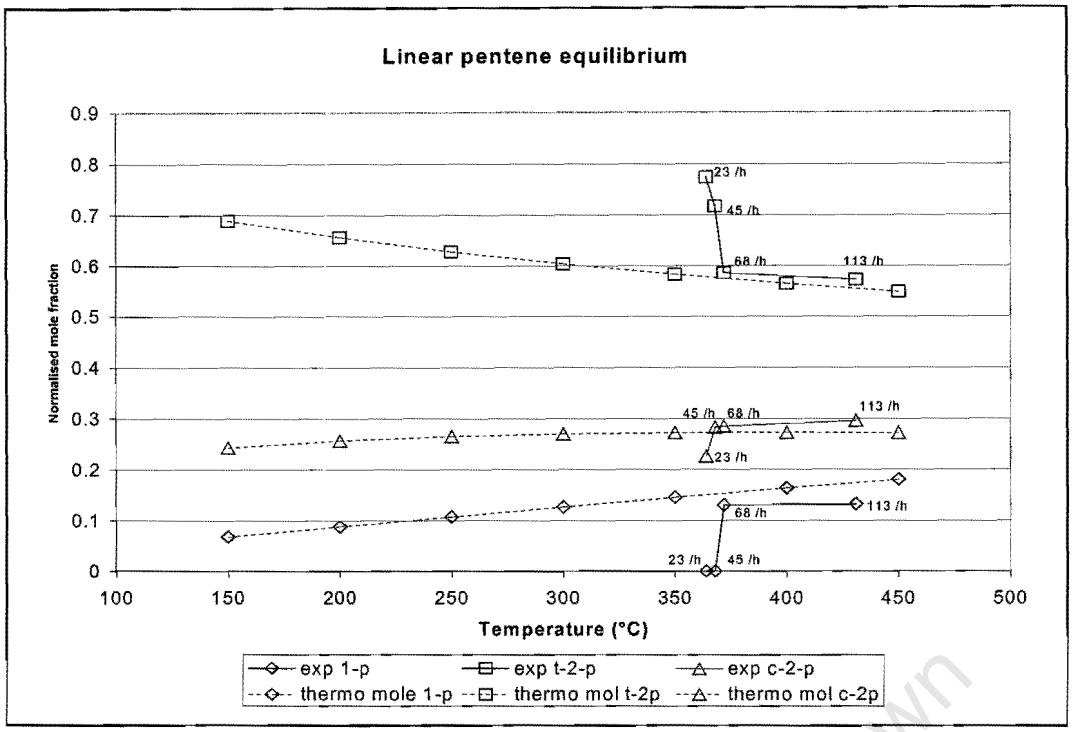

Figure 4.15 Linear pentene isomer equilibrium

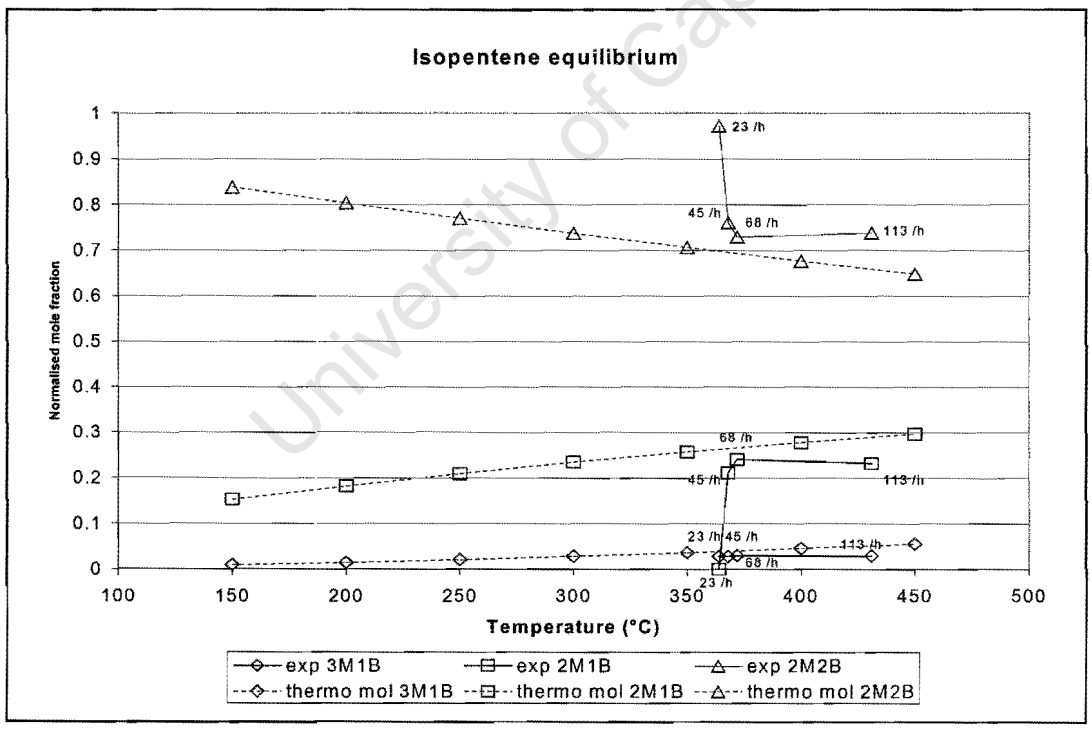

Figure 4.16 Isopentene equilibrium

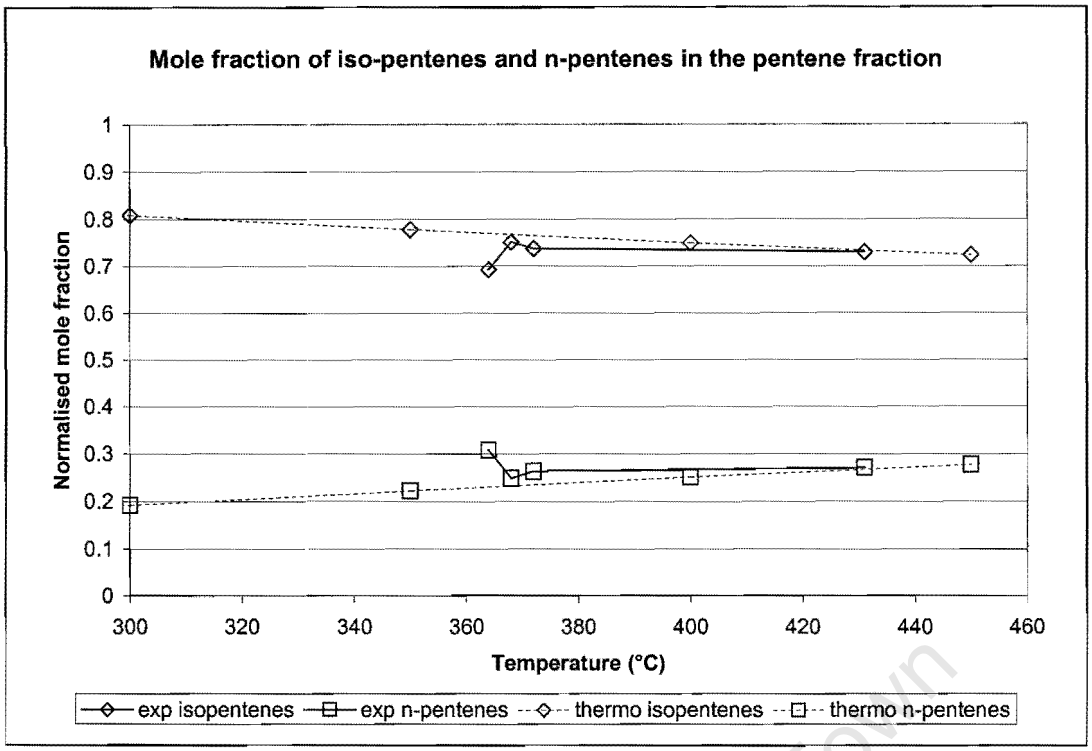

Figure 4.17 Total equilibrium in the pentene fraction

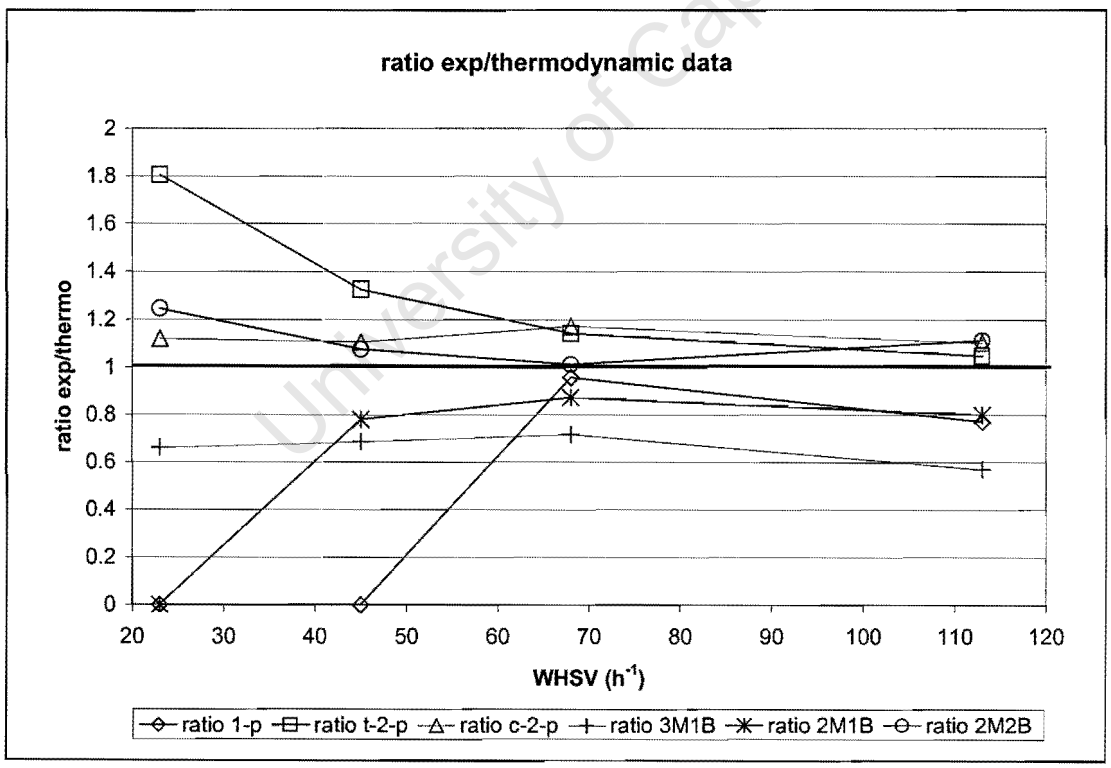

Figure 4.18 Thermodynamic equilibrium of pentenes as a function of WHSV

4.2.2.2 Oligomerisation

Oligomerisation trends as a function of WHSV could not be followed, since C_{10} and C_{15} olefins could not be distinguished on the GC trace in the range of WHSV and temperatures studied. This was also the case for temperatures above 268°C in the temperature runs (Chapter 4, Section 4.1.2.2). That oligomerisation is part of the reaction pathway is evident from the presence of compounds with carbon number higher than the C_5 feed.

4.2.2.2 Cracking

The light components (C_2-C_4) in the product are depicted in Figure 4.19.

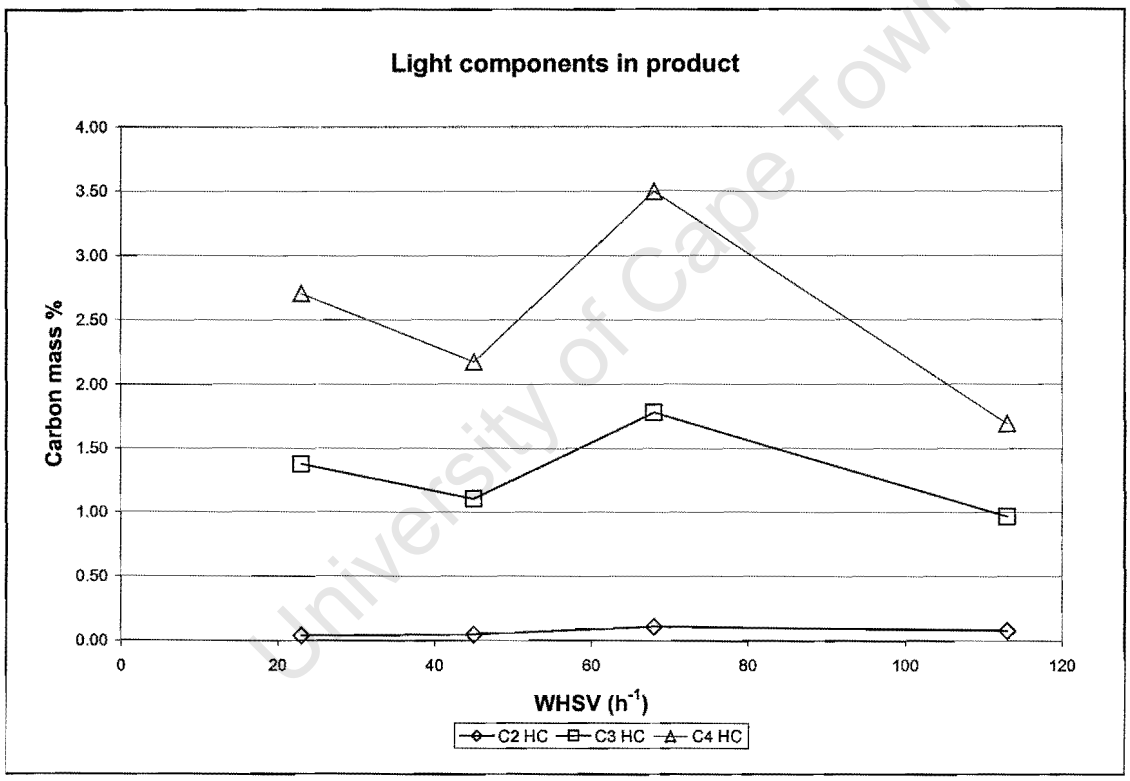

Figure 4.19 Light components in product

Increasing the WHSV resulted in a general decrease in C_3 and C_4 components, except for an increase at 68 h^{-1} WHSV. The shorter contact time presumably allows less time for secondary reactions such as cracking. The increase in C_2 compounds with increasing WHSV is probably due to the increase in temperature with increasing WHSV. An increase in C_2's

was also observed when increasing the temperature in the temperature runs (Chapter 4, Section 4.1.2.3).

4.2.2.4 Aromatisation

The BTX+ EB thermodynamic equilibrium is shown in Figure 4.20. Increasing the WHSV from 23 h^{-1} to 68 h^{-1} brought the toluene and o-xylene closer to thermodynamic equilibrium, with toluene attaining equillibrium at 68 h^{-1} and o-xylene close to equilibrium. At higher WHSV these aromatics departed from thermodynamic equilibrium. The other aromatics were not in thermodynamic equilibrium. The effect of increasing WHSV is not conclusive, since the temperature also increased with increasing WHSV. Increasing temperature while keeping the WHSV constant at 23 h^{-1} resulted in an approach to equilibrium (Chapter 4, Section 4.1.2.4). It is expected that high WHSV will cause a shift away from equilibrium. As this is not the case, the temperature effect dominates here.

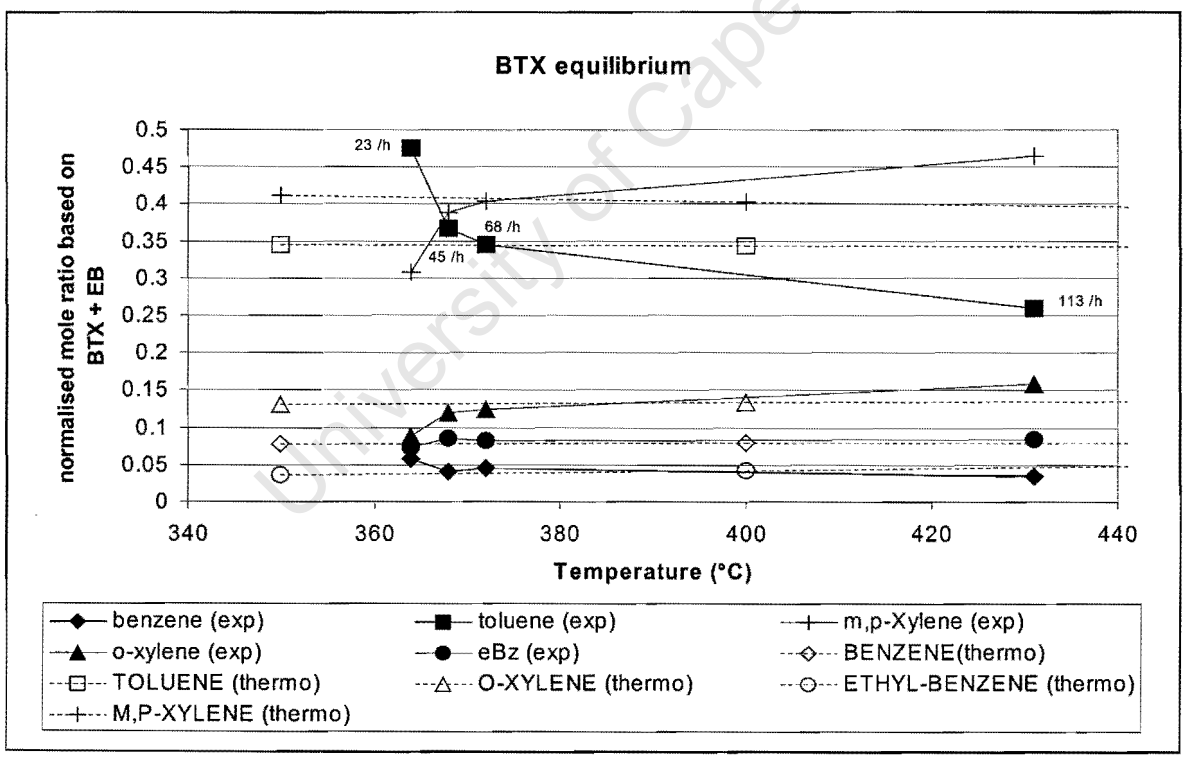

Figure 4.20 BTX+EB thermodynamic equilibrium

4.2.2.5 Coking

Coking as a function of WHSV was discussed in Chapter 3, Section 3.1.8. As shown in Figure 4.21, increasing the WHSV form 23 h^{-1} to 113 h^{-1} (with accompanying temperature increase from 364°C to 431°C) had essentially no effect on the C:H ratio of the coke on the spent catalyst. If any, it is rather a slight decrease. The C:H values of between 1.87 and 1.10 indicate that the coke formed is mostly aromatic in character. The results in Chapter 4, Section 4.1.2.5, where was kept at 23 h^{-1}, showed an increase in C:H ratio to 4 at the higher temperatures (around 400°C), indicating coke with a more graphitic nature. It seems therefore that increasing the WHSV at 400°C prevents the formation of graphitic coke.

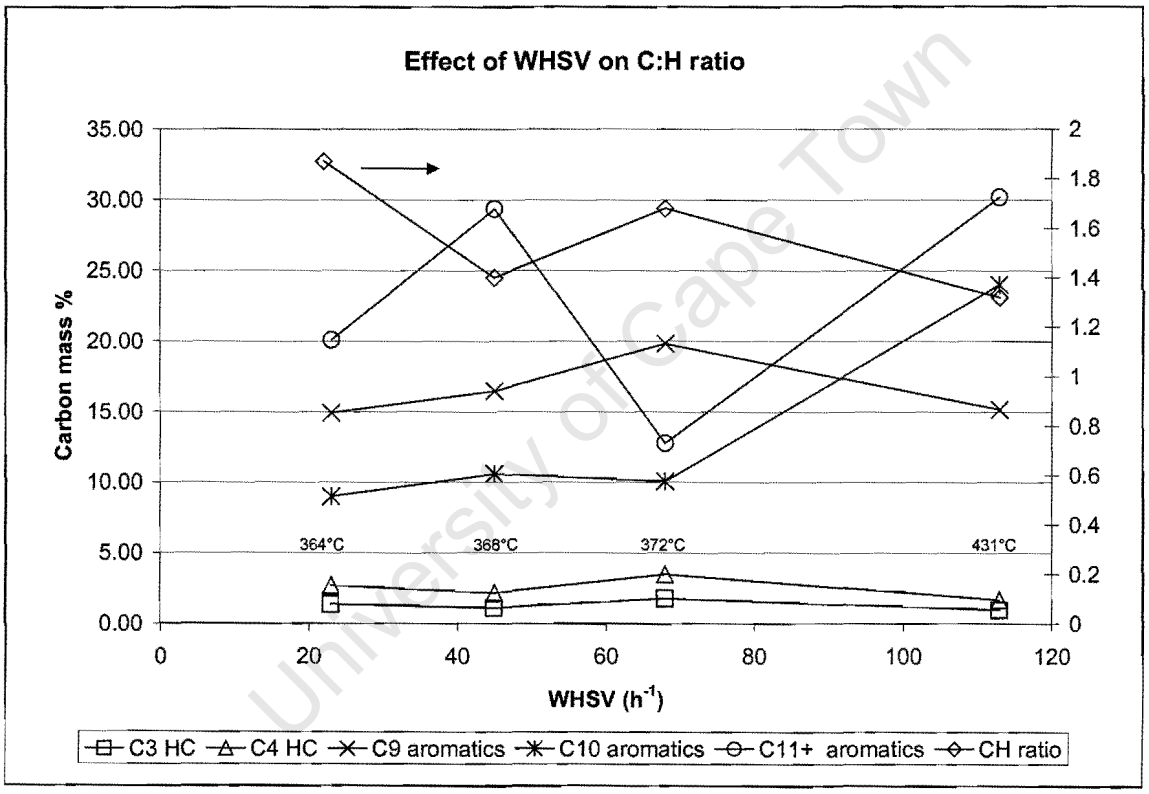

Figure 4.21 Effect of WHSV on C:H ratio

4.3 Influence of pressure and carrier

4.3.1 Conversion

Linear pentene and 1-pentene conversions were complete at both pressures and with both carrier gases (Figure 4.22).

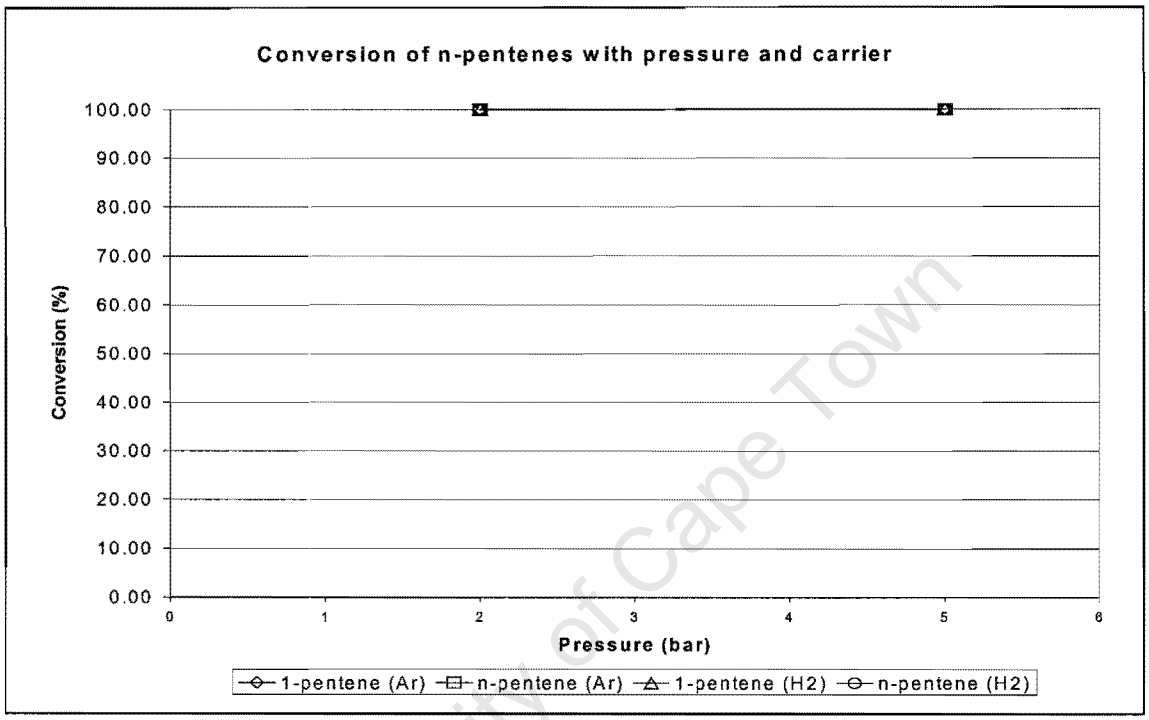

Figure 4.22 Conversion of n-pentenes as a function of pressure and carrier gas at T=364°C and WHSV=23 h^{-1}

4.3.2 Reaction types

4.3.2.1 Isomerisation

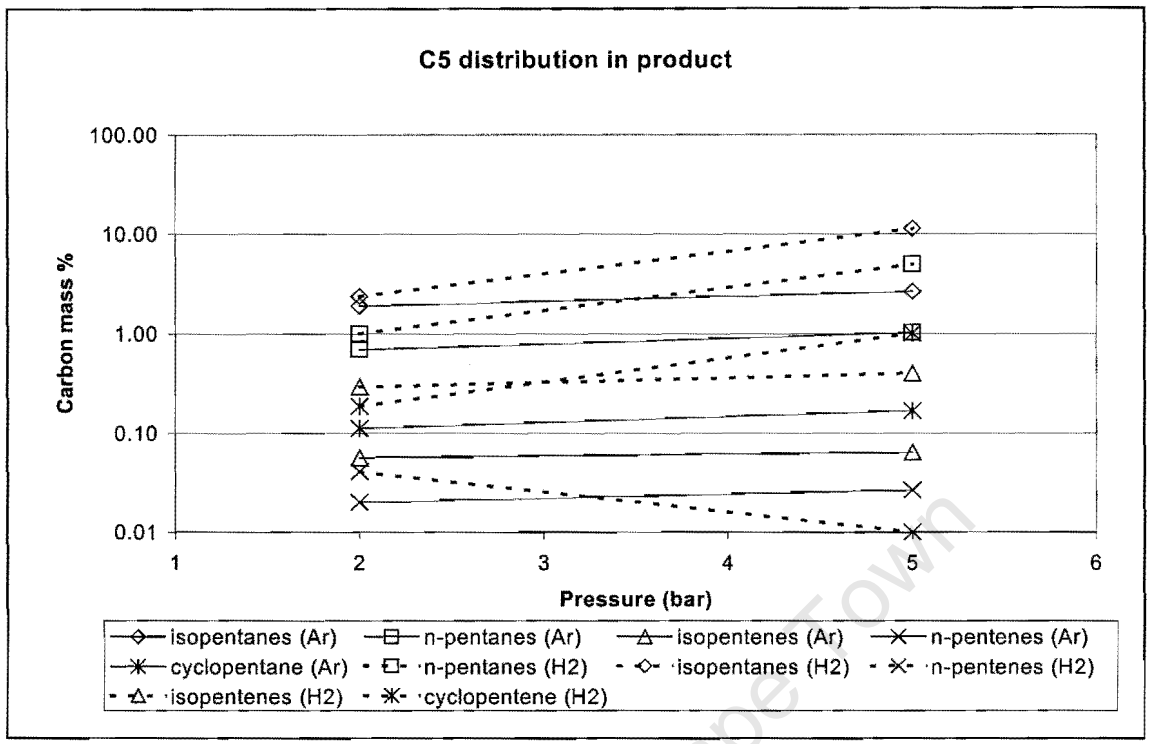

Figure 4.23 C_5 distribution in product

A break down of the C_5 components in the product is given in Figure 4.23. With argon as carrier, n-pentanes and isopentanes are the main C_5 components and show an increase with increase in pressure. With hydrogen as carrier, n-pentanes and isopentanes are also the main C_5 components, but in bigger quantities than with argon as carrier. The increase in n-pentanes and especially isopentanes with increase in pressure is more pronounced than with argon as carrier. The increase in pressure in the presence of hydrogen probably allows for more hydrogen transfer to form paraffins. With hydrogen as carrier, there is also a slight increase in isopentene and cyclopentane formation.

Double-bond isomerisation

Determining the extent of double-bond isomerisation was difficult due to the small quantities of n-pentenes in all the runs, as well as lack of linear pentene data at 5 bar pressure with hydrogen as carrier. The plot in Figure 4.24 shows that the linear pentenes were not in equilibrium.

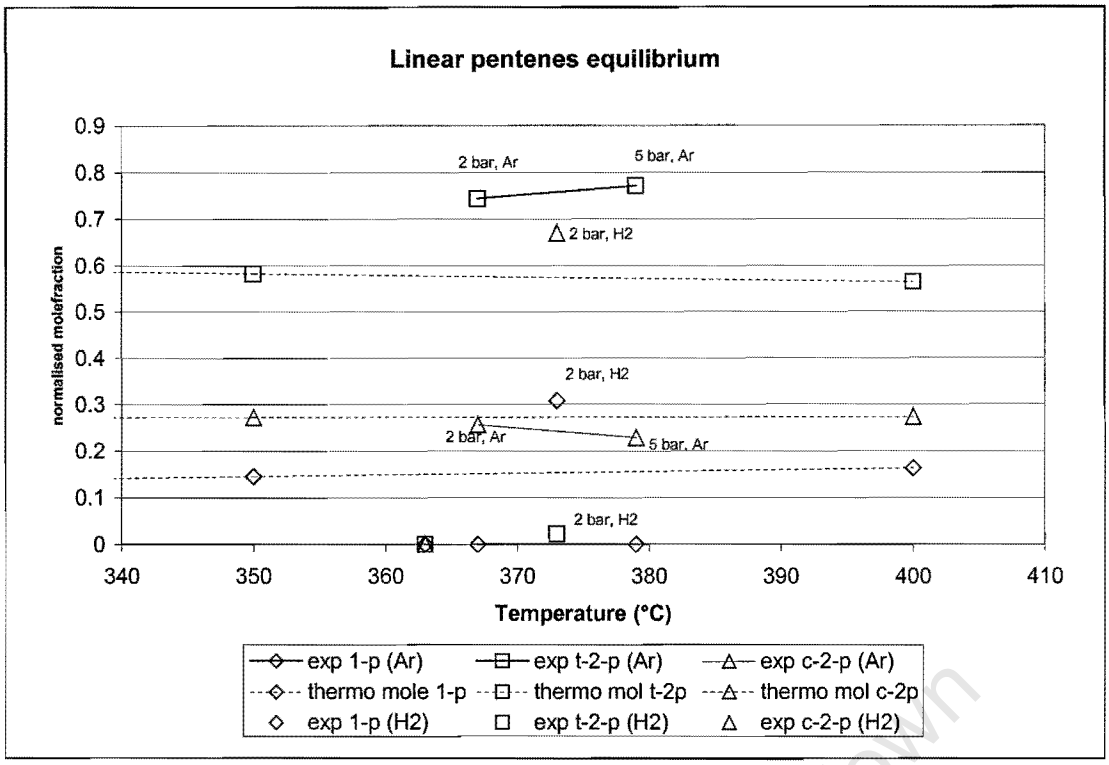

Figure 4.24 Linear pentene equilibrium

Skeletal isomerisation

Determining the extent of skeletal isomerisation was difficult for the same reasons given for double-bond isomerisation. In this case only 2M2B data was available at 5 bar hydrogen pressure. At 2 bar pessure with hydrogen as carrier, however, 2M2B and 2M1B are close to thermodynamic equilibrium (Figure 4.25). Grouping the linear pentenes and grouping the branched pentenes (Figure 4.26) shows that the linear pentenes as well as branched pentenes were closer to equilibrium at the lower pressure of 2 bar for both argon and hydrogen as carrier.

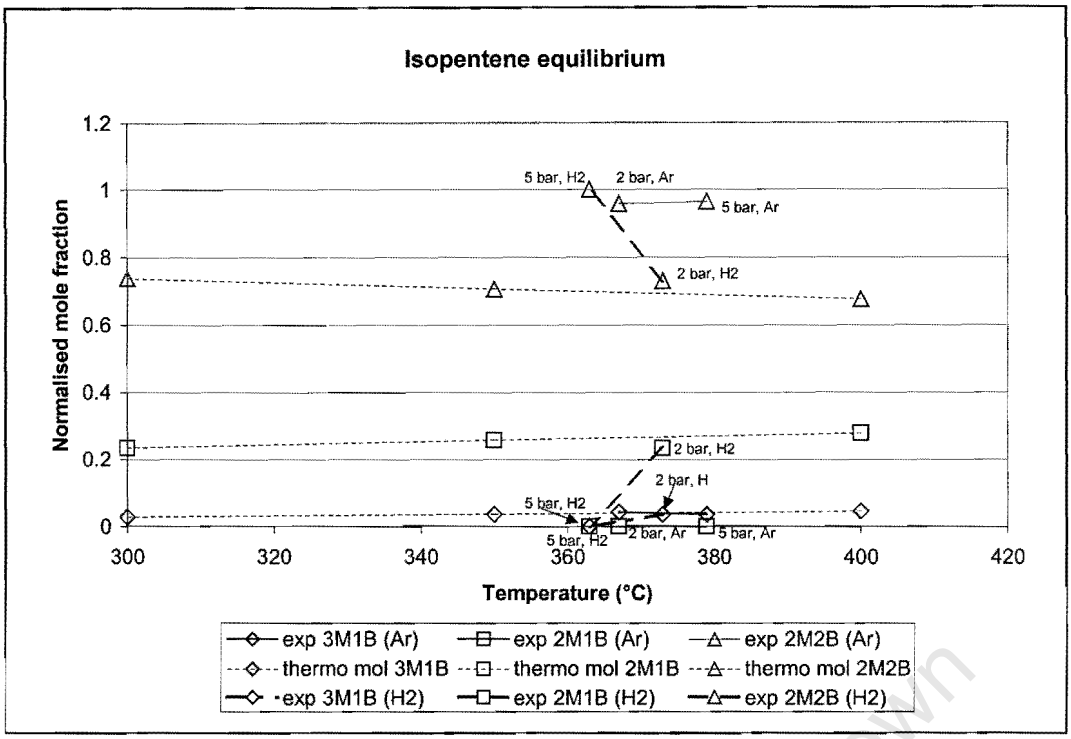

Figure 4.25 Isopentene equilibrium

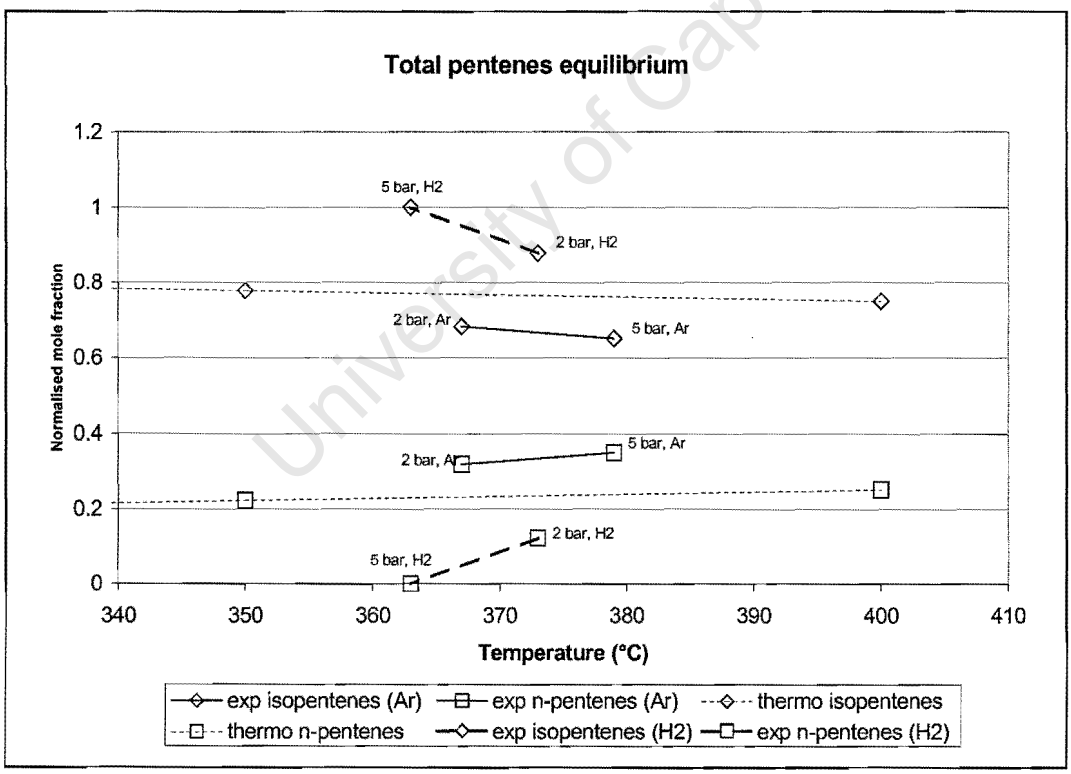

Figure 4.26 Total equilibrium in the pentene fraction

4.3.2.2 Oligomerisation

The oligomerisation reactions could not be followed for the same reasons mentioned in Section 4.2.2.2.

4.3.2.3 Cracking

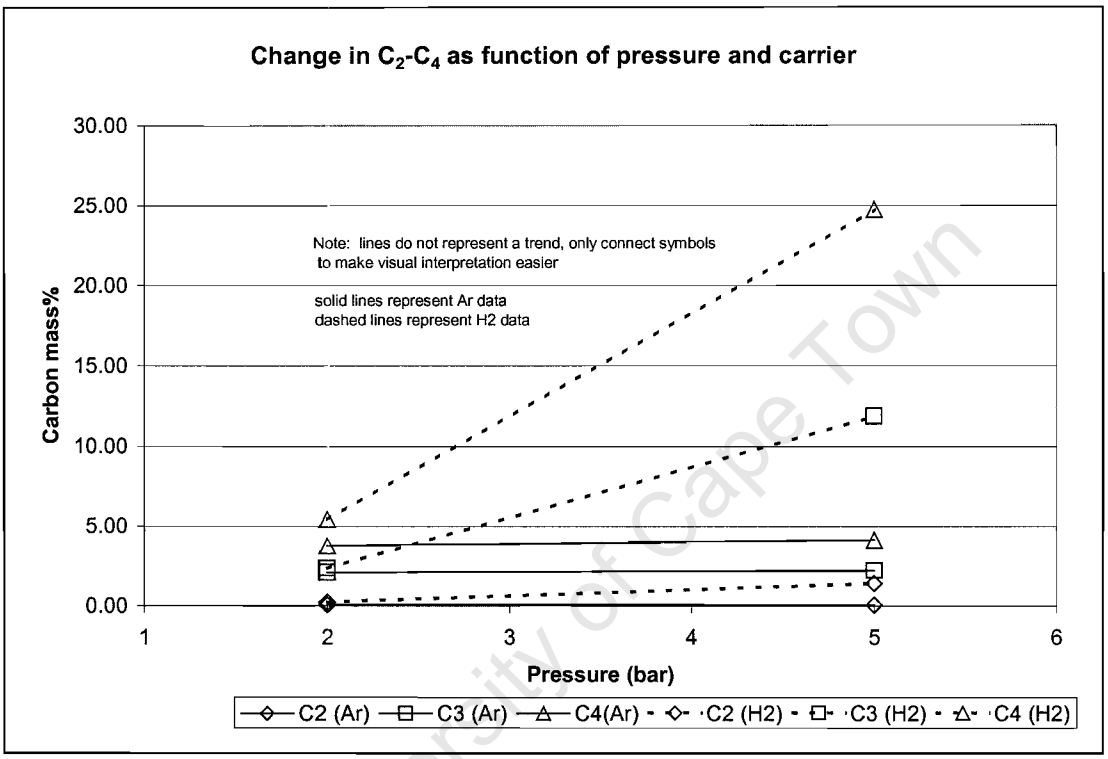

Figure 4.27 Light components in product

The formation of light products (C_2-C_4) is shown in Figure 4.27. The amount of C_2, C_3 and C_4 components stayed essentially the same upon increasing the pressure from 2 bar to 5 bar with argon as carrier gas. Using hydrogen as carrier, increasing the pressure resulted in a marked increase (approximately five-fold) for each of the C_2-C_4 compounds.

4.3.2.4 Aromatisation

At 2 bar argon, only toluene, o-xylene and m, p-xylene are in equilibrium. Increasing the pressure to 5 bar resulted in benzene approaching equilibrium, while the other BTX+EB aromatics moved further away from equilibrium (Figure 4.28). At 2 bar hydrogen pressure, none of the BTX+EB aromatics are in thermodynamic equilibrium. Increasing the pressure to 5 bar resulted in benzene attaining thermodynamic equilibrium for the BTX+EB fraction (Figure 4.29).

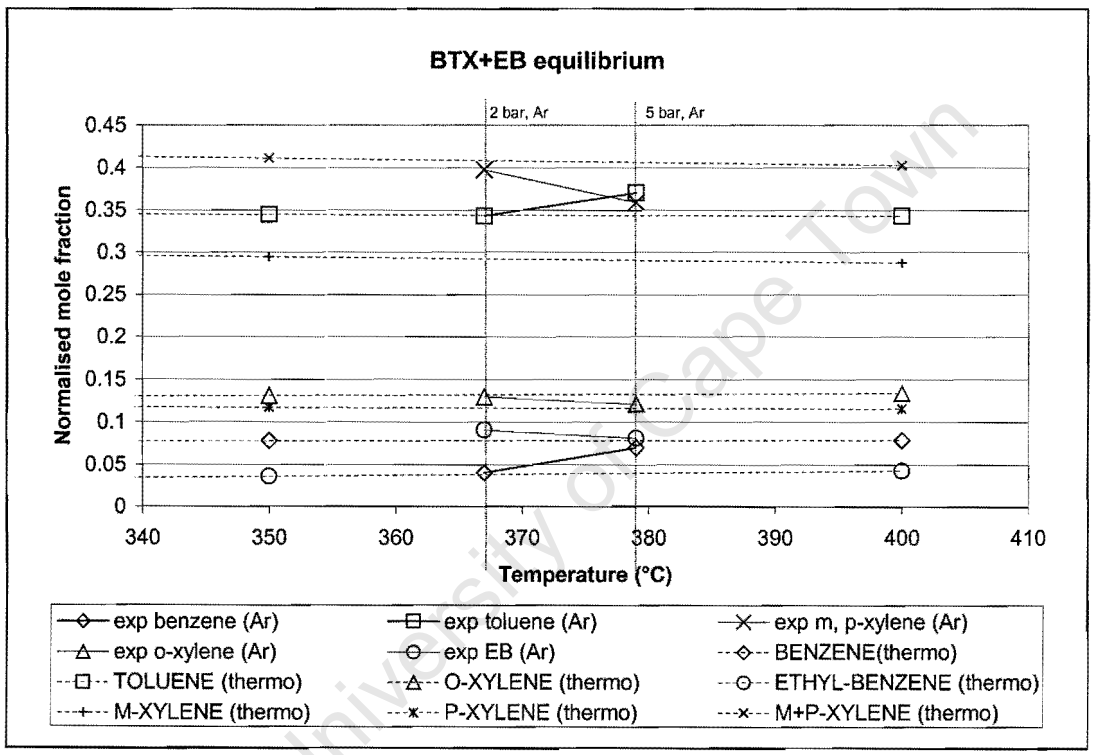

Figure 4.30 BTX+EB equilibrium with argon carrier gas

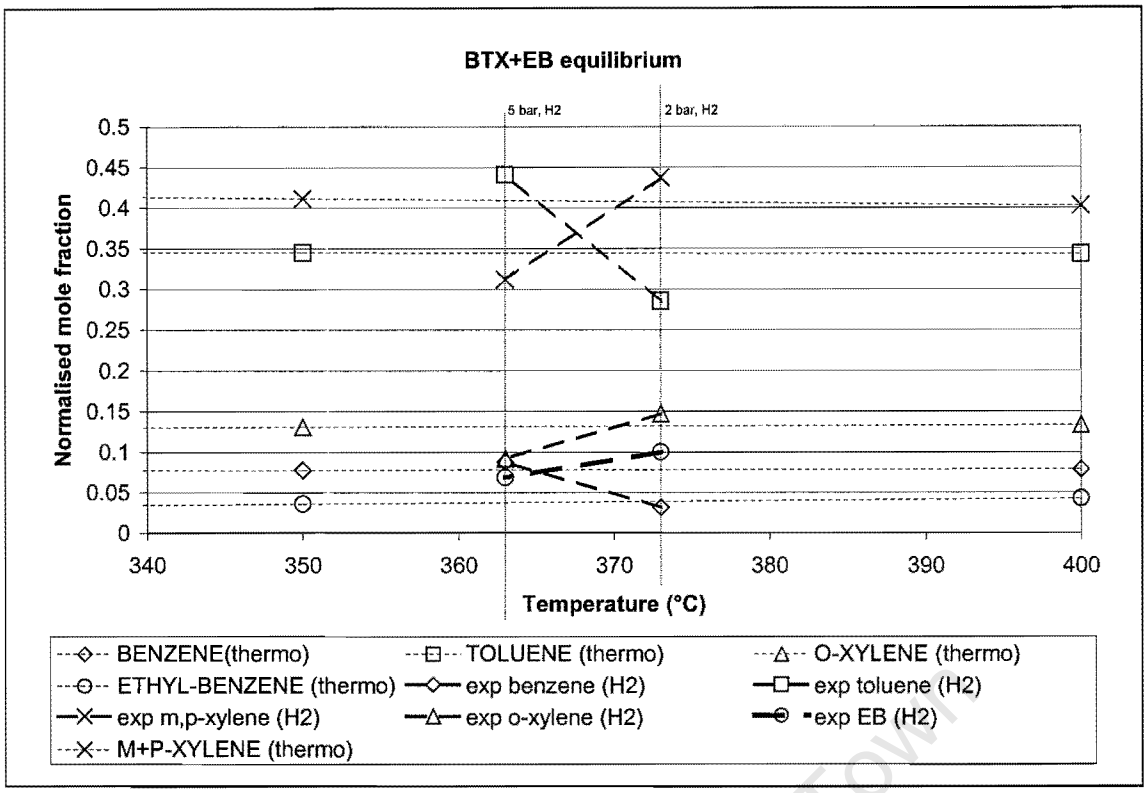

Figure 4.29 BTX+EB equilibrium with hydrogen carrier gas

4.3.2.5 Coking

The C:H ratio is shown in Figure 4.30. Increasing the pressure with argon as carrier led to an increase in C:H ratio from 1.4 to 1.78. Although this is an increase, it still indicates that the carbon laydown is aromatic in character. With hydrogen as carrier, very large C:H numbers were obtained at both 2 bar and 5 bar pressure. This suggests that the nature of the carbon laydown was graphitic. This is unexpected, since the presence of hydrogen should have prevented the formation of graphitic coke. The amount of carbon on the spent catalyst was, however, much less for the 5 bar hydrogen run than for the 5 bar argon run. This could be expected since the higher pressure in hydrogen resulted in the formation of less aromatics (Figure 4.31), which are thought to be precursors of coke.

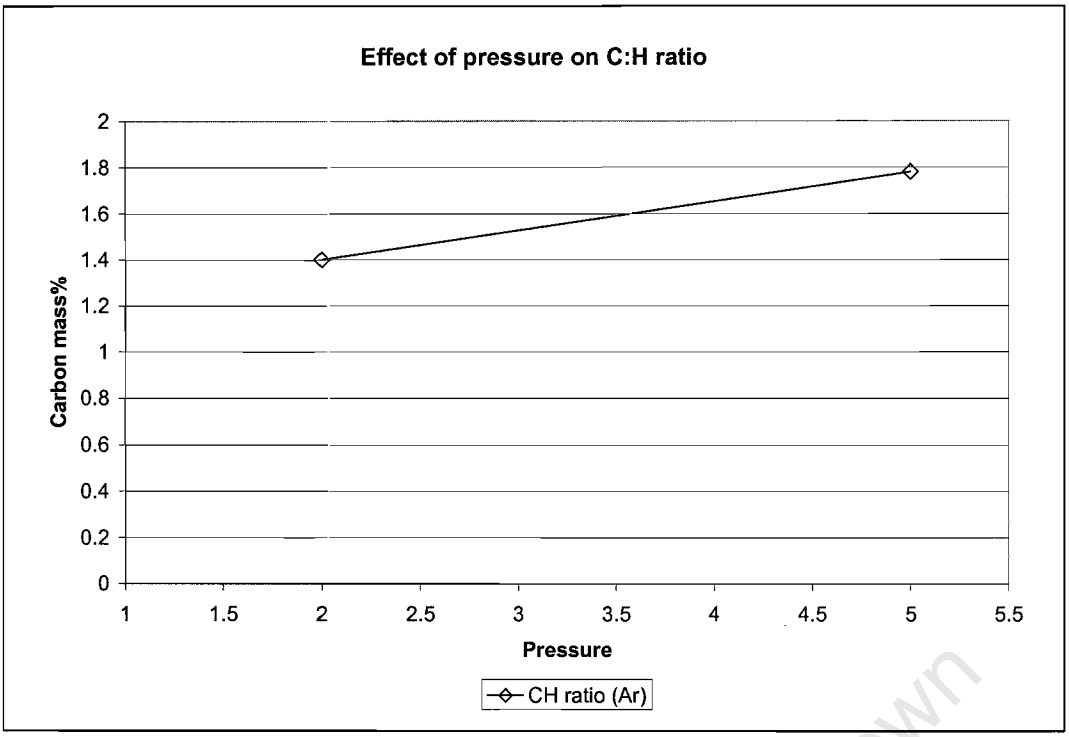

Figure 4.30 Effect of pressure and carrier on C:H ratio

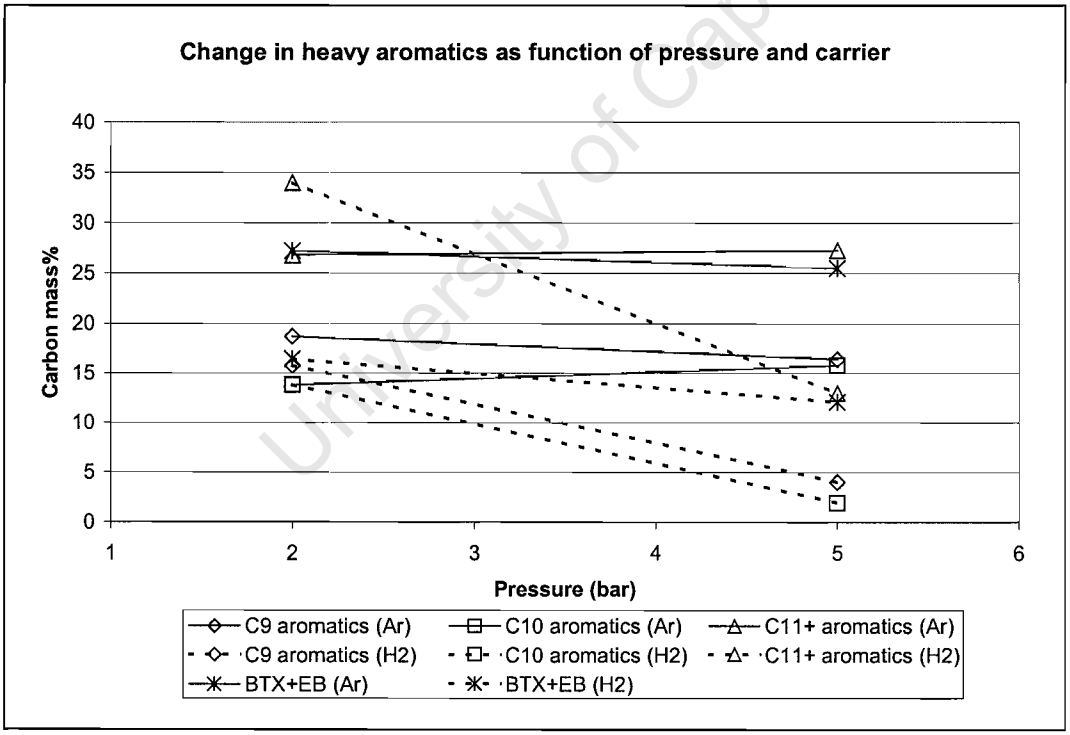

Figure 4.31 Change in heavy aromatics as a funcion of pressure and carrier gas

4.4 Reaction pathway

The results of the temperature data seem to suggest the following reaction pathway for the conversion of n-pentene over H-ZSM-5:

Double-bond isomerisation ⟶ Oligomerisation ⟶

Cracking + Skeletal isomerisation ⟶ Cyclisation ⟶ Aromatisation

At the lower temperatures (153°C-268°C), double-bond isomerisation, oligomerisation, cracking and skeletal isomerisation are dominant. Increasing the temperature increases aromatisation and cracking products, while skeletal isomers of the feed almost disappear. Although oligomerisation products of C_5 are not present at high temperatures, the reaction had to proceed via oligomers in order to explain the formation of products with carbon number above C_5.

Increasing the WHSV resulted in a slight increase in double-bond isomers and skeletal isomers of the feed, as well as an increase in naphtenes and C_{10} and higher aromatics. Light products (C_2-C_4) and BTX+EB decreased.

Increasing pressure with both argon and hydrogen as carriers resulted in a slight increase in double-bond isomers and skeletal isomers of the feed. Changing the carrier gas from argon to hydrogen at the same pressure had the same effect. Increasing the pressure with hydrogen as carrier, as well as changing the carrier from argon to hydrogen at the same pressure, resulted in more light products (C_2-C_4). Increasing pressure with both argon and hydrogen as carriers, as well as changing from argon to hydrogen as carrier, resulted in a decrease in BTX+EB and higher aromatic products. The formation of aromatics was greatly suppressed by increasing the pressure with hydrogen as carrier.

4.5 Conclusions

The product composition obtained for conversion of 1-pentene over H-ZSM-5 displayed a clear relationship with temperature. The temperatures at which specific reactions commenced, as well as the temperatures at which these reactions were dominant, could be observed. The product spectrum changed from mostly olefinic at the lower temperatures to mostly aromatic at the higher temperatures.

At 153°C the temperature was sufficient for the formation of n-pentene isomers (double-bond isomerisation), C_{10}-olefins (dimerisation), C_{15}-olefins (trimerisation) and isopentenes (skeletal isomerisation). The dominant reactions at this temperature were double-bond isomerisation and oligomerisation. At 200°C, branched olefins were formed and skeletal isomerisation and oligomerisation were the dominant reactions. Cyclisation and aromatisation products, as well as paraffins, were first detected at 320°C and were the dominant products at this temperature. Naphtenes decreased with increasing temperature. At temperatures above 320°C, aromatics were the main product.

References

Bhattacharya, D., Sivasanker, S., Aromatization of n-hexane over H-ZSM-5: influence of promoters and added gases, *Appl. Catal. A: General*, **141,** 105-115, (1996)

Biscardi, J.A., Iglesia, E., Reaction pathways and rate-determining steps in reactions of alkanes on H-ZSM5 and Zn/H-ZSM5 catalysts, *J. Catal.,* **182**, 117-128, (1999)

Brooks, B.T., in *The Chemistry of Petroleum Hydrocarbons Vol. III*, edited by Brooks, B.T., Boord, C.E., Kurtz S.S. Jr., Schmerling, L., Reinhold Publishing Corporation, New York, (1955)

Buchanan, J.S., Santiesteban, J.G., Haag, W.O., Mechanistic considerations in acid-catalysed cracking of olefins, *J. Catal.,* **158**, 279-287, (1996)

Chen, N.Y., Garwood, W.E., Dwyer, F.G., Shape selective acid catalysis, in *Shape Selective Catalysis in Industrial Applications,* Marcel Dekker, Inc., New York (1989)

Condon, F.E., in *Catalysis, (VI)*, Alkylation, isomerization, polymerization, cracking and hydroreforming, ed., Emmett, P.H., 98, Reinhold Publishing Corporation, Baltimore, (1958)

Cortright, R.D., Dumesic, J.A., Madon, R.J., Catalytic cycles for hydrocarbon cracking on zeolite, *Top. Catal.,* **4** (1,2 Acidity in aluminas, amorphous and crystalline silico-aluminas), 15-26, (1997)

Costa, C., Lopes, J.M., Lemos, F., Ramoa Ribeiro, F., *J. Molec. Catal. A: Chemical*, **144**, 207-220, (1999)

Csicsery, S.M., Shape selective cayalysis in zeolites, *Chem. Br.*, **21(5)**, 473-4, 476-7, (1985)

Derouane, E.G., Vanderveken, D.J., Structural recognition and preorganization in zeolite catalysis: direct aromatization of n-hexane on zeolite L-based catalysts, *Appl. Catal.,* **45** 419, (1988)

Egloff, G., Morrell, J.C., Thomas, C.L., Bloch, H.S., *The Catalytic Cracking of Aliphatic Hydrocarbons,* 3571-3580, (1939)

Ewell, R.H., Hardy, P.E., Isomerisation equilibrium among the branched chain pentenes, *J. Am. Chem. Soc.,* **63**, 3460, (1941)

Garwood, W.E., in *Intrazeolite Chemistry*, Stucky, G.D., Dwyer, F.G., Eds., ACS Symposium Series 218, American Chemical Society: Washington, D.C., 383-396, (1983)

Gnep, N.S., Bouchet, F., Guisnet, M.R., Comparative study of the oligomerization of C2-C6 olefins on HZSM-5, *Symposium on alkylation, aromatization, oligomerization and isomerization of short chain hydrocarbons over heterogeneous catalysts*, presented before the Division of Petroleum Chemistry, Inc. American Chemical Society, New York City Meeting, August 25-30, 1991, 620-626.

Höchtl, M., Jentys, A., Vinek, H., Isomerization of 1-pentene over SAPO, CoSAPO (EAL, AFI) molecular sieves and HZSM-5, *Appl. Catal. A: General,* **207**, 397-405, (2001)

Hölderich, W.F., van Bekkum, H., in *Introduction to Zeolite Science and Practice (Studies in Surface Science and Catalysis 58)* ed. van Bekkum, H., Flanigen, E.M., Jansen, J.C., Elsevier Science Publishers B.V., Amsterdam, (1991)

Horsley, J.A., Derouane, E., *Zeolite Advances in Petroleum and Organic Chemicals,* (1995)

Horsley, J.A., *New Zeolite Applications in the Petroleum and Petrochemical Industries,* Catalytica, Inc., California, (1993)

HSC Chemistry Ver. 2.03. Copyright (C) Outokumpu Research Oy, Pori, Finland, A. Roine

Humphries, A., Harris, D.H., O'Connor, P., in The nature of active sites in zeolites: influence on catalyst performance in fluid catalytic cracking: *Science and Technology*, (Eds,: Magee, J.S., Mitchel, M.M. Jr.), *Studies in Surface Science and Catalysis*, **76**, Elsevier, Amsterdam, (1993)

Jacobs, P.A., Martens, J.A., *in Introduction to Zeolite Science and Practice (Studies in Surface Science and Catalysis 58)* ed. van Bekkum, H., Flanigen, E.M., Jansen, J.C., Elsevier Science Publishers B.V., Amsterdam, (1991)

Jacobs, P.A., Kanai, J., Martens, J.A., On the nature of the active sites for ethylene hydrogenation in metal-free zeolites, *J. Catal.*, **133(2)**, 527-543, (1992)

Mäurer, T., Kraushaar-Czarnetzki, B., Thermodynamic and kinetic reaction regimes in the isomerization of 1-pentene over ZSM-5 catalysts, *J. Catal.*, **187(1)**, 202-208, (1999)

Maxwell, I.E., Stork, W.H.J., Hydrocarbon processing with zeolites, in *Introduction to Zzeolite Science and Practice (Studies in Surface Science and Catalysis 58)* ed. van Bekkum, H., Flanigen, E.M., Jansen, J.C., Elsevier Science Publishers B.V., Amsterdam, (1991)

Meier, W.M., Olsen, D.H., *Atlas of Zeolite Structure Types*, Third, revised edition, Butterworth-Heinemann, (1992)

Mériaudeau, P. and Naccache, C., Dehydrocyclisation of alkanes over zeolite-supported metal catalysts: monofunctional or bifunctional route, *Catal. Rev.-Sci. Eng.*, **39 (1&2)**, 5-48, (1997)

Morrison, R.T. and Boyd, R.N., *Organic Chemistry,* Fifth Edition, Allan and Bacon, Inc., Boston, (1987)

Nash, R.J., *Aromatization of alkenes by gallium/H-ZSM5 zeolite catalysts,* MSc. dissertation, University of Cape Town, (1994)

Oblad, A.G., Messenger, J.U., Brown, H.T., Isomerization of 1- and 2-pentenes, *Ind. Eng. Chem.*, **39**, 1462, (1947)

O'Connor, C.T., Aromatization of light alkanes, in *Handbook of Heterogeneous Catalysis, Vol. 5,* ed. Ertl, G., Knözinger, H., and Weitkamp, J., Wiley-VCH, (1997)

O'Connor, C.T., Kojima, M., Alkene oligomerization, *Catal. Today*, **6(3)**, 329-349, (1990)

Quann, R.J., Green, L.A., Tabak, S.A., Krambeck, F.J., Chemistry of olefin oligomerization over ZSM-5 catalyst, *Ind. Eng. Chem. Res.*, **27 (4)**, 565-570, (1988)

Roland, E., Kleinschmidt, P. in *Ullmann's Encyclopedia of Industrial Chemistry,* Sixth Edition, Electronic release, (1998)

Sano, T., Hagiwara, H., Okabe, K., Okado, H., Saito, K., Takaya, H., Olefin hydrogenation over zeolite H-ZSM-5, *Sekiyu Gakkaishi*, **29, (1)**, 89-92, (1986)

Santilli, D.S., Gates, B.C., Hydrocarbon reaction mechanisms, in *Handbook of Heterogeneous Catalysis*, *Vol.3,* ed. Ertl, G., Knözinger, H., and Weitkamp, J., Wiley-VCH, (1997)

Senger, S., Radom, L., Zeolites as transition-metal-free hydrogenation catalysts: A theoretical mechanistic study, *J. Am. Chem. Soc.,* **122**, 2613-2620, (2000)

Sie, S.T., Acid-catalysed cracking of paraffinic hydrocarbons. 1. Discussion of existing mechanisms and proposal of a new mechanism, *Ind. Eng. Chem. Res.*, **31**, 1881-1889, (1992)

Sie, S.T., Isomerization reactions in *Handbook of Heterogeneous Catalysis*, *Vol.4,* ed. Ertl, G., Knözinger, H., and Weitkamp, J., Wiley-VCH, (1997)

Shaheen, E.I., *Catalytic Processing in Petroleum Refining*, Penwell Publishing Company, Tulsa, Oaklahoma, (1983)

Sinfelt, J.H., Catalytic reforming, in *Handbook of Heterogeneous Catalysis, Vol. 4*, ed. Ertl, G., Knözinger, H., and Weitkamp, J., Wiley-VCH, (1997)

SRI International- Catalysts Supplement A, *Process Economics Program Report 153A*, Catalysts, 5-19, Menlo Park, California (1996)

Tabak, S.A., Krambeck, F.J., Garwood, W.E., Conversion of propylene and butylene over ZSM-5 catalyst, *AIChe Journal*, **32(9)**, 1526-1531, (1986)

Tamm, P.W., Mohr, D.H., Wilson, C.R., Octane enhancement by selective reforming of light paraffins, in *Catalysis 1987*, ed. Ward, J.W., Elsevier Science Publishers B.V., Amsterdam, (1988)

Thomas, J.M., Bell, R.G., Catlow, C.R.A., in *Handbook of Heterogeneous Catalysis, Vol. 1,* ed. Ertl, G., Knözinger, H., and Weitkamp, J., Wiley-VCH, 1997.

Thomas, J.M., Thomas, W.J., *Principles and Practice of Heterogeneous Catalysis*, VCH, Weinheim, (1997)

Viswanadham, N., Pradhan, A.R., Ray, N., Vishnoi, S.C., Shanker, U., Prasada Rao, T.S.R., Reaction pathways for the aromatization of paraffins in the presence of H-ZSM-5 and Zn/H-ZSM-5, *Appl., Catal., A:General,* **137**, 225-233, (1996)

Voge H.H, Good, G.M., Greensfelder, B.S., Catalytic cracking of pure hydrocarbons, secondary reactions of olefins, *Ind. Eng. Chem.*, **38**, 1033, (1946)

Von Ballmoos, R., Harris, D.H., Magee, J.S., in *Handbook of Heterogeneous Catalysis, Vol. 4,* ed. Ertl, G., Knözinger, H., and Weitkamp, J., Wiley-VCH, (1997)

Walendziewski, J. and Pniak, B., Skeletal isomerization of 1-pentene, *React. Kinet. Catal. Lett.,* **58(2)**, 359-365, jointly published by Elsevier Science B.V., Amsterdam and Akademiai Kiado, Budapest, (1996)

Zhao, S., Zeitliche Selektivitäts- und Aktivitätsänderungen bei der Umsetzung von Methanol und n-Dodecan am Zeolith HZSM-5 und anderen sauren Katalysatoren", *Fortschr.-Ber. VDI,* **Reihe 3 Nr. 256**, (1991)

APPENDIX I THERMODYNAMIC TABLES

Double bond isomerisation:
1-pentene to t-2-pentene
C5H10(Fg) = C5H10(Hg)

T C	deltaH kJ	deltaS J	deltaG kJ	K
25	-11.632	-3.452	-10.602	7.21E+01
50	-11.662	-3.551	-10.515	5.01E+01
75	-11.698	-3.656	-10.425	3.67E+01
100	-11.737	-3.764	-10.332	2.80E+01
125	-11.779	-3.875	-10.237	2.20E+01
150	-11.825	-3.986	-10.138	1.79E+01
175	-11.873	-4.096	-10.037	1.48E+01
200	-11.924	-4.206	-9.933	1.25E+01
225	-11.976	-4.314	-9.827	1.07E+01
250	-12.03	-4.421	-9.718	9.34E+00
275	-12.086	-4.525	-9.606	8.23E+00
300	-12.143	-4.626	-9.492	7.33E+00
325	-12.201	-4.725	-9.375	6.59E+00
350	-12.259	-4.82	-9.255	5.97E+00
375	-12.318	-4.912	-9.134	5.45E+00
400	-12.376	-5.001	-9.01	5.00E+00
425	-12.435	-5.087	-8.884	4.62E+00
450	-12.493	-5.169	-8.755	4.29E+00

Double bond isomerisation:
1-pentene to c-2-pentene
C5H10(Fg) = C5H10(Gg)

T C	deltaH kJ	deltaS J	deltaG kJ	K
25	-6.782	1.607	-7.261	1.87E+01
50	-6.973	0.992	-7.294	1.51E+01
75	-7.153	0.454	-7.312	1.25E+01
100	-7.325	-0.021	-7.317	1.06E+01
125	-7.487	-0.443	-7.311	9.10E+00
150	-7.642	-0.821	-7.295	7.95E+00
175	-7.79	-1.159	-7.27	7.04E+00
200	-7.93	-1.464	-7.237	6.30E+00
225	-8.064	-1.739	-7.197	5.69E+00
250	-8.191	-1.989	-7.151	5.18E+00
275	-8.312	-2.215	-7.098	4.75E+00
300	-8.428	-2.421	-7.04	4.38E+00
325	-8.538	-2.609	-6.977	4.07E+00
350	-8.642	-2.78	-6.91	3.80E+00
375	-8.741	-2.936	-6.838	3.56E+00
400	-8.835	-3.078	-6.763	3.35E+00
425	-8.924	-3.208	-6.684	3.16E+00
450	-9.009	-3.327	-6.603	3.00E+00

Skeletal isomerisation:
1-pentene to 3-methyl-1-butene
C5H10(Fg) = C5H10(Dg)

T C	deltaH kJ	deltaS J	deltaG kJ	K
25	-6.899	-9.56	-4.049	5.12E+00
50	-6.625	-8.675	-3.821	4.15E+00
75	-6.367	-7.906	-3.614	3.49E+00
100	-6.124	-7.234	-3.425	3.02E+00
125	-5.897	-6.643	-3.252	2.67E+00
150	-5.683	-6.123	-3.092	2.41E+00
175	-5.483	-5.662	-2.945	2.21E+00
200	-5.294	-5.253	-2.809	2.04E+00
225	-5.118	-4.89	-2.682	1.91E+00
250	-4.953	-4.565	-2.564	1.80E+00
275	-4.798	-4.276	-2.454	1.71E+00
300	-4.653	-4.017	-2.35	1.64E+00
325	-4.517	-3.785	-2.253	1.57E+00
350	-4.39	-3.578	-2.161	1.52E+00
375	-4.271	-3.391	-2.074	1.47E+00
400	-4.161	-3.223	-1.991	1.43E+00
425	-4.057	-3.072	-1.912	1.39E+00
450	-3.96	-2.936	-1.837	1.36E+00

Skeletal isomerisation:
1-pentene to 2-methyl-1-butene
C5H10(Fg) = C5H10(Bg)

T C	deltaH kJ	deltaS J	deltaG kJ	K
25	-16.071	-4.87	-14.619	3.64E+02
50	-15.982	-4.585	-14.501	2.21E+02
75	-15.903	-4.349	-14.389	1.44E+02
100	-15.833	-4.153	-14.283	9.99E+01
125	-15.769	-3.987	-14.181	7.26E+01
150	-15.711	-3.846	-14.083	5.48E+01
175	-15.658	-3.725	-13.989	4.27E+01
200	-15.61	-3.62	-13.897	3.42E+01
225	-15.565	-3.528	-13.808	2.81E+01
250	-15.524	-3.448	-13.72	2.34E+01
275	-15.486	-3.378	-13.635	1.99E+01
300	-15.451	-3.315	-13.551	1.72E+01
325	-15.419	-3.259	-13.469	1.50E+01
350	-15.388	-3.209	-13.388	1.33E+01
375	-15.36	-3.165	-13.309	1.18E+01
400	-15.333	-3.124	-13.23	1.06E+01
425	-15.308	-3.087	-13.153	9.64E+00
450	-15.283	-3.053	-13.076	8.80E+00

Skeletal isomerisation:
1-pentene to 2-methyl-2-butene
C5H10(Fg) = C5H10(Cg)

T	deltaH	deltaS	deltaG	K
C	kJ	J	kJ	
25	-20.500		-18.000	
50	-20.587		-17.787	
75	-20.693		-17.566	
100	-20.810		-17.338	
125	-20.933		-17.101	
150	-21.059		-16.857	
175	-21.185		-16.605	
200	-21.308		-16.346	
225	-21.428		-16.081	
250	-21.545		-15.809	
275	-21.658		-15.532	
300	-21.767		-15.251	
325	-21.872		-14.964	
350	-21.974		-14.673	
375	-22.073		-14.378	
400	-22.168		-14.080	
425	-22.260		-13.778	
450				

Skeletal isomerisation:
t-2-pentene to 2-methyl-2-butene
C5H10(Hg) = C5H10(Cg)

T	deltaH	deltaS	deltaG	K
C	kJ	J	kJ	
25	-10.700		-9.360	
50	-10.785		-9.244	
75	-10.867		-9.122	
100	-10.948		-8.994	
125	-11.026		-8.860	
150	-11.103		-8.722	
175	-11.178		-8.579	
200	-11.252		-8.432	
225	-11.323		-8.281	
250	-11.393		-8.126	
275	-11.461		-7.968	
300	-11.526		-7.808	
325	-11.589		-7.644	
350	-11.650		-7.478	
375	-11.708		-7.310	
400	-11.764		-7.140	
425	-11.817		-6.966	
450				

Cracking:
1-decene to 2-methyl-1-butene
C10H20(Cg) = 2C5H10(Bg)

T	deltaH	deltaS	deltaG	K
C	kJ	J	kJ	
25	49.882	138.582	8.563	3.16E-02
50	49.931	138.743	5.096	1.50E-01
75	49.948	138.792	1.627	5.70E-01
100	49.936	138.76	-1.842	1.81E+00
125	49.9	138.667	-5.31	4.97E+00
150	49.843	138.529	-8.775	1.21E+01
175	49.767	138.355	-12.237	2.67E+01
200	49.675	138.154	-15.693	5.40E+01
225	49.567	137.932	-19.144	1.02E+02
250	49.446	137.695	-22.59	1.80E+02
275	49.312	137.446	-26.029	3.02E+02
300	49.167	137.187	-29.462	4.84E+02
325	49.012	136.922	-32.888	7.45E+02
350	48.847	136.652	-36.308	1.11E+03
375	48.673	136.379	-39.721	1.59E+03
400	48.492	136.104	-43.127	2.22E+03
425	48.303	135.828	-46.526	3.03E+03
450	48.107	135.553	-49.918	4.04E+03

Aromatisation:
t-2-pentene to benzene
1.2C5H10(Hg) = C6H6(g) + 3H2(g)

T	deltaH	deltaS	deltaG	K
C	kJ	J	kJ	
25	122.24	252.541	46.945	5.95E-09
50	123.211	255.669	40.592	2.74E-07
75	124.19	258.587	34.163	7.48E-06
100	125.158	261.273	27.664	1.34E-04
125	126.101	263.719	21.101	1.70E-03
150	127.012	265.939	14.48	1.63E-02
175	127.887	267.948	7.806	1.23E-01
200	128.722	269.762	1.084	7.59E-01
225	129.517	271.399	-5.68	3.94E+00
250	130.27	272.875	-12.484	1.76E+01
275	130.982	274.203	-19.323	6.94E+01
300	131.651	275.398	-26.193	2.44E+02
325	132.279	276.47	-33.092	7.76E+02
350	132.866	277.432	-40.016	2.26E+03
375	133.413	278.293	-46.963	6.10E+03
400	133.921	279.062	-53.93	1.53E+04
425	134.391	279.748	-60.915	3.61E+04
450	134.824	280.358	-67.917	8.06E+04

Aromatisation:
t-2-pentene to toluene
1.4C5H10(Hg) = C7H8(Cg) + 3H2(g)

T C	deltaH kJ	deltaS J	deltaG kJ	K
25	95.864	235.87	25.539	3.35E-05
50	96.849	239.044	19.602	6.78E-04
75	97.809	241.906	13.59	9.14E-03
100	98.739	244.485	7.509	8.89E-02
125	99.632	246.804	1.367	6.62E-01
150	100.491	248.896	-4.829	3.95E+00
175	101.315	250.788	-11.076	1.96E+01
200	102.105	252.504	-17.367	8.27E+01
225	102.862	254.062	-23.7	3.06E+02
250	103.586	255.482	-30.069	1.01E+03
275	104.279	256.775	-36.473	2.99E+03
300	104.94	257.956	-42.907	8.14E+03
325	105.571	259.034	-49.37	2.05E+04
350	106.172	260.018	-55.858	4.82E+04
375	106.743	260.916	-62.37	1.06E+05
400	107.285	261.736	-68.903	2.22E+05
425	107.797	262.483	-75.456	4.43E+05
450	108.28	263.163	-82.027	8.42E+05

Aromatisation:
t-2-pentene to ethylbenzene
1.6C5H10(Hg) = C8H10(Dg) + 3H2(g)

T C	deltaH kJ	deltaS J	deltaG kJ	K
25	82.207	207.526	20.333	2.74E-04
50	83.244	210.865	15.103	3.62E-03
75	84.278	213.946	9.792	3.39E-02
100	85.298	216.777	4.408	2.42E-01
125	86.294	219.362	-1.045	1.37E+00
150	87.264	221.725	-6.559	6.45E+00
175	88.205	223.886	-12.129	2.59E+01
200	89.116	225.864	-17.751	9.12E+01
225	89.996	227.676	-23.421	2.86E+02
250	90.844	229.338	-29.134	8.11E+02
275	91.661	230.863	-34.887	2.11E+03
300	92.445	232.263	-40.676	5.10E+03
325	93.197	233.547	-46.499	1.15E+04
350	93.917	234.726	-52.352	2.45E+04
375	94.604	235.808	-58.234	4.94E+04
400	95.259	236.799	-64.142	9.50E+04
425	95.881	237.706	-70.074	1.75E+05
450	96.47	238.536	-76.027	3.11E+05

Aromatisation:
t-2-pentene to o-xylene
1.6C5H10(Hg) = C8H10(Gg) + 3H2(g)

T C	deltaH kJ	deltaS J	deltaG kJ	K
25	71.413	199.827	11.834	8.44E-03
50	72.557	203.515	6.791	7.98E-02
75	73.672	206.838	1.661	5.63E-01
100	74.75	209.83	-3.548	3.14E+00
125	75.786	212.517	-8.828	1.44E+01
150	76.779	214.937	-14.171	5.62E+01
175	77.73	217.121	-19.573	1.91E+02
200	78.639	219.095	-25.026	5.79E+02
225	79.507	220.883	-30.526	1.59E+03
250	80.335	222.506	-36.069	4.00E+03
275	81.124	223.979	-41.65	9.32E+03
300	81.875	225.319	-47.266	2.03E+04
325	82.589	226.538	-52.915	4.18E+04
350	83.266	227.647	-58.592	8.16E+04
375	83.906	228.655	-64.296	1.52E+05
400	84.512	229.572	-70.024	2.72E+05
425	85.083	230.405	-75.774	4.68E+05
450	85.621	231.162	-81.544	7.77E+05

Aromatisation:
t-2-pentene to m-xylene
1.6C5H10(Hg) = C8H10(Fg) + 3H2(g)

T C	deltaH kJ	deltaS J	deltaG kJ	K
25	69.668	204.342	8.743	2.94E-02
50	70.673	207.58	3.594	2.63E-01
75	71.66	210.521	-1.633	1.76E+00
100	72.62	213.185	-6.93	9.34E+00
125	73.547	215.589	-12.29	4.10E+01
150	74.439	217.764	-17.708	1.54E+02
175	75.297	219.734	-23.177	5.03E+02
200	76.119	221.521	-28.693	1.47E+03
225	76.908	223.144	-34.252	3.91E+03
250	77.662	224.622	-39.849	9.53E+03
275	78.383	225.969	-45.482	2.16E+04
300	79.071	227.196	-51.146	4.59E+04
325	79.726	228.315	-56.841	9.21E+04
350	80.349	229.336	-62.561	1.76E+05
375	80.941	230.266	-68.306	3.20E+05
400	81.501	231.114	-74.074	5.60E+05
425	82.03	231.886	-79.862	9.45E+05
450	82.528	232.588	-85.668	1.54E+06

Aromatisation:
t-2-pentene to p-xylene
1.6C5H10(Hg) = C8H10(Hg) + 3H2(g)

T C	deltaH kJ	deltaS J	deltaG kJ	K
25	70.379	199.145	11.004	1.18E-02
50	71.365	202.321	5.985	1.08E-01
75	72.327	205.188	0.89	7.35E-01
100	73.258	207.772	-4.272	3.96E+00
125	74.153	210.095	-9.496	1.76E+01
150	75.013	212.189	-14.775	6.67E+01
175	75.837	214.081	-20.104	2.21E+02
200	76.625	215.793	-25.478	6.50E+02
225	77.379	217.346	-30.892	1.74E+03
250	78.099	218.757	-36.344	4.26E+03
275	78.786	220.041	-41.829	9.69E+03
300	79.441	221.21	-47.345	2.07E+04
325	80.065	222.274	-52.889	4.16E+04
350	80.657	223.244	-58.458	7.95E+04
375	81.218	224.127	-64.05	1.45E+05
400	81.749	224.931	-69.663	2.55E+05
425	82.251	225.663	-75.296	4.31E+05
450	82.722	226.327	-80.946	7.04E+05

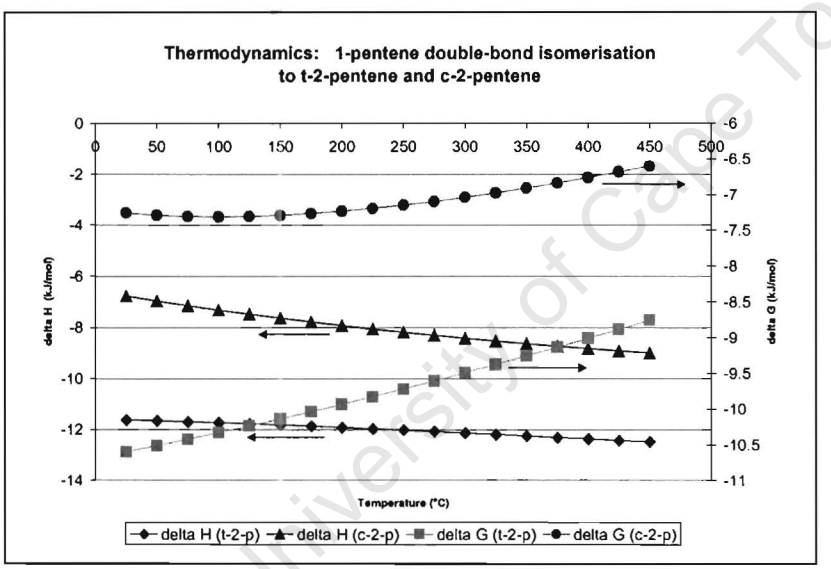

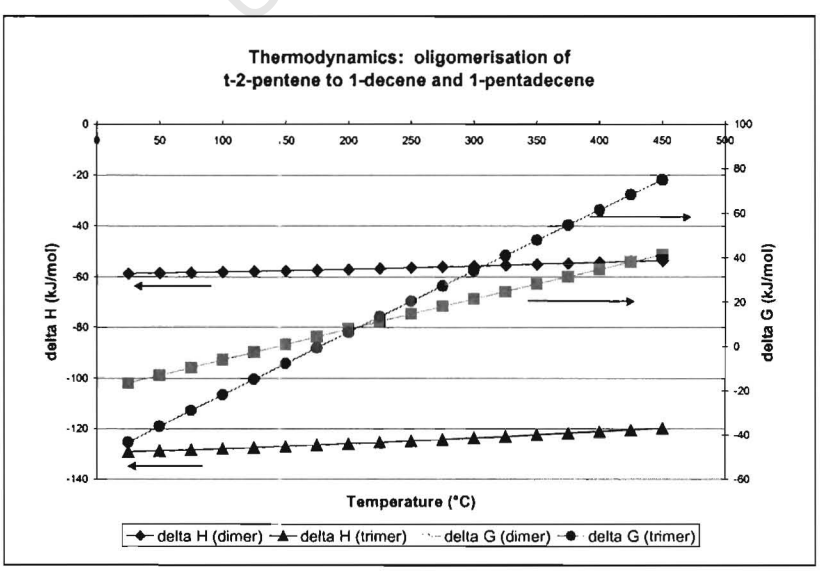

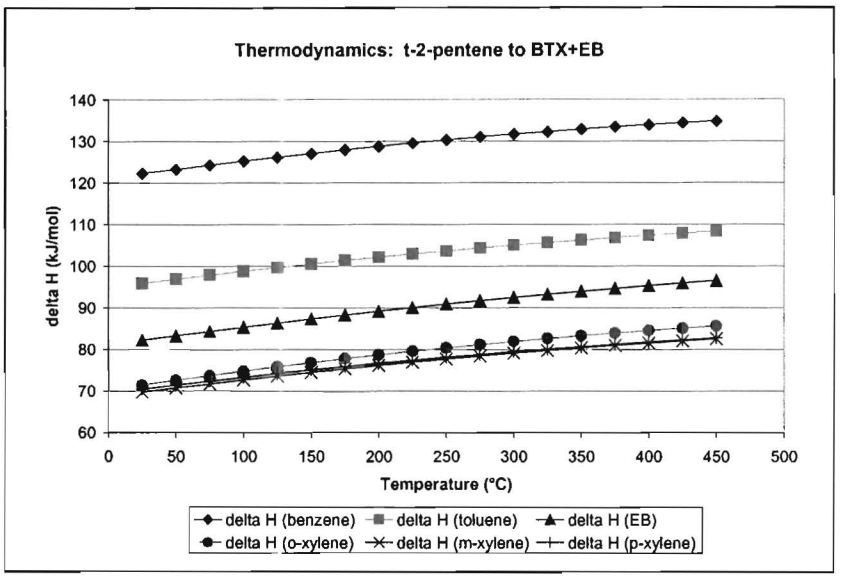

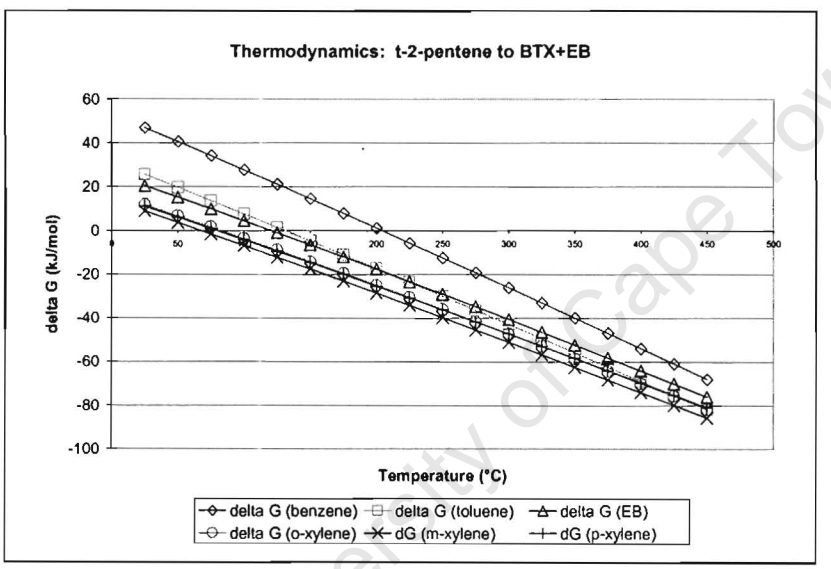

Appendix II Calibration graphs

The bubble flow meter was more accurate for the calibration of the Brookes used for argon due to the low flows (0-2 $l_n h^{-1}$).

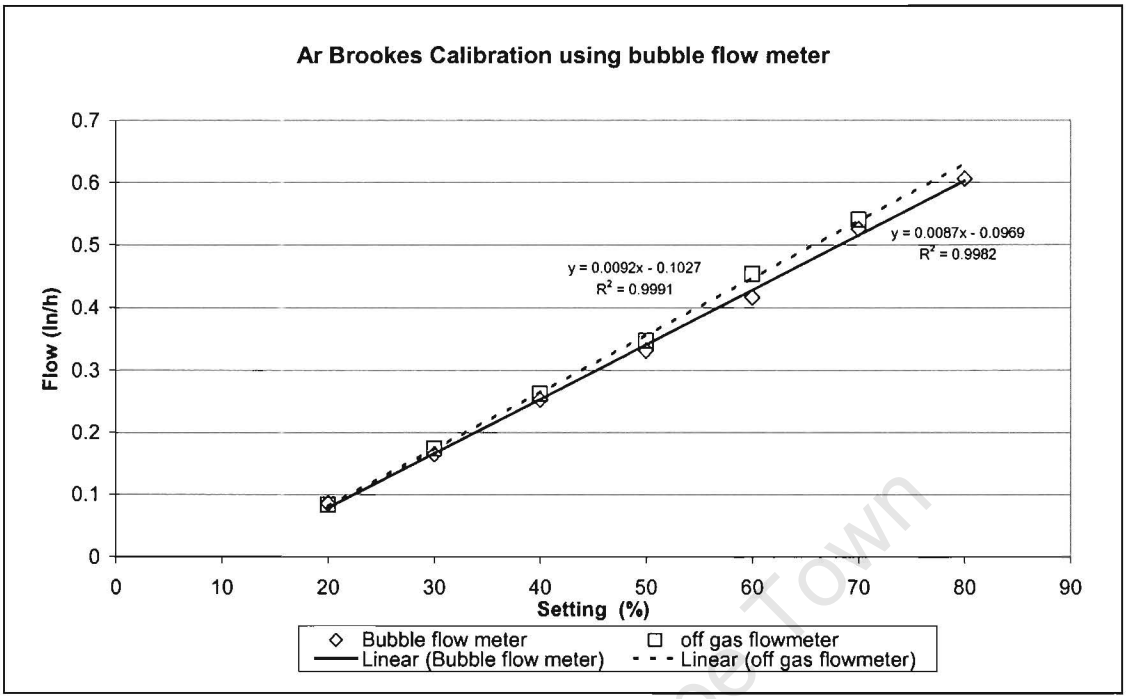

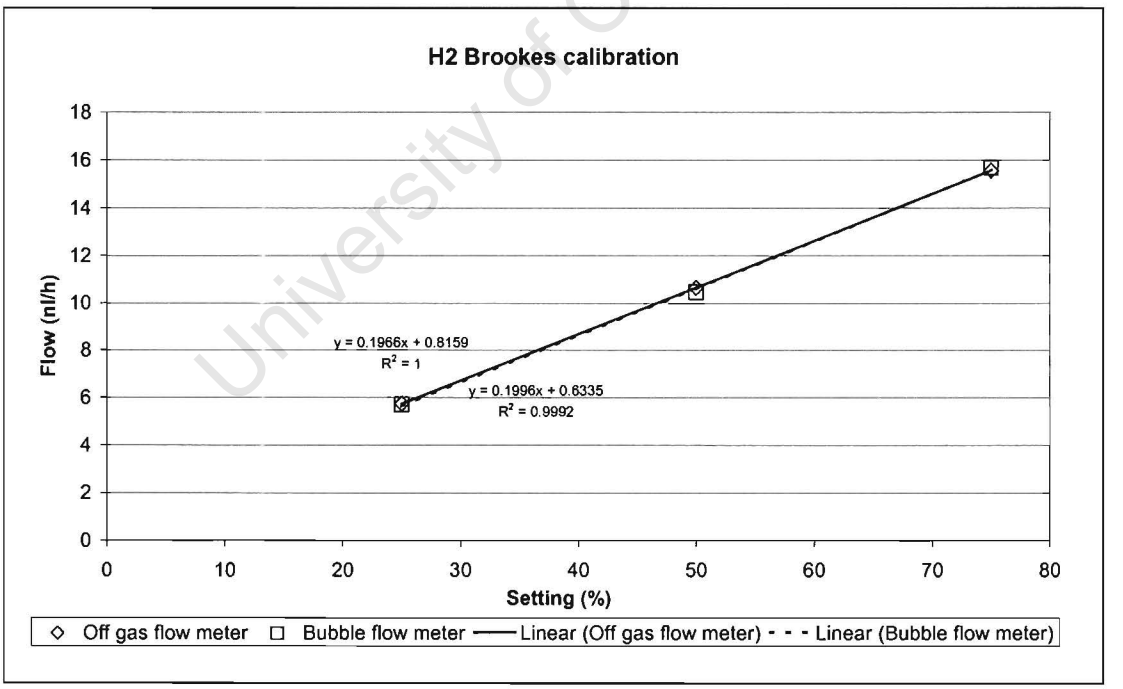

Mass balance

	Run 20z 153°C	Run 21z 360°C (blank run)
Liquid Feed		
Liquid feed ml/min	0.60	0.60
time (h)	6.00	6.00
total liq feed (ml)	216.00	216.00
density feed (g/ml)	0.64	0.64
total liq feed (g) (calc)	138.24	138.24
Gas Feed		
Ar (nl/h)	0.64	0.64
time (h)	6.00	6.00
total for run (nl)	3.84	3.84
Liquid Product		
Liquid prod (g)	19.25	26.50
time on stream (h)	6.00	6.00
Gas Product		
Total off gas (l)	12.06	12.58
Calib factor	0.95	0.95
off gasl flow (l)	11.43	11.92
off gas flow (nl)	8.88	9.26
time (h)	6.00	6.00
offgas (nl/h)	1.48	1.54
Ar (nl/h)	0.64	0.64
Actual Vol prod in off gas (nlh^{-1})	0.84	0.90
Total vol product in 6h (nl)	5.04	5.42
Total vol prod in 6h (l)	6.54	7.04
Density pentene (g/l)	2.98	2.98
Total mass (g) HC in off gas (6h) (assuming all HC are C5)	19.50	20.97
Total product (g) (6h)	38.75	47.47
HC in (g)	138.24	138.24
HC out (g)	38.75	47.47
Massbalance (%)	28.03	34.34

Appendix III Chromatograms

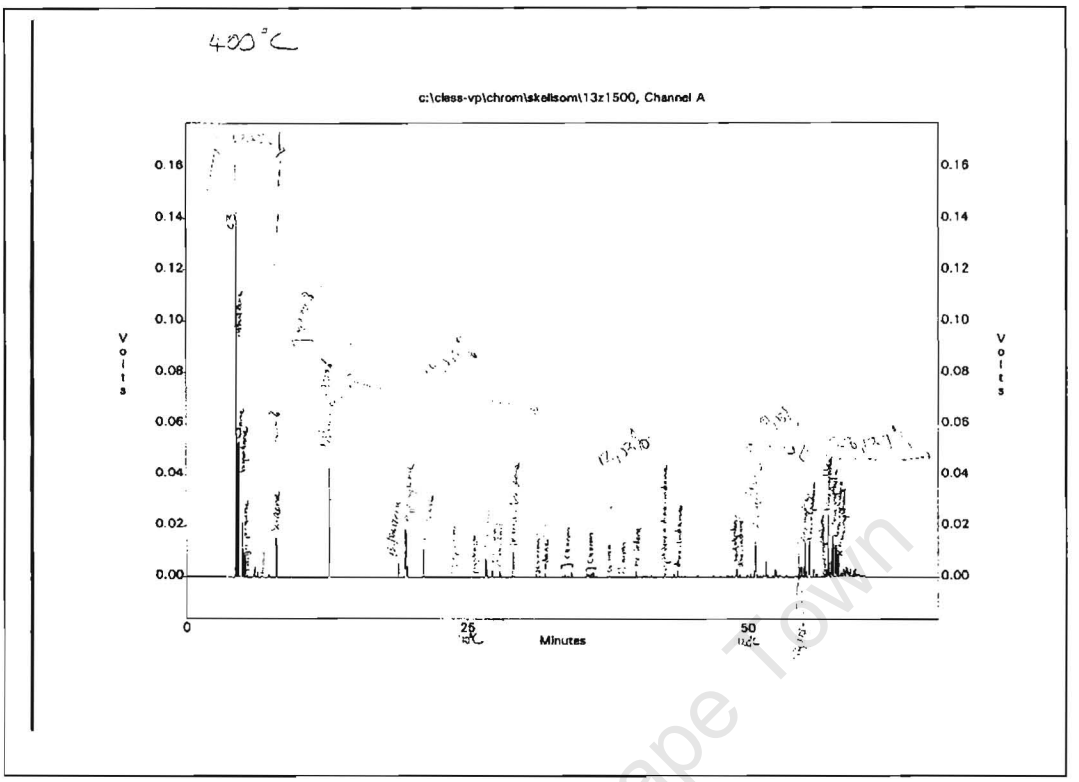

Figure 1 Run 13z

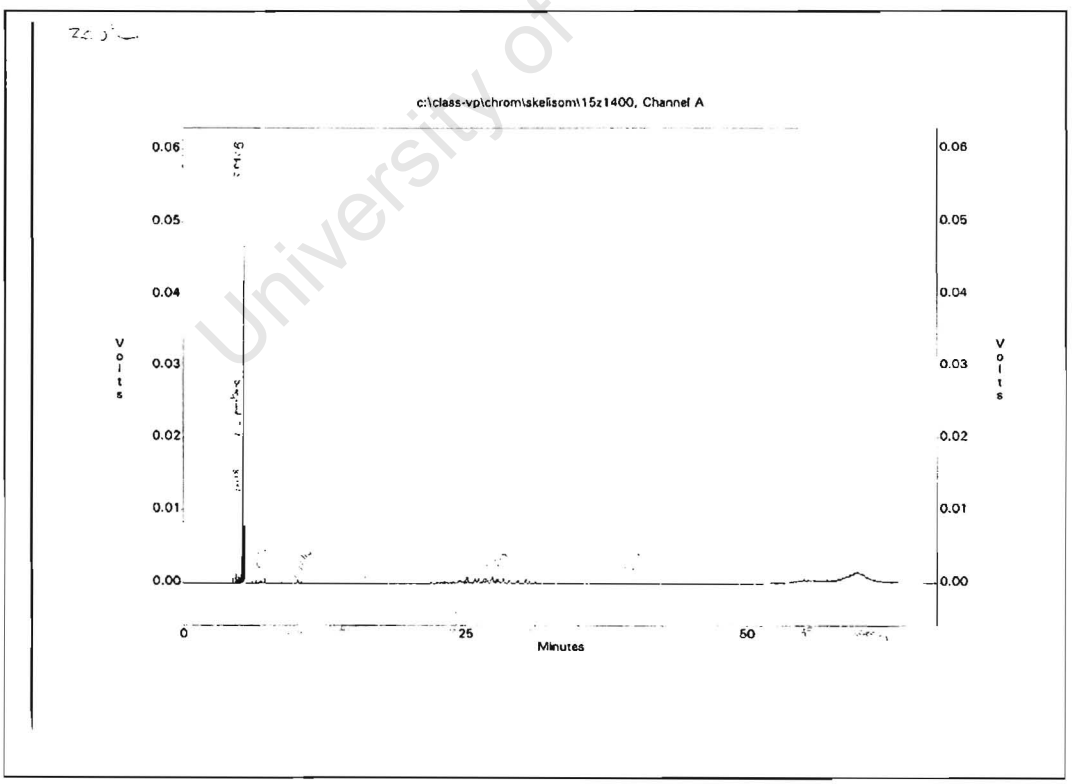

Figure 2 Run 15z

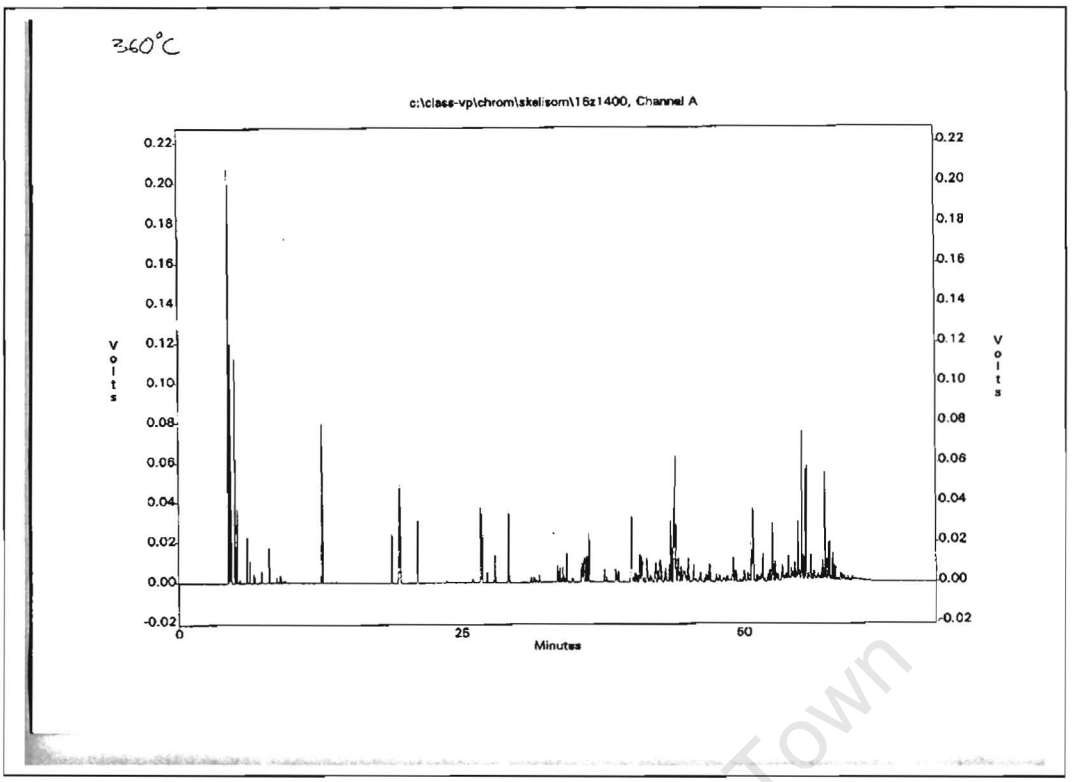

Figure 3 Run 16z

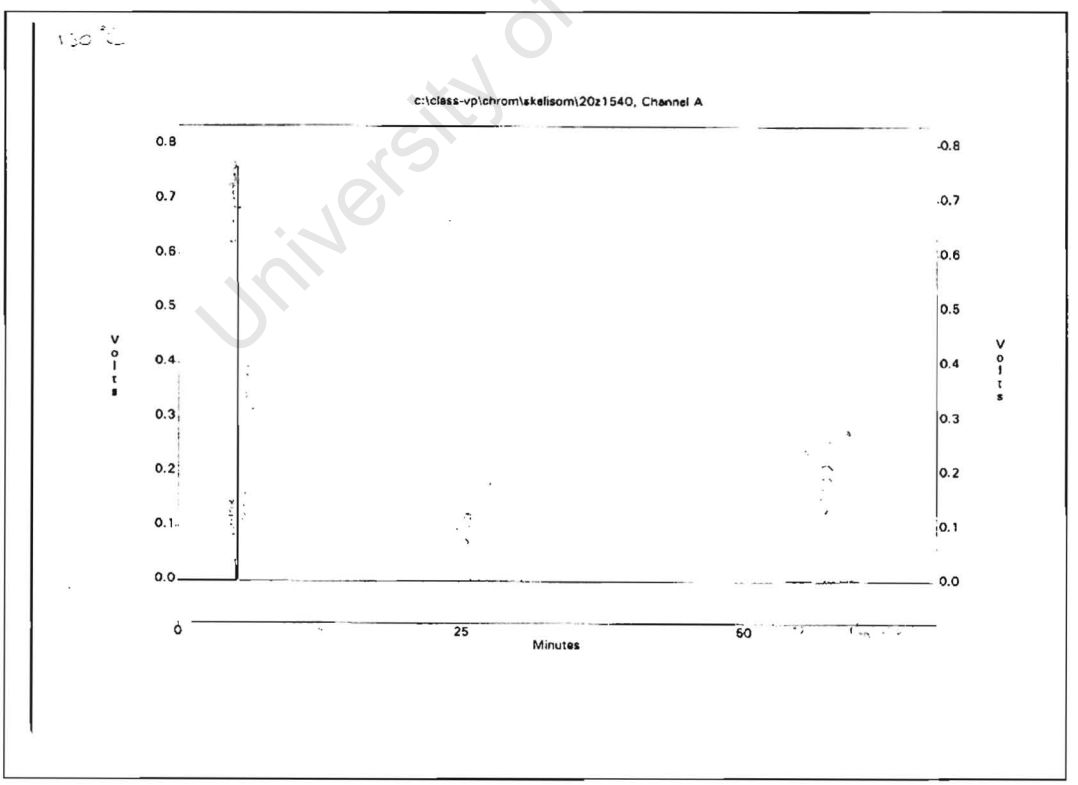

Figure 4 Run 20z

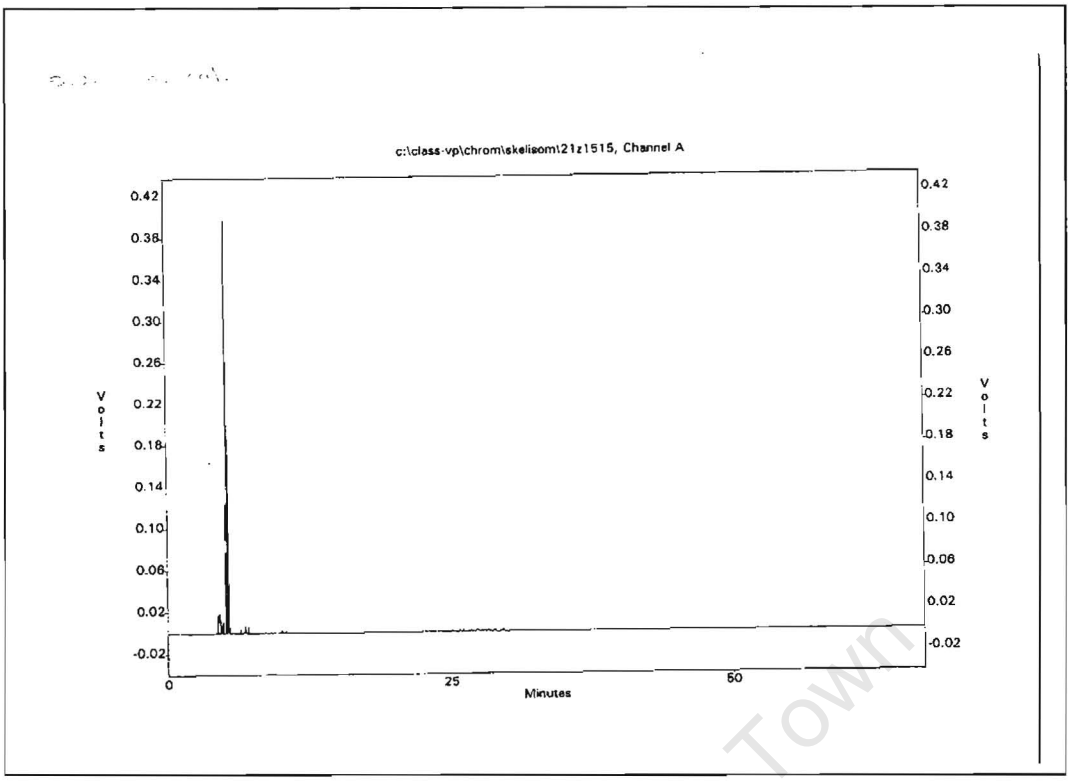

Figure 5 Run 21z

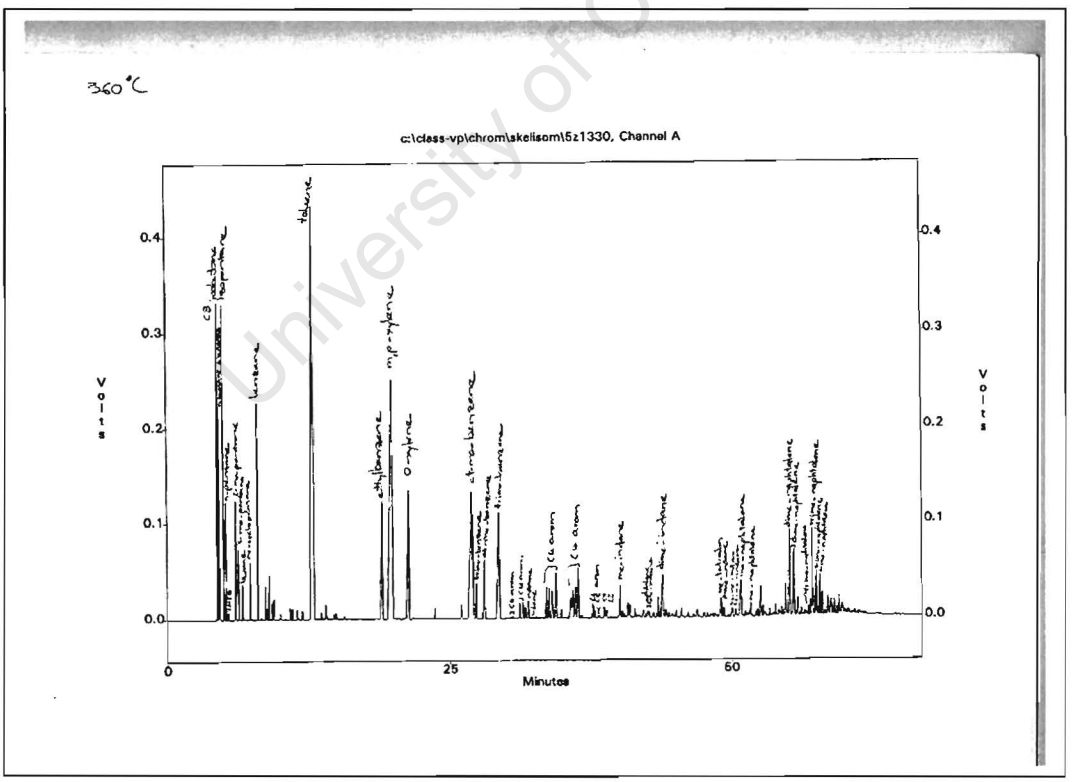

Figure 6 Run 5z

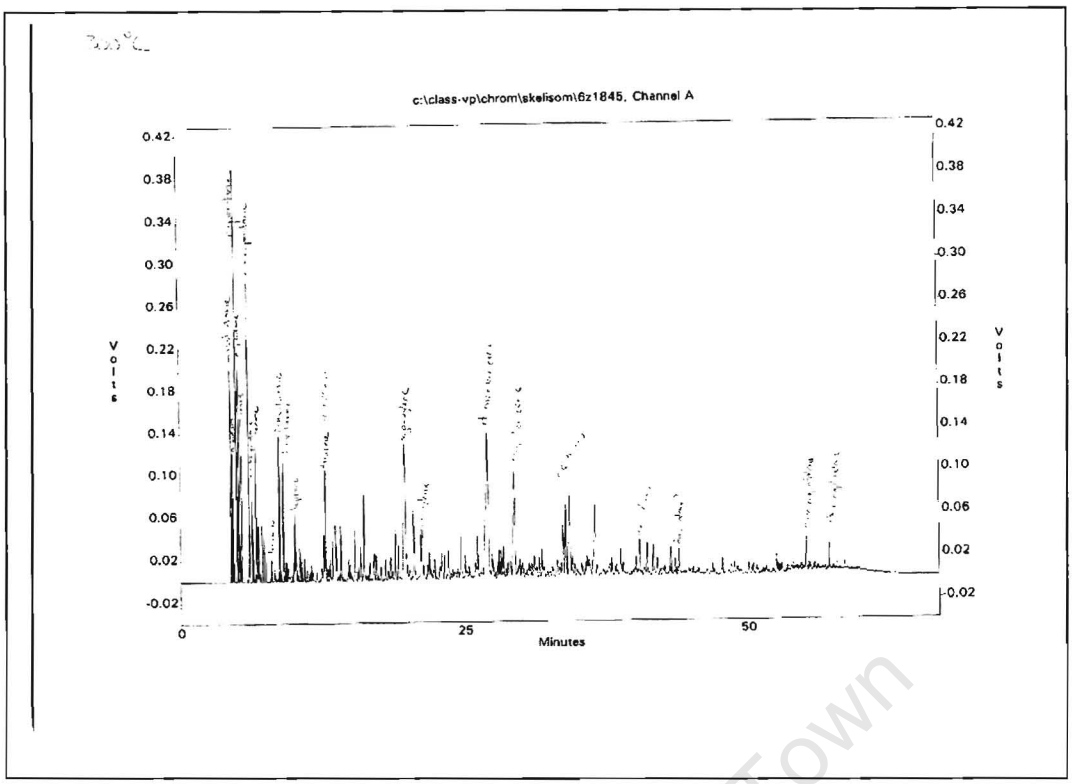

Figure 7 **Run 6z**

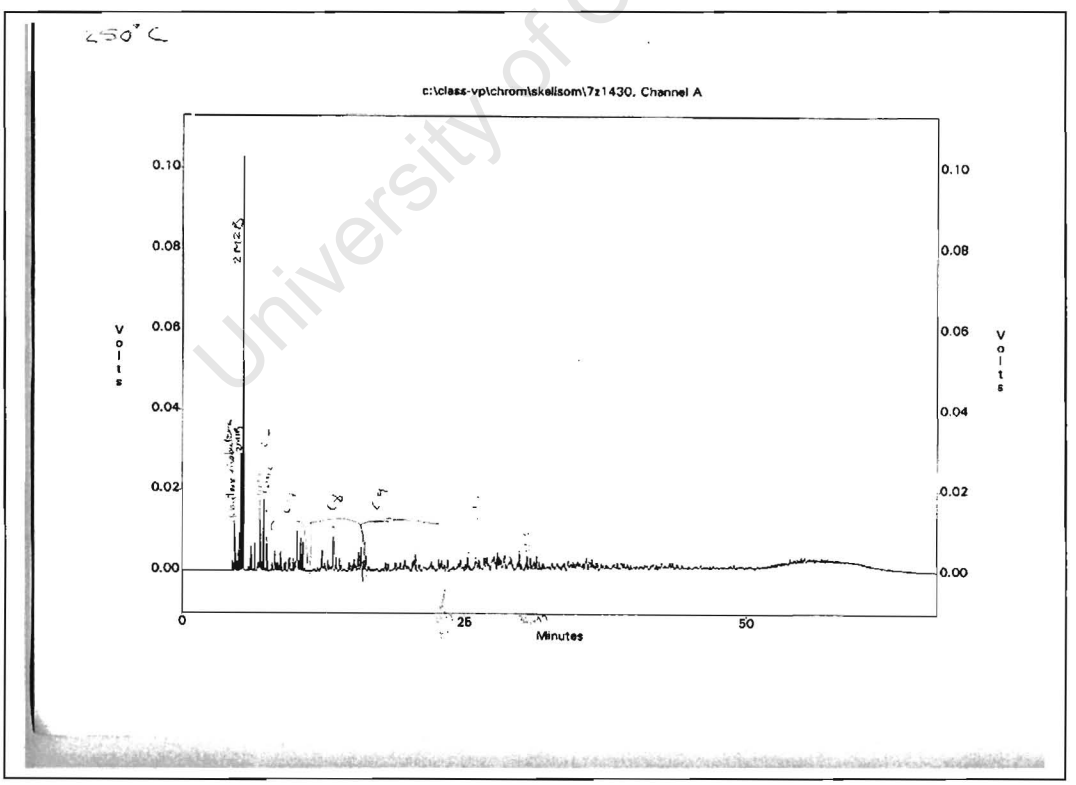

Figure 8 **Run 7z**

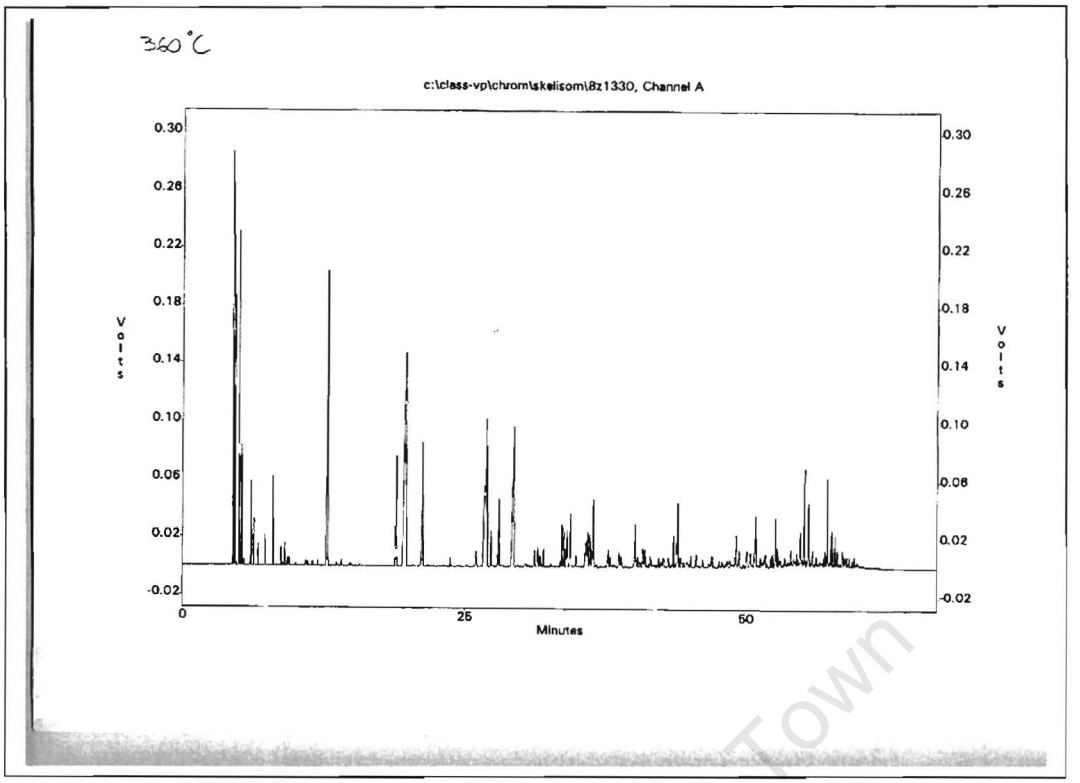

Figure 9 Run 8z

Table 3.5 (Extended) An example to show how assignment was carried out: Product distribution as a function of temperature

	Temperature (°C)	153	200	268	320	362	377	407	360
		20z	15z	7z	6z	5z	8z	13z	21z
C. no.	Component	C mass%	C mass%	C mass%	C mass%	C mass%	C mass%	C mass%	C mass%
2	C2 HC	0.00	0.00	0.00	0.01	0.04	0.06	0.65	0.00
3	C3 HC	0.00	0.20	0.11	0.39	1.37	2.09	10.07	1.05
4	C4 HC	0.02	1.05	1.03	2.01	2.70	3.77	10.00	2.43
5	isopentanes	0.06	0.40	0.40	1.78	1.70	1.89	2.62	0.21
5	n-pentanes	0.00	0.31	0.24	1.00	0.67	0.69	0.66	0.36
5	isopentenes	1.08	21.56	6.52	1.00	0.06	0.06	0.11	18.54
5	n-pentenes	65.26	9.03	1.11	0.25	0.02	0.02	0.02	45.54
5	cyclopentane+2,3-dimethyl butane	0.00	0.00	0.00	0.14	0.15	0.11	0.14	0.12
6	olefins	0.08	2.27	4.81	1.54	0.05	0.03	0.03	2.35
6	paraffins	0.00	0.00	0.54	3.13	1.42	1.11	0.59	0.56
6	naphtenes	0.00	0.00	0.00	0.37	0.46	0.27	0.13	0.01
6	aromatics								
6	Benzene	0.00	0.00	0.00	0.22	2.08	0.88	1.67	0.00
7	Toluene	0.00	0.00	0.00	1.44	18.38	7.91	7.69	0.00
8	m,p-Xylene	0.00	0.00	0.00	5.53	15.33	11.86	6.48	0.00
8	o-xylene	0.00	0.00	0.00	1.05	4.42	3.86	2.08	0.00
8	eBz	0.00	0.00	0.00	0.86	3.61	2.69	0.99	0.00
	BTX + eBZ	0.00	0.00	0.00	9.09	43.83	27.20	18.90	0.00
7	olefins	0.04	1.62	7.08	1.58	0.00	0.00	0.00	2.39
7	paraffins	0.00	0.00	0.00	5.05	0.96	0.55	0.12	0.13
7	naphtenes	0.00	0.00	0.00	2.61	0.86	0.44	0.10	0.00
7	aromatics				0.00				
8	olefins	0.02	1.53	9.45	1.53	0.00	0.00	0.00	2.06
8	paraffins	0.00	0.00	0.00	3.03	0.38	0.21	0.02	0.00
8	naphtenes	0.00	0.00	0.00	6.05	0.86	0.53	0.03	0.00
8	aromatics								
9	olefins	0.00	4.05	10.90	0.00	0.00	0.00	0.00	2.90
9	paraffins	0.00	0.00	0.00	2.23	0.04	0.04	0.00	0.00
9	naphtenes	0.00	0.00	0.00	13.13	0.46	1.65	0.00	0.00
9	aromatics	0.00	0.00	0.00	15.14	14.91	18.68	5.98	0.00
10	olefins	12.24	23.89	17.59	0.00	0.00	0.00	0.00	13.84
10	paraffins	0.00	0.00	0.00	0.00	0.00	0.00	0.00	0.00
10.	naphtenes	0.00	0.00	0.00	0.00	0.00	0.00	0.00	0.00
10	aromatics	0.00	0.00	0.00	16.90	8.98	13.79	5.39	0.00
11+	olefins	21.21	34.09	40.22	0.00	0.00	0.00	0.00	7.51
11+	paraffins	0.00	0.00	0.00	0.00	0.00	0.00	0.00	0.00
11+	naphtenes	0.00	0.00	0.00	0.00	0.00	0.00	0.00	0.00
11+	aromatics	0.00	0.00	0.00	12.78	20.08	26.79	44.44	0.00
	Total	100.00	100.00	100.00	100.77	100.00	100.00	100.00	100.00

Table 3.6 (Extended) The effect of WHSV on the product distribution

	WHSV (h^{-1})	23	23	23	45	45	68	168	113
		5z	8z	16z	4z	17z	3z	18z	14z
	Actual Average bed temperature (°C)	364	377	367	368	395	372	421	431
	Set temperature (°C)	360	360	360	360	360	360	360	360
C no.	Component	C Mass%	C Mass%	C Mass%	C Mass%	C Mass%	C Mass%	C Mass%	C Mass%
2	C2 HC	0.04	0.06	0.10	0.05	0.04	0.11	0.08	0.08
3	C3 HC	1.37	2.09	3.27	1.10	0.83	1.78	1.04	0.96
4	C4 HC	2.70	3.77	4.98	2.17	1.68	3.49	1.79	1.69
5	isopentanes	1.70	1.89	1.86	1.32	0.97	1.99	0.80	0.76
5	n-pentanes	0.67	0.69	0.61	0.56	0.41	0.87	0.34	0.32
5	isopentenes	0.06	0.06	0.05	0.13	0.17	0.34	0.28	0.32
5	n-pentenes	0.02	0.02	0.02	0.04	0.05	0.12	0.10	0.12
5	cyclopentane+2,3-dimethyl butane	0.15	0.11	0.08	0.12	0.08	0.21	0.08	0.09
6	olefins	0.05	0.03	0.02	0.14	0.18	0.32	0.28	0.38
6	paraffins	1.42	1.11	0.77	1.12	0.90	1.64	0.62	0.60
6	naphtenes	0.46	0.27	0.15	0.41	0.29	0.64	0.23	0.25
6	Benzene	2.08	0.88	0.48	1.01	0.60	1.39	0.37	0.44
7	Toluene	18.38	7.91	3.60	9.70	6.47	11.23	3.19	3.43
8	m,p-Xylene	15.33	11.86	5.14	13.29	12.59	17.02	6.82	7.95
8	o-xylene	4.42	3.86	1.66	4.08	3.91	5.27	2.25	2.70
8	eBz	3.61	2.69	1.14	2.93	2.71	3.47	1.38	1.43
	BTX + eBZ	43.83	27.20	12.02	31.01	26.27	38.37	14.01	15.95
7	olefins				0.12	0.24	0.25	0.20	0.43
7	paraffins	0.90	0.51	0.26	0.78	0.71	1.07	0.45	0.51
7	naphtenes	0.93	0.48	0.20	0.95	0.83	1.40	0.72	1.03
7	aromatics								
8	olefins								
8	paraffins	0.38	0.21	0.08	0.42	0.47	0.55	0.20	0.41
8	naphtenes	0.86	0.53	0.20	1.50	1.59	2.37	1.54	2.71
8	aromatics								
9	olefins								
9	paraffins	0.04	0.04	0.01	0.00	0.00	0.00	0.16	0.27
9	naphtenes	0.46	1.65	0.54	1.63	1.97	1.82	2.12	3.80
9	aromatics	14.91	18.68	7.55	16.47	16.23	19.82	15.11	15.14
10	olefins								
10	paraffins								
10	naphtenes								
10	aromatics	8.98	13.79	15.21	10.59	20.17	10.06	28.65	23.99
11+	olefins								
11+	paraffins								
11+	naphtenes								
11+	aromatics	20.08	26.79	52.05	29.37	25.41	12.78	31.18	30.17
	Total	100.00	100.00	100.00	100.00	99.49	100.00	100.00	100.00

Table 3.7 (Extended) The effect of Pressure and carrier gas on the product distribution

	Total Pressure (bar)	2	2	2	5	2	5	5
	H_2 (H_2:feed molar ratio)	0	0	0	0	1	1	1
	Actual average bed temperature (°C)	364	367	377	379	373	363	372
	Set temperature (°C)	360	360	360	360	360	360	360
		5z	8z	16z	9z	10z	12z	19z
C no.	Component	C Mass %	C Mass %	C Mass %	C Mass %	C Mass %	C Mass %	C Mass %
2	C2 HC	0.04	0.06	0.10	0.05	0.23	1.42	0.50
3	C3 HC	1.37	2.09	3.27	2.22	2.36	11.89	7.99
4	C4 HC	2.70	3.77	4.98	4.14	5.43	24.75	15.67
5	isopentanes	1.70	1.89	1.86	2.64	2.37	11.29	6.76
5	n-pentanes	0.67	0.69	0.61	1.02	1.01	4.96	2.35
5	isopentenes	0.06	0.06	0.05	0.06	0.29	0.40	0.27
5	n-pentenes	0.02	0.02	0.02	0.03	0.04	0.00	0.07
5	cyclopentane+2,3-dimethyl butane	0.15	0.11	0.08	0.17	0.19	1.01	0.45
6	olefins	0.05	0.03	0.02	0.05	0.15	0.03	0.13
6	paraffins	1.42	1.11	0.77	1.87	1.40	5.20	3.34
6	naphtenes	0.46	0.27	0.15	0.32	0.56	1.59	0.80
6	Benzene	2.08	0.88	0.48	1.45	0.41	0.89	0.73
7	Toluene	18.38	7.91	3.60	8.12	3.90	4.69	5.02
8	m,p-Xylene	15.33	11.86	5.14	10.18	7.74	4.28	6.41
8	o-xylene	4.42	3.86	1.66	3.42	2.60	1.26	1.98
8	eBz	3.61	2.69	1.14	2.29	1.77	0.94	1.55
	BTX + eBZ	43.83	27.20	12.02	25.46	16.42	12.07	15.68
7	olefins							
7	paraffins	0.90	0.51	0.26	0.72	0.68	1.80	1.30
7	naphtenes	0.93	0.48	0.20	0.62	1.37	2.68	1.54
7	aromatics							
8	olefins							
8	paraffins	0.38	0.21	0.08	0.24	0.38	0.79	0.56
8	naphtenes	0.86	0.53	0.20	0.52	1.64	1.16	1.36
8	aromatics							
9	olefins							
9	paraffins	0.04	0.04	0.01	0.00	0.02	0.00	0.08
9	naphtenes	0.46	1.65	0.54	0.48	1.94	0.10	0.56
9	aromatics	14.91	18.68	7.55	16.38	15.78	4.01	8.68
10	olefins							
10	paraffins							
10	naphtenes							
10	aromatics	8.98	13.79	15.21	15.75	13.82	1.92	5.19
11+	olefins							
11+	paraffins							
11+	naphtenes							
11+	aromatics	20.08	26.79	52.05	27.26	33.94	12.95	26.72
	Total	100.00	100.00	100.00	100.02	100.00	100.00	100.00

Note: The temperatures for all repeat runs were set to the same value at the start of the run. Differences in exotherms upon addition of the feed, led to different actual catalyst bed temperatures for these runs.